Spatial Modelling, formation and transformation of the Oldowan lithic artefact assemblages from Sterkfontein Caves, South Africa

By Raymond Alexander Couzens

A thesis submitted to the Faculty of Science, University of the Witwatersrand, Johannesburg, in fulfilment of the requirements for the Degree of Doctor of Philosophy
Johannesburg, 2021

Declaration

I, Raymond Alexander Couzens, declare that this thesis is my own unaided work. It is being submitted for the degree of Doctor of Philosophy at the University of the Witwatersrand, Johannesburg.

It has not been submitted before for any degree or examination in any other university.

___________________ on the Day of 31 May 2021, Johannesburg.
(Signature of candidate)

Abstract

This study focuses on the formation and transformation of the Oldowan artefact-bearing deposits in the eastern portion of Member 5 (M5) at Sterkfontein Caves. Karst systems can be naturally complex in their formation and deposition, and since 1936 much research has taken place at Sterkfontein to clarify the stratigraphy of the site's sedimentary genesis. In order to explain aspects of the site formation I first mapped the current M5 deposits and features exposed at surface and through excavations using a Geographic Information Systems (GIS) programme. This is now the most up-to-date plan for this part of the Sterkfontein site. The Oldowan assemblage in Member 5 East (M5E) has been published as the most intact examples of this early industry in southern Africa, which also has a large small flaking debris (SFD) component, as well as other lithic types, which served as the basis for this study.

I developed the first whole tool abrasion index for very small lithics by using a Micro Computerized Tomography (Micro-CT) scanner. I was able to produce Three-Dimensional (3D) geometries of over 400 SFD pieces, as well as 300 other lithics in different categories. I used statistical analysis to quantify the abrasion on an entire tool's surface mesh, thereby creating a new technique for edge angle analysis. My approach does not depend on a tool's orientation, unlike other existing and often problematic edge angle techniques. I compared SFD from the M5E Oldowan assemblage with SFD that originated in M5E but that had been shown to have winnowed down into a separate and lower chamber of the cave system called the Name Chamber. Using my method, I was able to quantify the different degrees of abrasion that had occurred within the M5E Oldowan and the underlying Name Chamber assemblage to assess the effects of reworking within the cave system. This study shows that the Sterkfontein Oldowan assemblage has not been significantly altered, despite its secondary context within an underground karst cave infill. Both my abrasion index and spatial plan should equip future researchers with tools for better understanding the intricate site formation at Sterkfontein Caves.

This thesis is dedicated to my mother, Diana Rosemary Wall, and my late father, Professor Timothy John Couzens

Acknowledgements

I would like to first and foremost extend my deepest gratitude to my main supervisors Kathleen Kuman and Dominic Stratford for guiding me in this research and helping me see it through to completion. I want to extend a huge thank you to my external co-supervisor Dr. Kristian Carlson, with whom I spent many hours discussing the philosophy of 3D surfaces and statistical analysis. Thank you to Dr. Kudakwashe Jakata for helping facilitate my scans and to the Evolutionary Studies Institute where this work was conducted. Thank you to the Sterkfontein staff, and especially Soloman Sheshoene, who helped in the preparation of the site and to Professor Ron Clarke who gave me advice right at the start of my PhD. Thank you to Laurent Bruxelles for teaching me about Sterkfontein geology and José Braga for including me in additional work at Kromdraai.

Additional thanks go out to: Jo Buitendach, Justin du Piesanie, George Kalapov, Kelly Gill, Nicholas Zachariou, Matt Lotter, Matt Caruana, Dan Apter, Craig Kirby, Erica Penfold, Ira Friedman, Andrew Paskaramoorthy, Sarah Byrne, Phil Setzer, Nathan Mckay, Leeshia Roopnarain Mitch Spargo, Charles Murcott, Henri Kotze, Seema Chita, Courtney Wendt and Mike Macdonald.

Thank you to my brother Hal Couzens and sister Kate Couzens who motivated me to persevere even in the absence of our beloved father's guidance.

I would like to thank the National Research Foundation (NRF) and the Palaeontological Scientific Trust (PAST) for the funding that made a majority of this research possible.

Table of Contents

List of Figures

List of Tables

Chapter 1

1. Introduction

Since the discovery of the first adult *Australopithecus* in 1936 (Broom 1936) in an older member of the site, Sterkfontein has played an integral role in the paleoanthropological sciences and in the earliest archaeology of southern Africa. The site has yielded a diverse range of fauna and a large number of hominid specimens of different species, including the largest number of *Australopithecus africanus* in the world in the oldest deposits. There are six main depositional units at Sterkfontein, which were identified and labelled as Members 1 to 6 by Partridge (1978). Member 2 (M2) has yielded the world's most complete *Australopithecus* skeleton (StW 573), which has been attributed to *Australopithecus prometheus* (Clarke 1998, 2013; Clarke 2019; Clarke & Kuman 2019). Member 4 (M4) has yielded over 700 hominid specimens representing two species: *A. africanus* and *A. prometheus* (Clarke 2013; and see also Clarke & Kuman 2019). Member 5 (M5) has yielded a few *Paranthropus* teeth and a fragment of hominid ulna from its lower levels, which have also yielded the largest and most intact Oldowan assemblage in southern Africa, ca 2.18 Ma (Kuman & Clarke 2000; Kuman & Field 2009; Granger *et al.* 2015). *Homo ergaster* (StW 80) and some fragmentary remains of early *Homo* have been found in the Early Acheulean tool-bearing deposits of M5 which has an age of ca 1.7- 1.4 Ma (Kuman & Clarke 2000).

Karst systems can be inherently complex in their formation and depositional histories (White 2007; Stratford 2011) and since 1936 much research has taken place at Sterkfontein to clarify the stratigraphy of the site's sedimentary record (e.g., Cooke 1938; Robinson 1957; Brain 1958; Tobias & Hughes 1969; Partridge 1978; Wilkinson 1983; Partridge & Watt 1991; Clarke 1994, 2006; Kuman & Clarke 2000; Ogola 2009; Pickering & Kramers 2010; Stratford *et al.* 2012, 2014; Bruxelles *et al.* 2014, 2019). However, much more work is needed to improve the stratigraphic resolution of the artefact-bearing infills at Sterkfontein in order to refine our understanding of the deposits, their contents and their contextual and chronological relationships with one another (see Stratford *et al.* 2016).

This research project focuses on the formation and transformation of the Oldowan artefact-bearing deposits in the eastern portion of Member 5 (M5) at Sterkfontein Caves (Figure 1.1).

The Sterkfontein M5 East (M5E) Oldowan Infill yielded a very large assemblage with 3500 artefacts, of which 84.17% is small flaking debris (SFD) less than 20 mm in size (specifically 65% < 10 mm, and 20% < 20 mm), with 93.6% of the entire assemblage in vein quartz (Kuman & Field 2009). This large amount of SFD attests to knapping activities occurring near the cave shaft entrance and its rapid burial in the M5 infill through a narrow opening (Clarke & Kuman 2000). In most cases SFD, which are small and lightweight compared to other tool components such as chunks or complete flakes, is swept away by water action during excessive rains or flooding. Compared to experimental assemblages discussed by Kuman and Field (2009), SFD between 10-19 mm is over-represented at the site, while the SFD < 10 mm is under-represented, and this pattern needed investigation. The large proportion of SFD, along with additional isotopic research on the fauna by Luyt & Lee-Thorp (2003), suggests that the catchment area for the Oldowan in M5E would have been stable, with shade trees attracting hominids to the area of the cave entrance, resulting in a long-term accumulation of lithics in a concentrated catchment area (Kuman 2003; Langejans 2012). The roots of these trees also may have influenced the stability of the land surface in the catchment area (Langejans 2012).

Regardless of this stable environment, Stratford's 2012 excavation of the Name Chamber, located directly below the Oldowan deposits in M5E and connected by a narrow feeding shaft (Clarke 1994), demonstrated that movement of deposits had occurred within the site. Avery *et al*. (2010), Stratford *et al.* (2012), and Stratford & Val (2015) have shown that, prior to the calcification of the M5 deposits, some material was transported into the lower gallery from the M5E Oldowan and filtered into the Name Chamber. The use of Micro-CT scanning will be beneficial to studying the abrasion that has taken place on artefacts from that have shifted within a redeposited context.

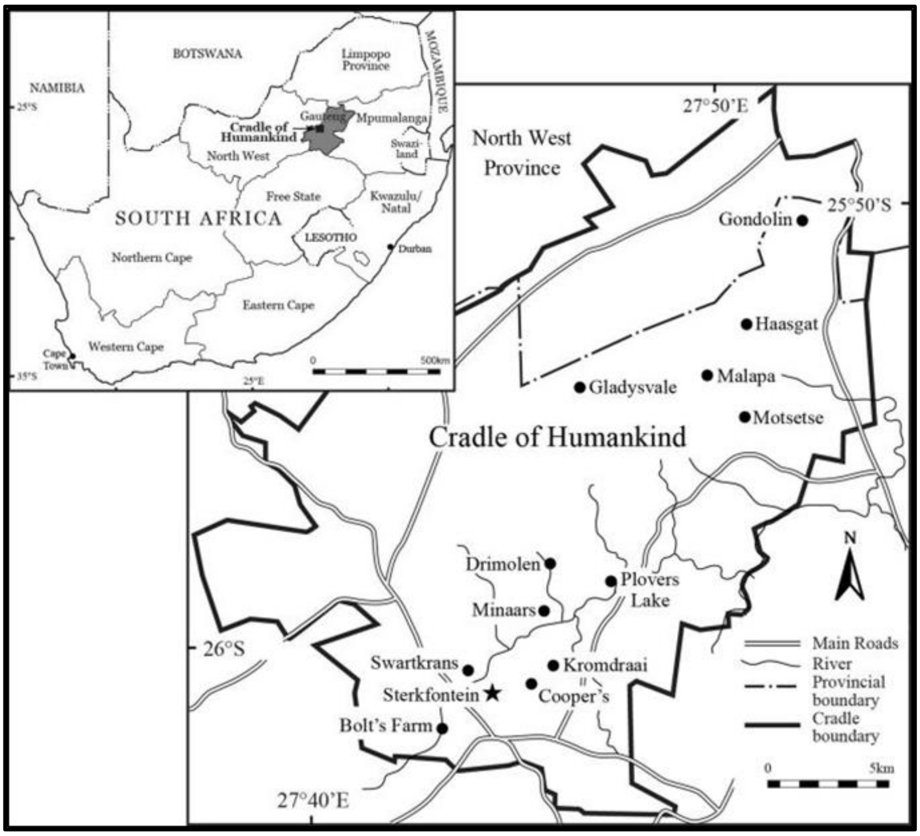

Figure 1.1. The location of the Sterkfontein Caves in relation to the Cradle of Humankind, South Africa (from Stratford *et al.* 2016: 2).

1.1 Aims of the thesis

The first aim of this thesis is to create a comprehensive high resolution understanding of the formation of the M5E Oldowan assemblage through Micro-CT analysis of artefact abrasion. The Name Chamber artefacts will be compared to the M5E Oldowan lithics because they are known to have experienced movement within the site through a feeding shaft leading to an underground cavern. Ultimately this research builds on existing knowledge of the site and its complex formation processes, through movement primarily within site infills and reworking of sediments, as previously described by Kuman & Clarke (2000), Ogola (2009) and Stratford *et al.* (2012). Furthermore, this thesis seeks to produce a condition index that will quantify the degree of abrasion undergone by the Oldowan artefacts, which will aid in analysing details of the site formation and transformation processes that have affected the material in the infill.

The second aim is to better understand and map the complex infills and deposits within M4 and M5 in a much higher spatial resolution than previous schematic plans and photographs provided. This is done using a Nikon Total Station to survey the outlines of important features, such as the remaining contacts between M4/M5, different types of rock, the excavation outline, solution pockets and flowstone within the extension site area. 3D georeferenced point clouds were used to create the highly accurate plan view to accurately depict the site.

Although M4 and M5 have been extensively discussed independently in terms of their respective fauna, hominids and sediments (Clarke 1994, 2006; Kuman 1994; Kuman & Clarke 2000; Stiles & Partridge 1979; Curnoe & Tobias 2006; Ogola 2009; O'Regan 2007), close examination of the boundary between the two members has been limited and challenging because the areas of contact had not been recognised during excavations prior to the 1990s. In the region of the supposed meeting of the two deposits, certain areas have been defined as M4 or M5 based on the presence and absence of certain fauna, stone tools or hominid representation. Given the significance of these earliest archaeological deposits in southern Africa, a dedicated site formation examination is crucial in establishing the relative integrity of the Oldowan assemblage. The high resolution study of artefact conditions in this study is a novel approach which will add to our understanding of the formation and transformation of the assemblages for the Oldowan and Early Acheulean periods.

1.2 Thesis outline

Chapter 1 provides a brief background, focused on the research questions and aims addressed in the thesis. Chapter 2 discusses the previous literature related to how the stratigraphic infills formed and were excavated, and how its members, flora, fauna and hominid fossils have been described and published. Chapter 2 also examines various published studies on methods used to measure the abrasion or edge angles of lithics. Chapter 3 describes the methodology of this research to create an accurate GIS map of the M5 area of the site (previously called the Extension Site) and explains how I created a new method for analysing and understanding the abrasion of the lithics of the Oldowan assemblage. Chapter 4 reports the descriptive and statistical results of the applied methodology, while Chapter 5 provides a discussion of the results and their implications. Finally Chapter 6 draws together the conclusions from this research and its importance for any further studies at Sterkfontein Caves.

Chapter 2

2. Literature Review

This section offers a comprehensive overview of excavations at Sterkfontein Cave and covers the complexity of site formation studies in karst sites. It further delves into the existing historical literature on lithic abrasion analysis and discusses some of the benefits that high resolution modern techniques can provide.

2.1 Sterkfontein Caves, location and formation of members

Sterkfontein is a karst underground cave network located in Gauteng's Blaaubank River Valley and forms part of South Africa's Cradle of Humankind UNESCO World Heritage Site (Fig. 1.1). Sterkfontein is an important site for African palaeoanthropology. Since the discovery of the first hominid fossil in 1936 (Broom 1936), the site has yielded hundreds of hominid specimens, many thousands of associated faunal remains, palaeoenvironmental indicators (based on faunal taxa, isotopic studies and fossil wood), and the largest intact Oldowan and Early Acheulean stone tool assemblages in southern Africa (Kuman & Field 2009; Kuman & Clarke 2000). Additionally, stratigraphic research has been an important focus, as these cave system infills can be complex and their chrono-stratigraphic sequences difficult to interpret (Cooke 1938; Robinson 1957, 1962; Brain 1958; Tobias & Hughes 1969; Wilkinson 1973, 1983; Partridge 1978; Clarke 1994, 2006, 2012; Partridge & Watt 1991; Kuman & Clarke 2000; Kibii & Clarke 2003; O' Regan 2007; Ogola 2009; White 2007; Kuman & Field 2009; Stratford *et al.* 2011, 2012, 2016; Bruxelles *et al.* 2019).

Two years after Broom's discovery of the first adult *Australopithecus* (Broom 1936), Cooke (1938) published a basic description, plan and section of the limestone quarry, which is now known as the Type Site (Figure 2.1), in which the famous cranium and many other fossils were exposed by lime miners. Until 1947, all fossils were derived from this locality, including Mrs Ples in 1947, for many years the most complete cranium of *Australopithecus africanus*.

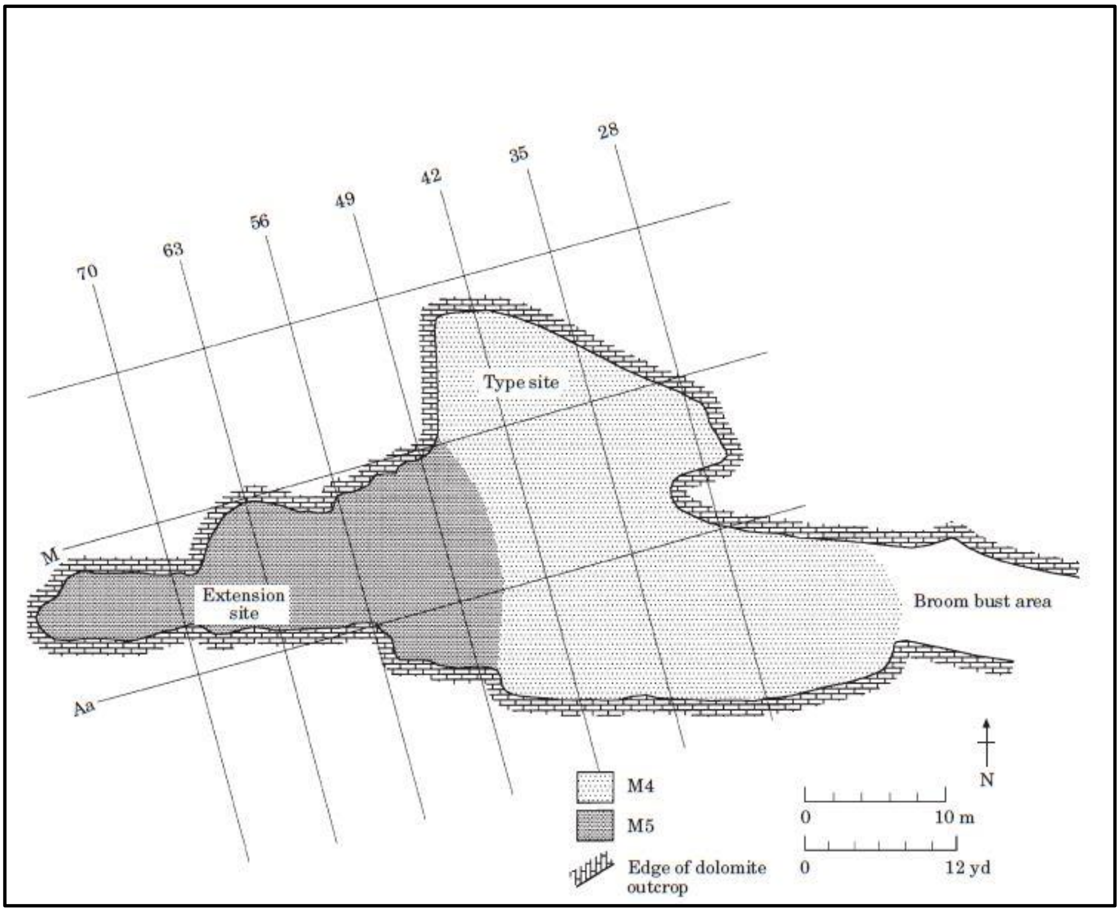

Figure 2.1. The historically presumed distribution of M4 and the Extension Site M5, with the excavation grid superimposed (from Kuman & Clarke, 2000: 830).

Although the Silberberg Grotto deposits (only named in 1979 by Professor Phillip Tobias) were known to Broom and were much deeper in the system, he suggested its fauna was similar in age to that of the Type Site (Clarke 2006). Subsequently, a near-complete *Australopithecus* skeleton was discovered in the Silberberg Grotto (Clarke & Tobias 1995, Clarke 1998, 2019) and was dated to ca 3.67 Ma (Granger *et al.* 2015).

In 1956, researchers turned their attention to the western end of the Sterkfontein breccias prompted by the discovery of 'archaic' tools by C.K. Brain. The first excavations by R.J. Mason and J.T. Robinson in 1957-1958, in what was then named the 'Extension Site' (see Figure 2.1), yielded artefacts and associated fossils (Mason 1962; Kuman 1994a) and demonstrated a separate infill from the eastern Type Site. The deposits were subsequently divided into the oldest breccia (in the Type Site), the younger Extension Site breccia to the west (also referred to as 'red-brown breccia') containing tools and *Equus* fossils, and the youngest breccia overlying the red-brown breccia containing *Equus* but no stone tools

(Robinson 1957). Robinson (1962) then re-defined these infills as: Lower Breccia, Middle Breccia (red-brown, containing artefacts) and Upper Breccia (brown breccia). He assumed nothing below the ‘Lower Breccia’ was older, as it was presumed to be a single infill. It was Tim Partridge (1978) who provided the first dedicated analysis of the full depth of the breccias at surface and in the underground Silberberg Grotto, naming the entire sequence the ‘Sterkfontein Formation’. He divided the breccias into six stratigraphic members with M1 being the oldest and deepest deposit preserved in the underground cave (Partridge 1978; Clarke 2006). Partridge’s terminology of the six members thus replaced Robinson’s (1962) definitions of Lower (now M4), Middle (now M5) and Upper (now M6) Breccias. Figure 2.1 shows how the distributions of the two main infills were referred to by researchers following Partridge (1978). Figures 2.2 and 2.3 provide additional representations of the stratigraphic members based on Partridge’s work.

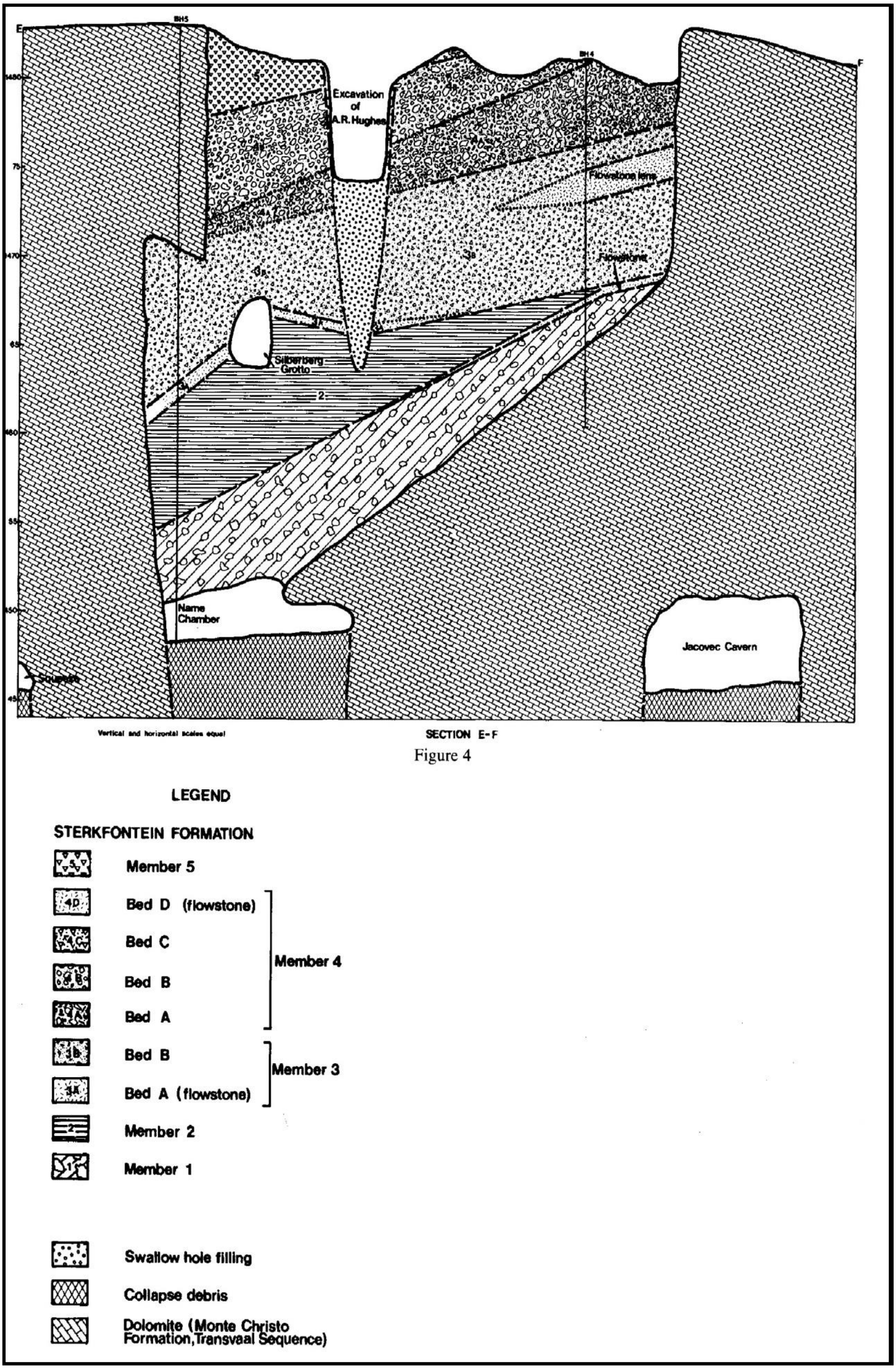

Figure 2.2. Partridge & Watt's stratigraphic sequence (from Partridge & Watt 1991: 39).

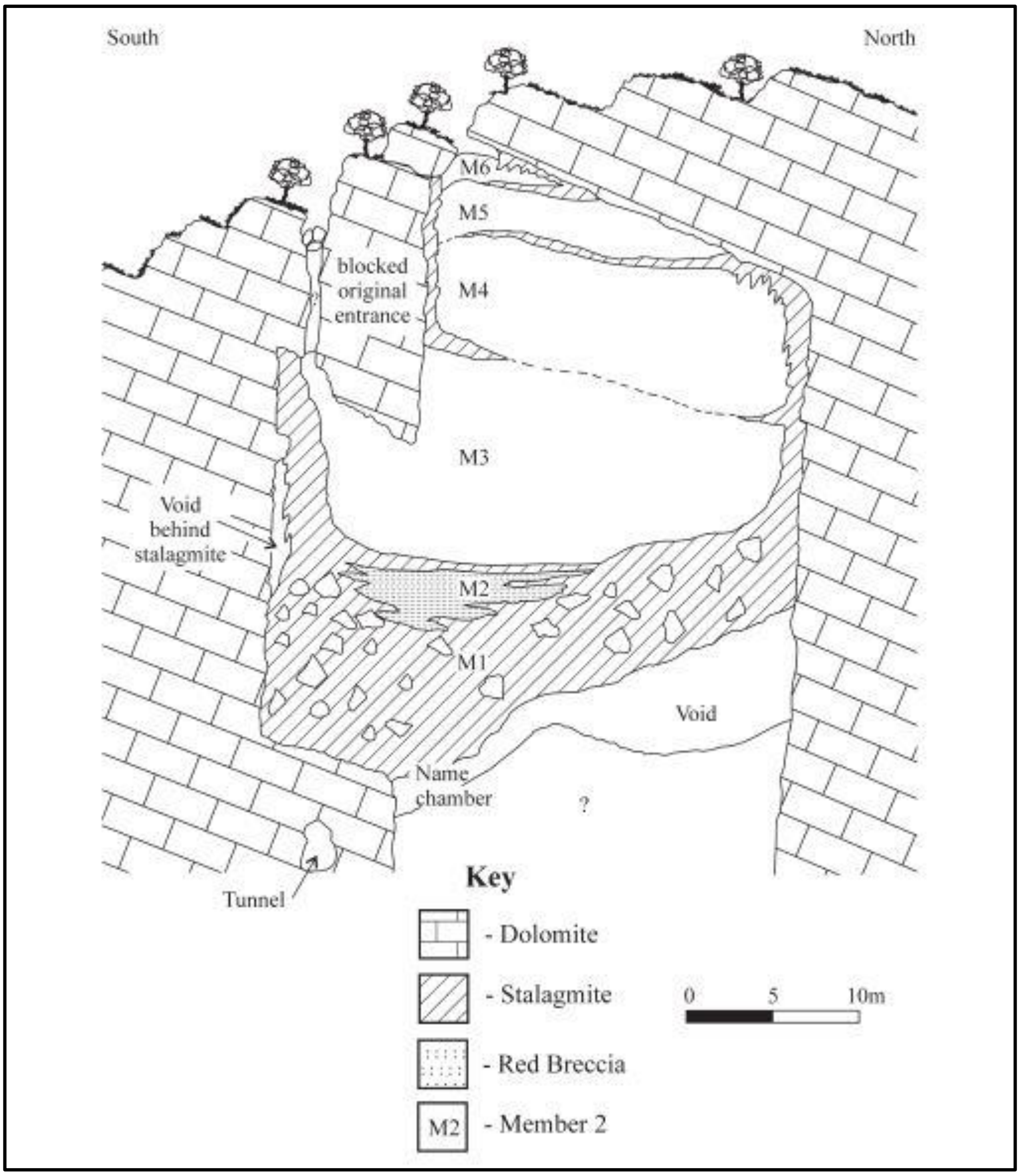

Figure 2.3. Clarke's stratigraphy (from Clarke 2006: 119).

Wilkinson (1983) later proposed that M1 was not the deepest deposit in the sequence and identified deeper deposits in the Jacovec Cavern, which he believed were older than M1 (Figure 2.2). Wilkinson (1983) tentatively proposed that the deposits continued down to 50 metres, contradicting Partridge's proposed maximum of 30 metres. In May/June of 1989, Partridge and Watt set out to test this hypothesis by drilling five cores at Sterkfontein that could provide suitable stratigraphic information as well as samples for paleomagnetic dating (Partridge & Watt 1991). Their study showed that the six members in the Sterkfontein Formation ranged in thickness from 12.0m - 29.75m with an average of about 20m, and that a dolomite floor existed at the base of the Sterkfontein Formation. However, this paper did not address the Jacovec Cavern. Pickering & Kramers (2010) later commented that Partridge and

Watt's cores did not in fact sample the lowermost deposits but rather hit uneven dolomite walls of the cave, and thus the maximum depth of the caves was said to be inconclusive. A further interesting point captured by their study concerns the complex nature of the M4/M5 contact. Partridge & Watt (1991) argued that an almost vertical contact existed between the two members in a fairly wide area with an angle of not more than 20º. The drilled cores tentatively showed that, although that part of the site experienced some vertical movement of about 5m after deposition, this proposed downward movement was quite localised, and the stratigraphic structure appeared to be largely intact, minus some inevitable mixing of sediments during the downward shifting. They were careful to suggest that this was the action of a 'swallow hole' because a large amount of breccia has been displaced, but it was not a solution pocket or what they call a "makondo". Solution pockets are more common in the upper calcified cave infills. They are defined by limited movement of insoluble sediment within a capsulated section or pocket where trees and vegetation causes dissolution of calcium cement (Partridge & Watt 1991).

The core study proposed that the localised vertical M4/M5 contact probably formed through this movement of the uncalcified or decalcified sediment as opposed to an erosion of the talus cone of M4 prior to the deposition of M5. It should be noted that this has not yet been confirmed, but is the subject of dedicated studies.

With regard to the six members of the Sterkfontein Formation, it is agreed that M1 comprises autogenic sediments, formed before the opening of the caves to the surface, and it contains no fossils (Martini *et al.* 2003). M2 was deposited against the large stalagmite 'boss' that covered the eroded remnants of M1 (Martini *et al*. 2003). A further influx of perhaps eight metres of bone-bearing sediments built up to create M3 on top of a flowstone that sealed M2, but it has not yet been excavated due to limited accessibility (Clarke 2006). Between 1978 and 1980, Tobias instructed Hughes to supervise the removal of lime miners' rubble from the floor of the Silberberg Grotto, yielding significant fossils mainly attributed to M2. In 1992, Clarke then blasted out M2 breccia at the eastern end of this cavern, which resulted in the retrieval of fauna accumulated as a death-trap assemblage including mainly monkeys and carnivores. From the western end of the cavern (which was not blasted) Clarke discovered four hominid foot bones that had gone unrecognised in the fauna processed between 1978 and 1980 (Clarke & Tobias 1995). In 1997, Clarke identified further foot and leg bones of the same individual and commenced excavating a near-complete skeleton *in situ*, which is the most complete *Australopithecus* ever found, StW 573 (Clarke 1998, 1999, 2002, 2006, 2007, 2008, 2019). Members 1, 2 and 3 are exposed in the Silberberg Grotto (Partridge 1978), the type section for the lower units of the Sterkfontein Formation. A taphonomic analysis of these bones by Pickering *et al*. (2004) suggested a death-trap scenario as the main accumulation agent of the fauna. However, artefacts are not preserved until the Oldowan deposit in M5E.

Member 4 (M4)

M4 formed above M3 (Figure 2.3) and is described by Clarke (1994, 2006) as a partly decalcified breccia series formed over a few hundred thousand years, forming a talus cone proposed to slope toward the north and west. It may have formed below a vertical shaft (Partridge 1978). Many researchers have tried to date this Member, using bovid/primate biochronology (Vrba 1976, 1982; Delson 1984, 1988), faunal seriation (McKee 1993), Electron Spin Resonance (ESR) (Schwartz *et al*. 1994), palaeomagnetism (Partridge 2005), Uranium-Lead (Pickering & Kramers 2010) and Uranium-Thorium isotopes (Herries & Shaw 2011). The general estimate is that it lies roughly between 3.3 and 2.14 Ma (Clarke 2013).

Following the early years that involved blasting, Hughes spent 10 years from 1966 clearing and processing the lime miners' dumps that covered both the Member 4 and 5 breccias that had become exposed at the surface breccias (Hughes & Tobias 1977). Their first *in situ* hominid discovery was the StW 53 cranium in 1976 at the southern end of M5 (Hughes & Tobias 1977). It was assigned to *Homo habilis*, largely on the incorrect designation of this part of the site as M5 (Tobias 1978), which has more recently been described as a remnant of M4 (Clarke 1994; Kuman & Clarke 2000). Although debated, this fossil has been re-assigned to *Australopithecus* by Clarke (see Clarke & Kuman 2019 for detail).

The enormous infill of breccia now known as M4 has yielded hundreds of *Australopithecus* fossils but no *in situ* stone tools, which only occur in M5. Although the site was methodically excavated for Tobias by Hughes for many years, no stratigraphic records were kept of this work, and thus the approximate boundary with M5 has been identified by differences in faunal taxa, the distribution of fossil wood in M4, and the occurrence of artefacts in M5 (Kuman & Clarke 2000). In addition to the large number of *Australopithecus* fossils in M4, there are abundant faunal and floral specimens with which researchers have been able to accurately analyse the paleo-environment (Bamford 1999; Clarke 2013). The presence of fossilized wood, mainly of a species of liana associated with tall trees, indicates a subtropical gallery forest in M4 times and a moister environment than at present (Bamford 1999). The fauna distinguishes M4 as forming within a medium-density woodland (Kuman & Clarke 2000; Luyt & Lee-Thorp 2003; Clarke 2006). The *Australopithecus* StW 431 pelvic reconstruction suggests that morphologically these hominids could have been ''part-time climbers and part-time terrestrial bipeds'' (Kibii & Clarke 2003: 226 after Susman *et al.* 1984).

Clarke (2013, 2019) suggests, mainly based on cranial morphologies, that two species of *Australopithecus* exist within M4, *A. africanus* and *A. prometheus*, and that the complete StW 573 skeleton in M2 falls into this second group (Clarke & Kuman, 2019). *Australopithecus* fossils have also been found within the Jacovec Cavern which is broadly similar in age to M2, even though it is separate from the members in the Sterkfontein Formation (Partridge *et al.* 2003; Clarke 2006, 2013).

Dating of fossils and lithics was previously estimated based on comparisons with well-procured and radiometrically dated East African assemblages from sites like Olduvai Gorge, which was followed by attempts to use more absolute methods that have been highly debated (e.g., Walker *et al.* 2006; Pickering *et al.* 2011; Herries *et al.* 2011; Bruxelles *et al.* 2019). Most recently M2 was dated to ca. 3.67 Ma using cosmogenic burial dating (Granger *et al.* 2015). Currently M4 is estimated on fauna to be ca 2.4 - 2.8 Ma based on the bovids (Vrba 1982) or ca. 3.3 Ma (Clarke 2013), but cosmogenic dating is being applied. The Oldowan breccia in M5E is now cosmogenically dated to ca. 2.18 Ma (Granger *et al.* 2015), but the younger Acheulean breccia in M5 is still estimated to be ca 1.7-1.4 Ma based on the fauna and the early archaeology (Kuman & Clarke 2000). Given the many fossils from Sterkfontein and its early archaeology, higher resolution mapping of the M5 breccia and its interface with M4 is important to address.

As noted above, faunal evidence from M4 and M5 supports the idea that during the accumulation of M4 the environment would have been medium density woodland, with much carnivore activity around the openings (Reed 1997). Isotopic analysis of fauna by Luyt & Lee-Thorp (2003) suggests that the M5E Oldowan deposit fauna represent only slightly more open conditions than M4, whereas the M5 West Acheulean breccia is substantially more open. They thus contrast the Oldowan and Acheulean environments as showing a drying trend from about 1.7 Ma, the upper estimated age of the Acheulean accumulation. This isotopic environmental analysis is more recent than the analysis presented in Kuman & Clarke (2000), which was based on certain informative taxa such as the presence or absence of horse, springhare and ostrich representing more open environments in M5. Kuman (2003) noted that the artefact distribution may have been accumulated within a 15ft (~5m) wide space, leading to the assumption that the Oldowan opening was quite narrow. Pickering (1999) also indicated that the fauna is death-trap accumulated, with some minor contribution from slope wash, which supports the idea that the opening at this time was narrow.

In comparison, M4 is suggested by Kibii (2004) to have had accumulated under more varied scenarios, following the opening of the original entrance in M2, which had also been narrow, fostering a death-trap accumulation. While the M4 cave opening, which was mainly in the southern part of the site, had enlarged following M2, the opening that had admitted the M5E Oldowan sediments was not continuous with M4 but may have been created as a result of subsidence that occurred around 2.2 Ma (K. Kuman, pers. comm.). By the time the M5 Acheulean deposits accumulated, the cave entrance had become larger once again (Kuman 2003), and the environment surrounding Sterkfontein was a drier and more open grassland (Kuman & Clarke 2000; Luyt 2001; Luyt & Lee-Thorp 2003; Clarke 2013).

Member 5 (M5)

M5 comprises two archaeological subdivisions: the Oldowan and the early Acheulean. Figure 2.6 shows a plan of Sterkfontein with the last schematic outline of M5 as presented by Kuman & Clarke (2000).

The Oldowan deposits

The deeper of the artefact-bearing infills is an Oldowan tool-bearing breccia in M5E that is dated to ca. 2.18 Ma (Granger *et al*. 2015). It is found below a depth of 22 feet (~6.7 m), with *Paranthropus robustus* teeth found in the same deposit (Kuman 1994; Kuman & Clarke 2000). The assemblage contained therein is the most complete and best preserved Oldowan artefact assemblage in southern Africa (Kuman & Clarke 2000; Kuman & Field 2009; Stratford *et al.* 2012). In total, 3500 pieces have been recovered, of which 84.17% consist of artefacts under 20 mm in size. Table 2.1 shows the complete Oldowan assemblage compared to the Name Chamber assemblage.

Table 2.1. A table displaying artefact types and raw materials for the Member 5E Oldowan (STK M5E) and the Name Chamber (NC) (after Kuman & Field 2009: 154; Stratford 2008: 109).

Location	Artefact Types	Quartz	Chert	Quartzite	Other	Total	%
STK M5E	Small flaking debris < 10 mm	321	24	0	-	345	**9.8%**
NC		537	29	2	-	568	**54.1%**
STK M5E	Small flaking debris 10-19 mm	2343	175	9	-	2527	**71.9%**
NC		363	23	3	-	389	**37.0%**
STK M5E	Small flaking debris < 20 mm	2744	204	9	-	2957	**84.17%**
NC		900	52	5	-	957	**91.2%**
STK M5E	Incomplete flakes and Flake fragments ≥ 20 mm	231	22	38	-	291	**8.28%**
NC		24	26	5	-	55	**5.1%**
STK M5E	Complete flakes ≥ 20 mm	57	7	20	-	84	**2.39%**
NC		9	9	3	-	21	**2.1%**
STK M5E	Cores	17	0	7	-	24	**0.68%**
NC		-	1	1	-	2	**0.2%**
STK M5E	Core fragments	1	1	3	-	5	**0.14%**
NC		-	-	1	-	1	**0.1%**
STK M5E	Core tools	0	0	1	-	1	**0.03%**
NC		-	-	-	-	-	**0%**
STK M5E	Manuports	2	1	7		10	**0.28%**
NC		-	-	1	1	2	**0.2%**
STK M5E	Manuports?	1	0	2	-	3	**0.09%**
NC		-	-	-	-	-	**0%**
STK M5E	Chunks	120	0	11		131	**3.73%**
NC		1	2	-	-	3	**0.3%**
STK M5E	Indeterminate	-	-	-	-	-	**-**
NC		7	1	-	-	8	**0.8%**
STK M5E	Total	3180	236	97	-	**3513**	**100%**
NC		**941**	**91**	**16**	**1**	**1049**	**100**
STK M5E	%	90.52%	6.72%	2.76%	-	**100**	
NC		**89.6**	**8.8**	**1.5**	**0.1**	**100**	

The dominant material is quartz, which is resistant to weathering, and in this context it would require movement (abrasion) to appear weathered (Kuman & Field 2009). It is clear that the Oldowan artefacts entered through a narrow opening, as Pickering's (1999) study of the Oldowan fauna suggests a death-trap scenario. Animals would have fallen into the narrow shaft and slope wash from the surface would have aided in accumulation of some additional fauna. However, a major question remains as to why the SFD in the 10-19 mm size category is over-represented in the Oldowan assemblage, while the SFD <10 mm is under-represented, when compared with assemblages created experimentally using the same raw materials (Kuman & Field 2009). Has small material from a wider catchment been incorporated in the deposit through slope wash? This discrepancy remains the case even though some of the Oldowan sample has been shown by Stratford *et al.* (2012) to have winnowed into the underlying Name Chamber, situated 12 metres below M5E (Kuman & Field 2009). Additionally, Shackley (1974) states that although tools can appear fresh to the naked eye, a study of ridge widths can be beneficial in determining exactly how abraded a piece has become due to any number of erosional processes. With this technique, the rate of weathering through abrasion can be determined relative to the intrinsic nature of that material.

Essentially, the Sterkfontein material is a long-term accumulation within a re-deposited context (Kuman & Field 2009). A portion of the smaller pieces <20 mm were winnowed into the deposits in the Name Chamber and therefore must have been present in the original assemblage before reworking (Kuman & Field 2009; Stratford *et al.* 2012). Components of this size require good preservation conditions, and the fact that they are present suggests that a stable land surface existed around the cave entrance. Some evidence to support this suggestion is found in Partridge's (1993) sedimentology study, which noted that the Oldowan sediments showed a higher clay and silt content than other M4 or M5 deposits. Later, Luyt & Lee-Thorp's (2003) isotopic work on faunal teeth argued for a moderately wooded biome. Together these analyses would suggest a stable land surface that was less prone to erosional processes.

The Acheulean deposits

By ca 1.7-1.4 Ma, sediments with Acheulean artefacts entered through a shaft enlarged by erosion and created a more widespread infill, probably situated across both M5E & M5W (Kuman & Clarke 2000; Kuman & Field 2009). The Acheulean at Sterkfontein is estimated in M5W to ca 1.7 - 1.4 Ma, and the presence of two bifaces and a cleaver, along with sediment changes, differentiate it from the Oldowan (Kuman & Clarke 2000). The M5E breccia above 22 feet, however, shows some mixing with surface rubble containing Middle Stone Age (MSA) artefacts through pockets of decalcification, thus limiting its usefulness for study. This contrasts with the M5W deposits that are calcified and better preserved. A larger proportion of manuports and a greater shift in raw material use from quartz to quartzite occur in the M5W Acheulean assemblage (Kuman & Clarke 2000). The Acheulean assemblage also contrasts heavily with the Oldowan because of its large number of cores and manuports and a greater emphasis on heavy-duty tools. Of additional interest, artefacts under 20 mm are not well preserved in the Acheulean levels, suggesting that they were subject to long-term surface exposure and erosion. Luyt & Lee-Thorp's (2003) isotopic study on faunal teeth in M5W showed that open grassland would have existed and we would expect less vegetative covering and more erosion and slope wash to have taken place (Kuman & Field 2009; Luyt & Lee-Thorp 2003). Some *H. ergaster* fossils are associated with the Acheulean at Sterkfontein.

Member 6 (M6)

M5 is terminated by a capping flowstone and Member 6 (M6), which dates to the Middle Pleistocene, is deposited directly on it. Not much is known about M6 and the only lithic, a manuport, was stolen by someone visiting the site before it could be excavated (Robinson 1957). Large portions of the flowstone and underlying breccia have eroded, leaving M6 as a hanging remnant (Kuman & Clarke 2000).

2.2 The Name Chamber

Robinson (1962) had noted a few stone tools at the top of the talus in the Name Chamber. Then during excavations in the 1990s, Clarke uncovered a connection between the Oldowan infill and the Name Chamber (Clarke 1994), which revealed that sediments and Oldowan artefacts had filtered into this lower cavern through a shaft about 12.5 m long (Clarke 1994). Subsequent work in the Name Chamber by Stratford described the flow of material through this narrow 'feeding shaft' (Figure 2.4; Stratford *et al.* 2012).

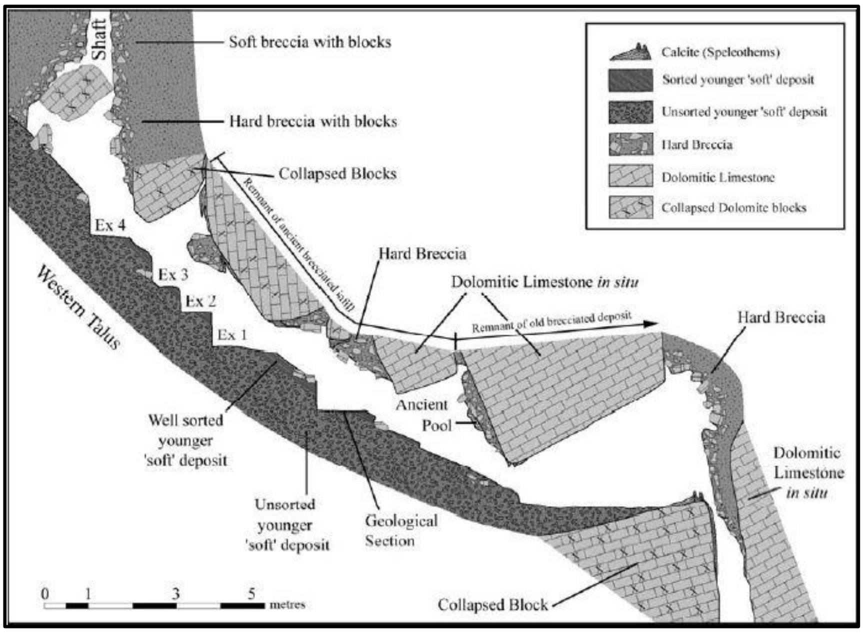

Figure 2.4. A cross-section of the feeding shaft linking the Name Chamber to the overlying Oldowan infill (from Stratford *et al.* 2012: 166). Abbreviation: Ex = excavation.

History of the Name Chamber deposits

Robinson (1962) was the first to propose a physical connection between the Name Chamber and deposits in the Extension Site. He ascended to the top of the steep underground talus and discovered three large artefacts from unconsolidated breccia (Robinson 1962). He hypothesized that this area was directly below the western boundary of the Extension Site. In his interpretation, the Name Chamber contained a collapse of what we now call M4 deposit, followed by subsequent infilling with M5 or 'middle breccia.' In time, the spaces left by a re-adjustment of material were filled by 'upper breccia' (now M6) (Robinson 1962; Clarke 1994). After taking over work on site from Hughes in 1991, Clarke (1994) focused on the M5 excavations. He encountered a hole at the bottom of the M5E Oldowan deposit and a hose pipe was inserted, which emerged at the top of a talus in the Name Chamber.

Continued excavations enlarged the size of the hole large enough for two speleologists, Gawie Moen and Andre Keyser, to climb down on a steel rope ladder, and they emerged on the top of the talus. Clarke (1994) illustrated the collapse of Oldowan sediments into the Name Chamber, which fits very well into current understanding of how the Name Chamber came to be formed (Fig. 2.4; Stratford *et al.* 2012). The roof of the Name Chamber is located 12m below Square R/57, where the hole initially opened in the Oldowan deposit during excavations (Clarke 1994). Following some initial excavations of the Name Chamber talus by Clarke, more extensive excavations and closer study of the strata were carried out by

Dominic Stratford and were published in Stratford *et al.* (2012). Due to the low ceiling and steep slope of the talus, work was primarily focused on the younger 'soft' Western Talus deposits, but the deposits were classed into three phases, described below (see Stratford *et al.* 2012). In the first phase an internal collapse occurred, which was possibly caused by the cave morphology changing from phreatic to vadose. A dark stony breccia (known as 'the Ancient Brecciated Deposit' or M1) filled the chamber and was then capped by a flowstone causing parts of the breccia to adhere strongly to the walls and ceiling (Martini *et al*. 2003). When the cave opened to the surface, water filtering into the shaft led to the erosion of some of M1 and the feeding shaft is thought to have begun developing.

Feeding shaft into the Name Chamber

Based on the description of both speleologists, the feeding shaft in the R/57 area of the M5E excavations was described as decalcified (Clarke 1994). The shaft consists of a sequence of collapse, large closely locked dolomite blocks that restrict the movement of larger deposits but allow the flow of smaller sediments and fossils to accrue in the lower reaches of the Chamber (Stratford *et al.* 2012). The opening of the feeding shaft brought with it the 'Old Brecciated Deposit, a coarser iron-rich sand deposited in multiple phases. This deposit did not fill the chamber, but remnants can be seen *in situ* as high as 16m from the opening of the feeding shaft. Eventually it was capped by flowstone and eroded away by the decalcification process (Stratford *et al*. 2012). The last infill was also deposited from above through the feeding shaft. It consists of a sediment rich in micro-fauna and artefacts, with lithics mainly <20 mm in size (*n* = 957), excavated and classified by Stratford (2008), which resemble the SFD component of the Oldowan East excavations (Kuman & Field 2009). See Table 2.1 for the Name Chamber lithic component.

The artefacts excavated from the Name Chamber suggested a redeposited secondary context for this small-sized material. This sediment is thought to have filled the remaining gaps in the chamber talus. This deposit is called 'the younger soft deposit' and was found in three distinct regions of the geometry known as the Far Western Talus (FWT), Western Talus (WT) and Eastern Talus (ET). Although these sediments are thought to be similar in depositional source, the differences in locality are attributed by Stratford *et al.* (2012) to changes within the feeding shaft matrix. The authors state that is possible that before the 'soft' sediment filled the cave, a collapse of M4 material into the lower reaches of the chamber may have formed the base of the talus upon which the softer breccia was subsequently deposited. At about 14 metres depth, a large fallen dolomite block (possibly from M1 collapse) separates the ET from the WT; however, below this, both deposits converge to form an inter-fingering stratigraphy (Stratford *et al.* 2012).

The far western talus (FWT) and western talus (WT)

The FWT and WT deposits (Figure 2.5) entered the feeding shaft together but split into different areas of the cave as they flowed around a dolomitic wall, first described by Robinson in 1962. This partition divides the Eastern Milner Hall from the Name Chamber. A substantial portion of the FWT has settled in the far eastern limit of the Milner Hall. The sediment of the FWT, what is known as the younger 'soft' deposit, is unmixed, and is a well stratified loam to silt loam (Stratford *et al.* 2012). This sediment shows no evidence of hydraulic assistance and material larger than 50 mm has been filtered by the feeding shaft and is absent in the FWT. The WT is contained within the Name Chamber and is identical to the FWT in terms of its sedimentary, faunal and archaeological composition, except that it differs from the FWT in that it is not as well stratified. This is thought to be because the extreme gradient of the talus combined with the formation of the deposits around abundant fallen dolomite blocks have limited the development of clear stratigraphy (Stratford *et al*. 2012).

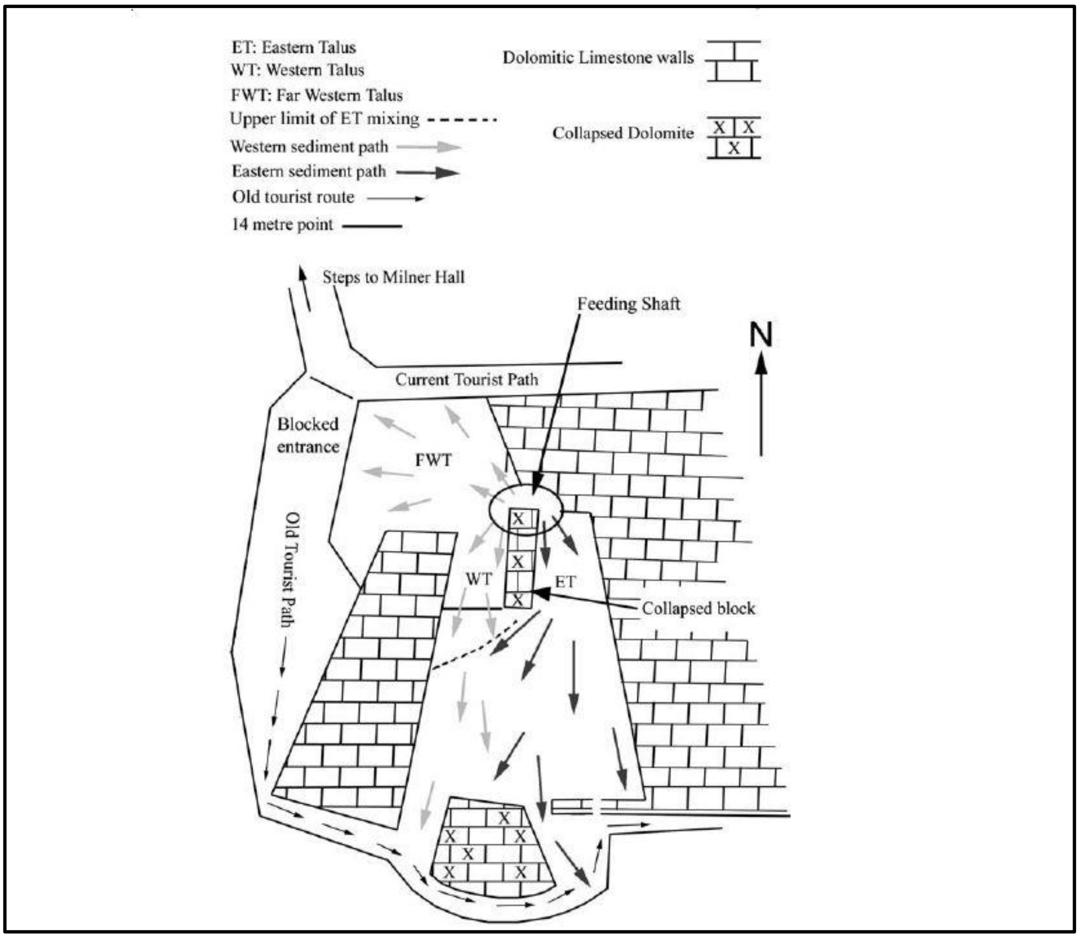

Figure 2.5. The deposition direction of the FWT, ET and WT (from Stratford *et al.* 2012: 164).

The eastern talus (ET)

The extreme gradient of the ET made it impossible to safely excavate the upper structure of this talus. However, some preliminary studies of the lower exposed deposit showed that, at the time of the deposition of the younger 'soft' material, the eastern side of the feeding shaft was more open and allowed larger dolomitic clasts to enter. Fossils larger than 50 mm are limited due to the possible breakage of a readily moving jumble of entering clasts and fossils (Avery *et al*. 2010; Stratford *et al.* 2012). ET material passed into the WT and is characterized by thick horizons of stonier sediments with a maximum clast size of 150 mm comparable to the WT's 50 mm clast size (Avery *et al*. 2010).

Name Chamber summary

A combination of Stratford *et al.'s* (2012) stratigraphic assessment and Avery *et al.'s*. (2010) micro-faunal studies has provided a comprehensive understanding of processes leading to the formation of the Name Chamber infills. At present, it is understood that reworking of sediments has occurred from the lower M5E Oldowan and Acheulean, as well as from M4 with lesser effect. Stratford *et al.* (2012) explain that M1 (or 'Ancient Brecciated Deposit') filled the Name Chamber with collapsed material as the cave opened up, and then much of this was eroded away when the feeding shaft opened and allowed fresh water to flow into the chamber. Then a second infill known as the 'Old Brecciated Deposit' came in through the feeding shaft and filled the chamber to just over half-full before the shaft was choked. Water rich in calcium carbonate calcified the deposit and M4 was deposited in the area above the feeding shaft. Fresh water then once again decalcified and eroded some of the Old Brecciated Deposit, as it had done to the 'Ancient Brecciated Deposit', allowing some material from the upper M4 to fall into the chamber and form the base of the talus atop which the Younger 'Soft' Deposit would later be transported. M5E sediment was then deposited above the feeding shaft into the gaps left by the collapsed M4 deposit. Before the upper deposits could be calcified, varying amounts of M5E Oldowan artefacts and associated fauna from the lower Oldowan deposits winnowed down through the feeding channel and came to rest in the Name Chamber (Avery *et al*. 2010; Stratford *et al.* 2012; Stratford & Val 2015).

2.3 StW 53 infill

The StW 53 infill represents an important area that lies to the south of the M5 artefact-bearing deposits. In 1976, it yielded a hominid cranium that Hughes & Tobias (1977) proposed appeared to belong to early *Homo* with affinity to *Homo habilis*, and which Tobias (1991) later assigned to *Homo habilis*. This interpretation was influenced by the fossil's assumed association with the stone tools found in the western part of M5 (see Figure 2.1), but also by its similarity to OH 24, assigned to *Homo habilis* from Olduvai Bed 1 (Tobias 1991). However, stratigraphic observations by Clarke (1994) revealed that this infill is separated from and different to M5 and that no *in situ* stone tools are present in the infill. Clarke also argued that the StW 53 cranium belongs morphologically to *Australopithecus africanus* (Kuman & Clarke 2000), and that OH 24 also belongs to *Australopithecus* (Clarke 2017). *Theropithecus oswaldi* (a grassland indicator) is found in the StW 53 infill, suggesting a drier climate to M4. This prompted Kuman & Clarke (2000) to propose that the StW 53 infill represents a deposit intermediate in chronology and dating between M4 and M5. However, new research by L. Bruxelles (pers. comm.) has now identified this breccia as a remnant of M4, and it may be a deposit that is late in the formation of M4 (D. Stratford pers. comm.).

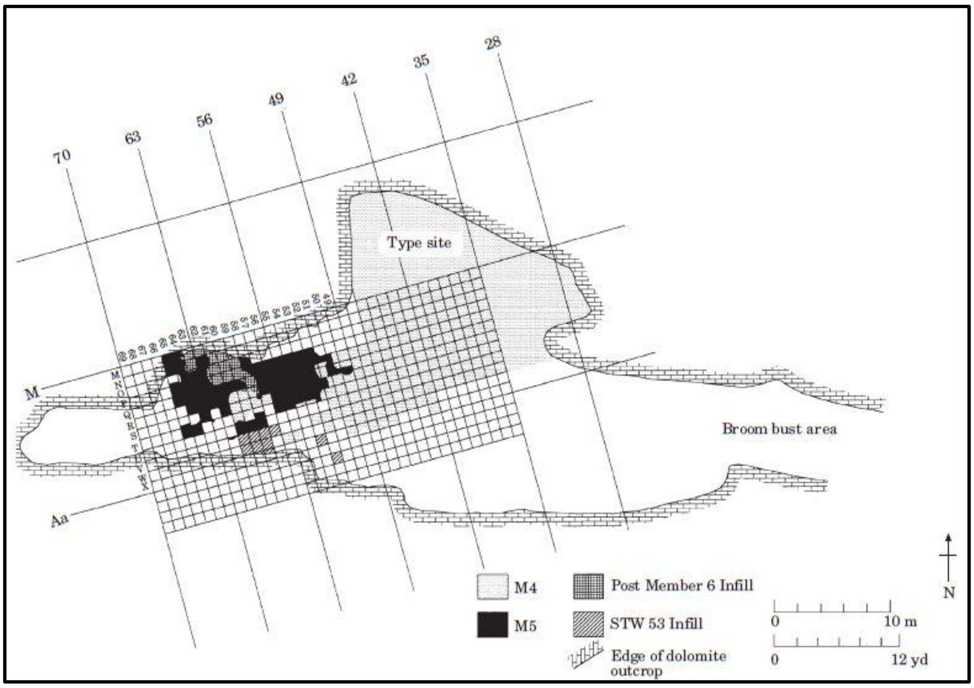

Figure 2.6. A revised plan of excavations that depicts M4, M5 and the StW 53 infill (from Kuman & Clarke 2000: 833).

2.4 Lincoln Cave and Post-Member 6 Infill

The Lincoln-Fault cave structure is 1665 metres in length and lies to the north of M5, about seven metres north of the Square L/63 in Fig. 2.6 (see Reynolds *et al.* 2007: Fig. 2.7). This cave system was previously considered unrelated to the Sterkfontein Caves because a substantial chert barrier described by Boshoff *et al.* (1990) separated the two. However, excavations in 1997 have proven this to be false (Reynolds *et al.* 2007). The Lincoln cave system was shown to be continuous and in a state of complex geological interaction with Sterkfontein (Reynolds *et al.* 2003, 2007).

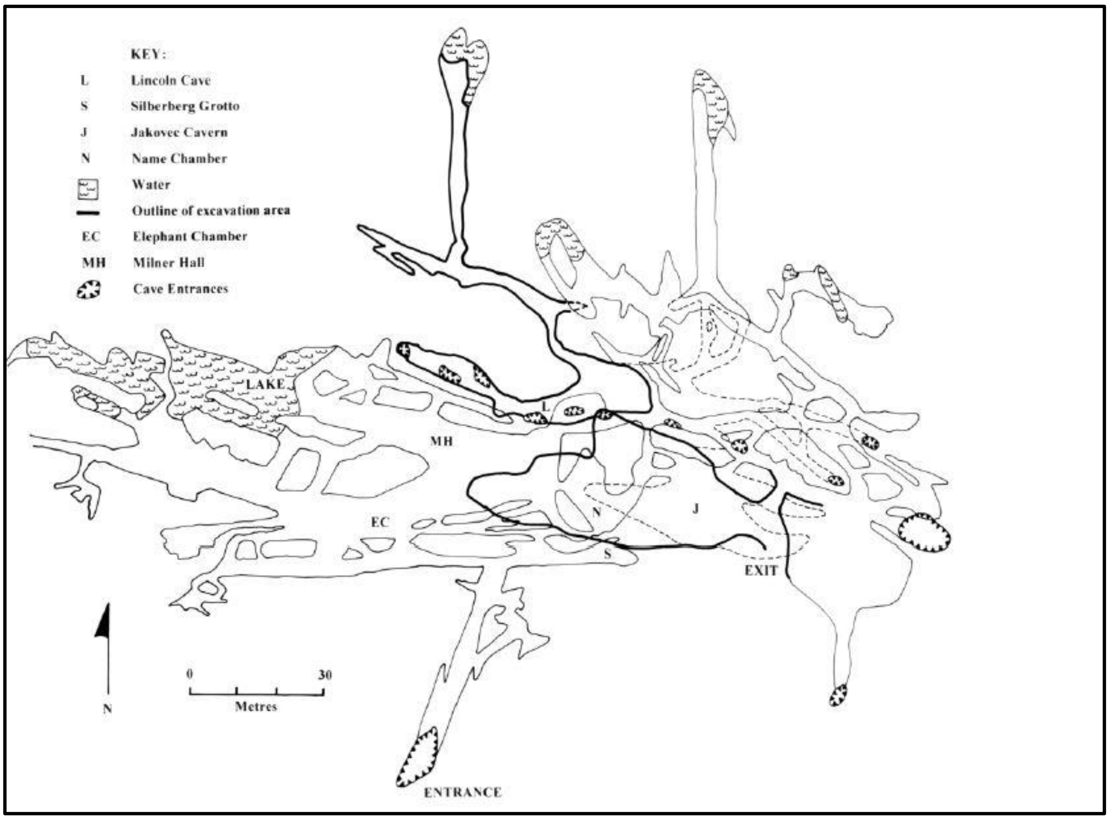

Figure 2.7. Map of Sterkfontein, with Lincoln Cave labelled (L) north of the main site, in the centre of the image (from Reynolds *et al*. 2003: 286).

Lime miners left a ramp of rubble (Figure 2.8) inside the cave which separates the cave into the Lincoln Cave North and South deposits. Uranium series dating was applied to a section in the North where breccia is sandwiched between two flowstones. The two flowstone layers provide an upper date of 115 300 ± 7700 years and a lower date of 252 600 ± 35 600 years ago for at least the northern deposit, while the southern deposit has yielded artefacts that clearly belong to the MSA, an era poorly represented in the Sterkfontein artefact-bearing deposits (Reynolds *et al*. 2003, 2007).

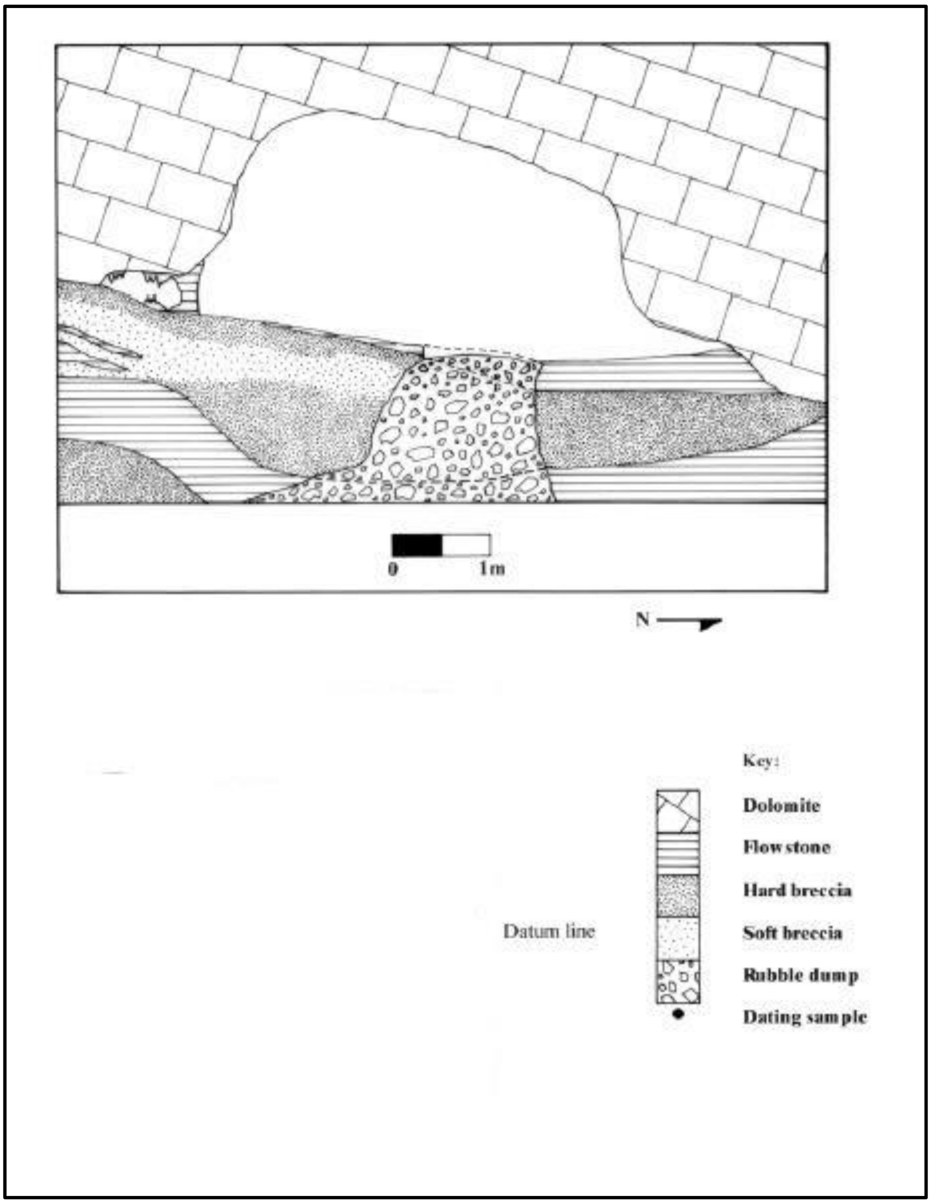

Figure 2.8. Lincoln Cave North (to the right) and South (to the left) are separated by a rubble dump left by miners (after Reynolds *et al.* 2003: 287).

In Lincoln Cave North, very few stone tools were recovered, except for a few polyhedral cores (n = 5) similar to those in the Acheulean in M5W (n = 701), and no SFD was present (Kuman 1994; Field 1999; Reynolds *et al.* 2007). In contrast, the southern excavation yielded not only a large proportion of SFD absent in the northern excavation, but also a large number of flakes (46.4%), which is uncharacteristic of the Acheulean in M5W. A diabase blade present is diagnostic of the MSA. In contrast, the recovery of a bifacial chopper core resembling the early Acheulean and various manuports suggests some incorporation of older material into the southern Lincoln Cave deposit (Reynolds *et al.* 2003, 2007). Also the main site excavation of Square L/63 and the surrounding area shows material with a strong similarity to that found in Lincoln Cave South. Thus, the artefacts within the Lincoln Cave are attributed to mixing of the MSA and Early Acheulean that occurred during the erosion of the M5 West Acheulean deposit and the infilling of this channel with younger sediments (Reynolds *et al.* 2003, 2007). Such mixing of artefacts and contamination of a younger infill were readily detected, but a similar situation was also represented by the fossils. Three hominid teeth from two individuals, a child (StW 591, 592) and an adult (StW 593), were excavated from Lincoln Cave South, along with a hominid cranial fragment (StW 594). One tooth (StW 585) was found in the L/63 area (Reynolds *et al.* 2007). Based on morphological comparisons, the teeth found in Lincoln South appear to belong to *Homo ergaster,* which is associated with the Early Acheulean-bearing M5W deposit, while the tooth from the L/63 area appears to belong to archaic *Homo sapiens,* contemporary with the MSA lithics in that part of the site and in Lincoln Cave South. Faunal evidence further substantiates the differences in formation between the Lincoln Cave and L/63 area deposits with the M5W deposits. Fauna reflecting a wetter climate were found within the northern deposits, including *Hippopotamus amphibius* (which is primarily aquatic) and a bushbuck (*Tragelaphus scriptus*) that specifically inhabits riparian thicket (Reynolds *et al.* 2003, 2007). This contrasts with the grassland environment represented in M5W that does not contain such fauna.

Reynolds *et al.* (2007) conclude that Acheulean tools eroded out of part of the M5W deposit sometime between 1.4 Ma and 115 000 years ago and were deposited into the northern (wetter) Lincoln Cave deposit, thought to have formed between 253 000 and 115 000 years ago. The MSA artefacts accumulated in the Southern Lincoln Cave deposit concurrent with the L/63 finds suggest that these deposits formed around the same time (Reynolds *et al.* 2007). Overall, the Lincoln Cave system is a good example of how intricate cave systems can be and how much research must be undertaken in all facets of a site in order to understand a complex cycle of erosion, reworking and re-deposition. A channel had been eroded into M5 between M5W and M5E, and this space was filled during MSA times with the Post-M6 Infill shown in Fig. 2.6. This research thus emphasises the importance of accurate mapping of deposits and their features.

2.5 Importance of stratigraphic and geological studies to karst sites

Geoarchaeology and site formation analysis

This section will provide an overview of how and when the linkage between archaeology and earth sciences came about. It also includes some of the theoretical, as well as methodological, considerations associated with the study of site formation processes.

Some of the earliest theories about site formation were proposed by Michael B. Schiffer in the early 1970s, who suggested that, for archaeologists to truly understand prehistoric behaviour within the archaeological record, they would need to understand what patterns implicitly affected the artefacts as they lay in place waiting to be discovered (Schiffer 1972). This echoed statements previously made by earth scientist Karl Butzer (1964, 1982), who had had been advocating palaeo-environmental approaches and reconstructions of deposition in regions as diverse as Egypt, North America, Europe and South Africa. Other authors that added weight to the movement included Francois Bordes (1961) in France, Vance Haynes (1964) in Northern America, George Rapp Jr. in Greece (Kraft *et al.* 1975) and Myra Shackley (1975) in Great Britain. Studies of site formation processes require consideration of three basic transformations. The first and second of these are well defined by Schiffer (1972) as cultural and natural processes (C-transforms and N-transforms). First, the cultural processes can be viewed as stages--the procurement, use, maintenance and eventual discard of artefacts. It is important to study these closely to try to determine which stage is being actively viewed at any given time. Some examples of attempts to understand such processes involve experimental replication studies, as these help to determine the context of an assemblage and lead to more nuanced information useful to archaeologists (Jewell 1963; Schiffer 1983; Schick & Toth 1994; Stein 2001; Schick & Clark 2003; Eren *et al.* 2005; Andrefsky 2009; Kuman & Field 2009; Caruana 2017). C-transforms can also modify or obscure the original behaviours. For example, Schiffer (1983) suggested that the re-use of a space for unrelated activities can alter existing patterns or destroy them completely. Secondly, Schiffer described N-transforms as processes that are non-cultural, i.e., geogenic or biogenic, which affect the original spatial integrity and preservation of the artefacts. An example of a significant historical N-transform is the sudden burial of Pompeii after the eruption of Mount Vesuvius, where the entire city was covered in significant amounts of ash and volcanic mud that led to differential preservations (Renfrew & Bahn 2004). Biogenic and geogenic processes are closely tied to geomorphology and environmental conditions. A well-known and ongoing experimental study of the Overton Down earthworks in the United Kingdom was started in the early 1960s. In this case, an experimental deposition scenario with a 21 m long, 7 m wide and 2 m high bank was created next to an artificially cut ditch. The aim of the study was to assess soil pH, porosity, organic matter content, carbonates, and buried artefact conditions, as well as earthworm activity and stratigraphic integrity of the bank and the ditch over a period of 128 years. The preliminary results (at the 32 year mark) have helped researchers describe what types of soil are more susceptible to subsidence, weathering and biological or chemical decay (Crabtree 1971; Crowther *et al.* 1996).

The partnership between archaeologists and earth scientists gained popularity in the early 1970s, as it became increasingly clear that many sites showed signs of post-depositional processes affecting the deposits (e.g., weathering, erosion and fluvial displacement). It was appreciated that earth scientists, with their broad knowledge of sedimentary processes, could help clarify and provide finer resolution on processes that were responsible for the different conditions of the archaeological record (Nash & Petraglia 1987; Stein 2001). It was in 1983 that Schiffer concluded that sufficient research had not been carried out concerning the natural processes of site formation (Schiffer 1983).

As the shift in focus towards an integrated earth sciences approach was being attempted, many archaeologists experienced difficulties in describing the complex depositional and post-depositional processes affecting sites (Hassan 1979; Stein 1993: Butzer 2008). The very real need for inter-disciplinary collaboration between archaeologists and earth scientists led to the development of a new sub-discipline of archaeology, referred to as geoarchaeology. Although the definition of geoarchaeology has been expressed in a number of ways over the years (Renfrew 1976; Butzer 1982; Waters 1992; Rapp Jr. & Hill 1998), it broadly refers to the united study of both archaeological and geomorphological histories and the acknowledgement of how natural and human-induced processes modify landscapes. This view of geoarchaeology has been described by French (2003) and Karkansas & Goldberg (2018) as more than just the study of geological features such as soils and sediments, but rather as inextricably linked to concepts within the earth sciences as a pool of knowledge that helps archaeologists implicitly study the development of the archaeological record (e.g., field stratigraphy, landscape reconstruction).

Thus archaeologists across the globe have become increasingly aware that in order to properly study the context of their assemblages they would need to employ earth science methods. As a result of this new type of thinking, the archaeological community is now more aware of the importance of geoarchaeology (e.g., Butzer 1982; Weiner & Bar-Yosef 1990; Waters 1992; Brown 1997; Ferring 1994; Holliday 1997; Goldberg & Macphail 2006). In order to properly interpret site formation processes there has been a marked shift toward multi-scalar approaches that often include broader geographical considerations combined with the dating of localised fossils or sediments (Bicket *et al.* 2009).

Scale in geoarchaeology

The traditional definition of an archaeological deposit has been critiqued as too simplistic because it suggests a single depositional episode, but most are affected by complex cumulative processes (Stein 2001).

The job of a geoarchaeologist is to closely study the lifespan and interaction of all particles within the deposit by analysing the types of modification processes, within the broader environmental and geomorphological context (Birkeland *et al.* 1991; Hassan 1978; Salvador 1994; Reading & Levell 1996). In geoarchaeology, deposits, as a collection of sedimentary units, are described based on their shape, size, distribution, composition, and degree of consolidation and are defined in a variety of ways and at a range of scales, such as their sedimentary composition and organisation of constituent particles – a facies approach, and by their stratigraphic association with other contacting units – an allostratigraphic approach. An historical definition of facies given by Walker (1984: 1) is: 'the sum total of lithological and palaeontological aspects of a stratigraphic unit'. Facies approaches are often used to distinguish units by depositional and post-depositional processes, which are generally indicated through patterns in particulate composition and organisation, the sedimentary frameworks of which are based on extensive work in the Earth Sciences. Facies-based research can include the targeted study of deposits based on their intrinsic properties such as clast size, matrix composition, overall sorting, mineralogy, etc. (Flügel 2004). The facies approach is a versatile method that allows multi-scale and multidisciplinary integrative analyses with particular suitability within high-resolution stratigraphic and site formation studies. An example of facies-based research includes work done on multiple stratigraphic ashy layers analysed in thin section from Sibudu rock shelter, which ultimately helped develop a framework for understanding multiple phases of burning and occupation (Goldberg *et al.* 2009). Allostratigraphy defines units by their lateral, upper and lower unconformities (NACSN 1983). The approach can be applied at different scales but focusses on grouping deposits and units into sedimentary packages that were deposited between distinct episodes of erosion or hiatuses in deposition. Typical examples of allostratigraphic deposits include stream terrace, lacustrine and glacial deposits which are created by successive episodes of deposition and erosion (Goldberg & Macphail 2006; Räsänen *et al.* 2009; Hughes 2010). The goal of allostratigraphy is to develop detailed sequences of deposition, rather than assessing the processes of deposition, and is particularly useful for tracking deposits across lateral space (from landscape to intra-site scales), where facies variables may change laterally within units. A combination of these approaches is often utilised to provide the greatest potential for the creation of robust stratigraphic frameworks that can be applied on sediment units across expansive areas (Hughes 2010).

A major contribution to geoarchaeology over the last two decades has been the appreciation of the scale at which sites can be studied. The three scales of resolution for studying sedimentological data are described by French (2003) and Butzer (2008). First is the macro-scale or regional context, which encompasses an extensive area and takes into account factors such as climate, geology and topography. Second is the meso-scale, which is the immediate area in which the site is located and factors such as position and land-use. Lastly the micro-scale is considered to account for micromorphological changes within a site. French (2003) explains that all these scales need to be reviewed in an interconnected theorem in order to completely understand a given site and the processes affecting it.

2.6 Overview of cave site formation processes

Cave systems can be considered as distinctive geoarchaeological environments that are often semi-closed sediment traps where geological or human-derived sediment can enter from the outside environment (exogenous) or accumulate within the cave itself (endogenous). Deposits within caves are nonetheless prone to transformation and reworking through internal climate change, and animal or fluvial activity (Butzer 2008; Karkansas & Goldberg 2018). Closed cave environments provide an opportunity for the accurate study of historical human activities such as fire production, trampling or ritual processes, as they generally preserve these aspects better than open air sites. This section will explain some of the depositional and post-depositional processes that can either aid or obscure how geoarchaeologists view the archaeological record (Goldberg & Sherwood 2006).

Anthropogenic processes

Anthropogenic processes include all primary and secondary human activities that accumulate and/or modify archaeological sediments or artefacts. Examples of this include, but are not limited to: trampling (Nielsen 1991), construction of hearths and preparation of bedding (Wadley *et al.* 2011), accumulation of bones and lithics due to onsite processing (Henshilwood *et al.* 2001b, combustion and/or its by-products (Berna *et al.* 2012), and burials.

Biogenic processes

Biogenic processes refer to the primary and secondary actions that can lead to the accumulation or redistribution of components that are human, animal or plant-based residues, or more specifically, any organic remnants derived from dung, guano, bone, carnivore coprolites, nesting residue from birds or rodents, wood ash, shell (snails) and root activity (Karkansas & Goldberg 2018). In cave systems these accumulations usually enter through cracks in the roof that become what are known as 'keyhole sites' or as a result of high energy fluvial transport. Typically, biogenic components register on common chemical tests such as Fourier Transform Infrared Spectrometry (FTIR), which detects phosphates, carbonates, or amino acids (Goldberg & Macphail 2006; Karkansas & Goldberg 2019). Biogenic chemical compounds are difficult to study without micromorphological examination of sediments as they are often prone to movement between sedimentary levels. Micromorphology entails the study of soils, sediments and any associated archaeological remnants (e.g., hearths, occupation floors) at a microscopic level, often through the analysis of thin slides viewed under a microscope (Goldberg & Sherwood 2006). These slides often reveal intrinsic properties that are useful for producing a comprehensive understanding of deposition or post-depositional alteration, used to infer environmental conditions or provide linkages to prehistoric human activities (Goldberg & Sherwood 2006; Goldberg & Berna 2010).

An example where the study of biogenic processes using micromorphology has been useful is that of Sibudu rockshelter in Kwazulu-Natal, South Africa (Wadley & Jacobs 2006). The sediments at Sibudu have been very carefully excavated to reveal phases of combustion at the macro scale. However, micromorphological comparisons enabled Goldberg *et al.* (2009) to differentiate microfacies, which delineate different combustible materials used in unique anthropogenic burning activities.

Geogenic processes

Geogenic processes include natural processes of sediment accumulation, re-deposition or removal. Some examples of these within caves include aeolian, colluvial and/or water-based flow and freeze-thaw processes. Sometimes geogenic processes include the cementation of deposits through precipitating calcium carbonate ($CaCO_3$) within caves (Butzer 2008). Geogenic fluvial processes can either transport anthropogenic materials such as lithics and pottery or independently create new sediment accumulations perhaps while transforming other natural formations (Karkansas & Goldberg 2018). Geogenic processes are further subdivided into types of sediments-utocthonous (internal) and allocthonous (external) (Goldberg & Sherwood 2006). Under certain conditions, endogenic cave sediments (sometimes referred to as autocthonous sediments) can facilitate sediment accumulation through, e.g., the detachment of speleothems and bedrock clasts from cave walls via solution of rock, gravity, tectonic activity, or frost shattering (Goldberg & Karkansas 2006; Butzer 2008).Allocthonous sediments enter the cave from outside, with the aid of processes such as fluvial flow within extensive cave corridors, which can lead to broadly dispersed size ranges and sediments influenced by the rate of flow. However, aeolian (wind-blown) deposits are rare or difficult to track in karst environments because they often consist of very fine particles that can either be mixed into existing sediments or buried by successive depositional events (Goldberg & Sherwood 2006).

2.7 High-resolution studies Micro-CT scanning, Geographic Information Systems (GIS) and other methods

Micro-CT scanning, although more commonly used in the field of archaeology, has been used in micromorphological studies with great effect. Micro-CT uses x-rays to create highly accurate 3D renderings of specimens, and it can be used to digitally recreate specimens encased in soil or hard breccia. Re *et al.* (2015) used Micro-CT scanning in Italy to non-invasively study blocks of soil where a ritual burial containing various artefacts was thought to have taken place. The sediments of these burials contained culturally produced sediments from pollen and seeds. Thus, Micro-CT proved invaluable because it was a non-destructive method. Resulting scans helped archaeologists surmise that features of geochemical processes caused by biogenic breakdown had affected the artefacts within the sample, and they were thus able to lead to a better understanding of post-depositonal processes within the stratigraphy as a result Re *et al.* (2015).

In Brazil, a study by Villagran *et al.* (2019) used Micro-CT scanning to study soil sections from the rockshelter site Lapo do Santo. The focus concerned fragmented termite mounds that were later shown to have been purposely mixed into ashy combusted sediments. A mixture of clay and organic termite residues (saliva, bodily fluids) cemented the mounds at the site. When analysed under thin section, this clay revealed very little. However Micro-CT penetration was able to identify successive and distinct organic and mineral features. Thus Micro-CT was extremely useful in describing anthropogenic processes at a much higher resolution (Villagran *et al.* 2019).

The use of digital cameras and aerial photography are methods for studying regional-scale environments and includes topographical data obtained with geophysical methods, such as magnetic survey or land remote-sensing satellite (LANDSAT). These methods are also used in geoarchaeology to locate sites and reveal hidden archaeological features or unique geomorphologies (Renfrew & Bahn 2004).

GIS is another method frequently used by multiple disciplines because of its flexibility. GIS originated from Computer- and Map-Aided Design (CAD and CAM), which were both developed in the 1970s and are used today both academically and industrially. GIS digital platforms can be used to create, analyse, orientate, integrate and display geographically positioned data in relative space. The programme enables users to visualise data that are both macro- and micro-scale-specific, and it is perhaps most useful for accurate recording of site components and the production of predictive models (Renfrew & Bahn 2004). GIS can also be used on individual artefacts. For example, Caruana *et al.* (2014) applied GIS to percussive stone tool technologies in order to compare very specific individualised wear-patterns on an experimental sample to hammerstones from the Koobi Fora and Galana Boi Formations in Kenya.

Summary of site formation

As clearly demonstrated above, karst cavern deposits can be highly complex and involve multiple phases of accumulation, subsidence and reworking during and after deposition. Thus, high resolution multi-scalar studies are necessary to best understand the stratigraphic succession, context and integrity of the artefacts from Sterkfontein. A detailed GIS spatial study of the artefacts from M5 and the limits of the M5 infills should help describe this member in greater detail. Furthermore the mapping of specific features which contributed to site formation and disturbance helps create a reference for futures excavations and can eventually be integrated into part of a greater GIS spatial framework that also covers subterranean caverns at the Sterkfontein Caves. The high resolution Micro-CT study of the Oldowan assemblage provides new data to explain the transformation of lithics and furthers our knowledge for understanding abrasion features at a microscopic level. Little literature currently exists for quantifying abrasion over an entire 3D surface and this multi-scalar study seeks to provide a method with which to do this.

2.8 Importance of artefact edge analysis

The study of post-depositional edge wear informs us about site formation, hence the importance of it in this study. The analysis of artefact edge angles and microwear research have pervaded archaeological study for decades, (for some of the earliest work on these topics see: Wilmsen 1970; Gould *et al.* 1971; White & Thomas 1972; Tringham *et al.* 1974; Burgess & Kvamme 1978; Dibble & Bernard 1980). Studies of tool edge wear patterns provide important information on settlement activities and the *modus operandi* of prehistoric communities, adding a new dynamic to lithic analysis as a whole (Tringham *et al.* 1974). Microwear studies are important in examining the complete surfaces of lithics and in understanding the nature of any natural damage that may have occurred. Studies of surface microwear are particularly important here because they form the groundwork for the research presented in this paper. In the early 1930s, Sergei Semenov began work on a book called *Prehistoric Technology* that would revive interest in functional studies (Semenov 1964). Semenov's publication was not the first of its kind to focus on microwear, but it definitely introduced a more innovative approach to lithic research (Tringham *et al.* 1974).

Semenov made use of higher magnifications and focused on experimental use wear, even though he admitted he was not the first to study microwear as a functional indicator (also see: Curwen 1930; Sonnenfeld 1962). His work aimed at compiling positive answers about the causes of such wear. He is regarded as the first to define different kinds of microwear and record them using enlarged photographs, stereoscopic microscopy (or binocular microscopy) and colourizers or metalization on plates under examination (Keeley 1974). From 1971 onwards, Tringham (after contact with Semenov) performed a variety of early experimental use-wear tests on a multitude of materials that she defined as 'soft' (skin, flesh), medium (some woods) and 'hard' (stone, antler) (Tringham *et al.* 1974). The experiments involved replicating transverse and longitudinal cutting and sawing actions and boring mechanisms and analysing them under a low power microscope.

An early description of 'edge angle' in microwear studies was "the angle to the plane at which a micro-flake is detached as a result of wear'' (Wilmsen cited in Tringham *et al.* 1974: 179). Wilmsen (1970) proposed that specific functions could be ascribed for each size range of angle. A similar edge angle was later described by Tringham *et al.* (1974: 179) as the 'spine-plane angle', which is "measured from the plane of the ventral surface of a flake to the plane of the dorsal surface which is nearest to the edge''. Figure 2.9 shows the difference between the spine-plane angle described by Tringham and Wilmsen's edge angle.

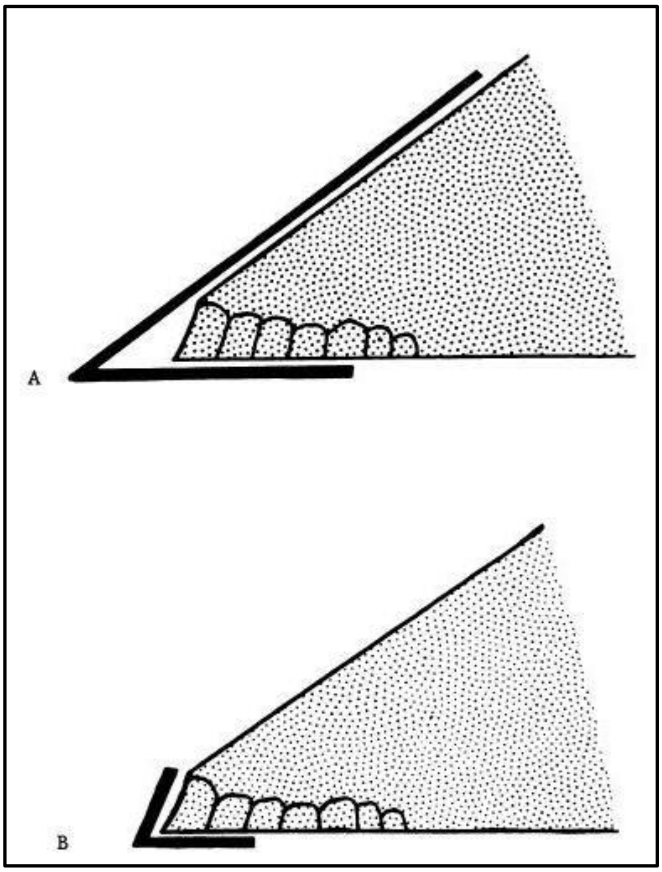

Figure 2.9. Measurements of the Spine-Plane Angle (A) and Edge Angle (B) (from Burgess & Kvamme 1978: 483)

The theory of edge angle measurement is an important one, yet the practical implications of producing the most suitable way to measure an edge angle is one that has troubled researchers who use complicated technologies. As Grosman *et al.* (2008: 3102) more recently declare: "The intrinsic impossibility to find a 'true' or 'unique' positioning is a mathematical fact which cannot be circumvented." This holds true because it is often difficult to decide where on a specific artefact the measurement should be applied, and this can also be complicated by the research question at hand (Dibble & Bernard 1980). Several methods have been proposed, each with their own strengths and weaknesses, and they are explained below.

Polar co-ordinate or graph method

This is a technique introduced by Wilmsen (1970) where an artefact is positioned on a piece of polar co-ordinate graph paper. The interior flake surface adjacent to the edge to be measured is positioned in line with the horizontal axis and the angle of the edge is read off the graph paper (see Figure 2.10). This method is perhaps the most widely known, yet is also the most problematic in some fundamental ways (Burgess & Kvamme 1978; Dibble & Bernard 1980). Both sets of authors state that alignment along the horizontal graph axis is not always possible, as the control of parallax and depth of field can be problematic due to the artefact position above the graph. Observer bias seems to be the biggest problem for this method. The method is also not suitable for measuring angles where large or inconstant edge lengths occur because one's eye cannot focus on both the edge angle and polar graph at the same time in order to make an accurate assessment (Patterson 1980).

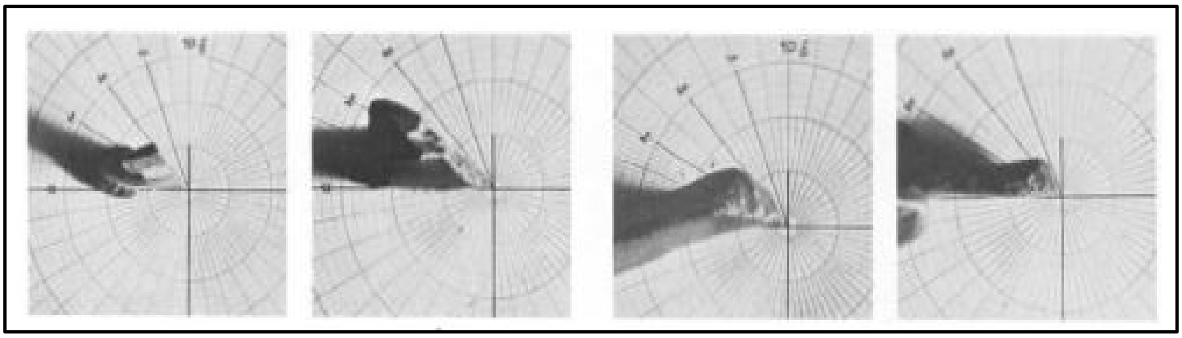

Figure 2.10. The Polar Co-ordinate method for measuring edge angles (from Wilmsen 1970: 21).

Clay method

The clay method, devised by Burgess & Kvamme (1978), involves two steps where an impression of an artefact edge is made in a strip of soft clay and the angle of the impression is then viewed and recorded using a magnifying comparator (Figure 2.11). This method is useful because it controls for parallax to a degree and allows the measurement of any chosen angle along an edge, something that is not possible with the graph method (Dibble & Bernard 1980). The only problem noted is that by magnifying an edge, irregularities in that edge can become more apparent. Similarly the authors state that prior to examination the research parameters need to be exclusively defined (Burgess & Kvamme 1978).

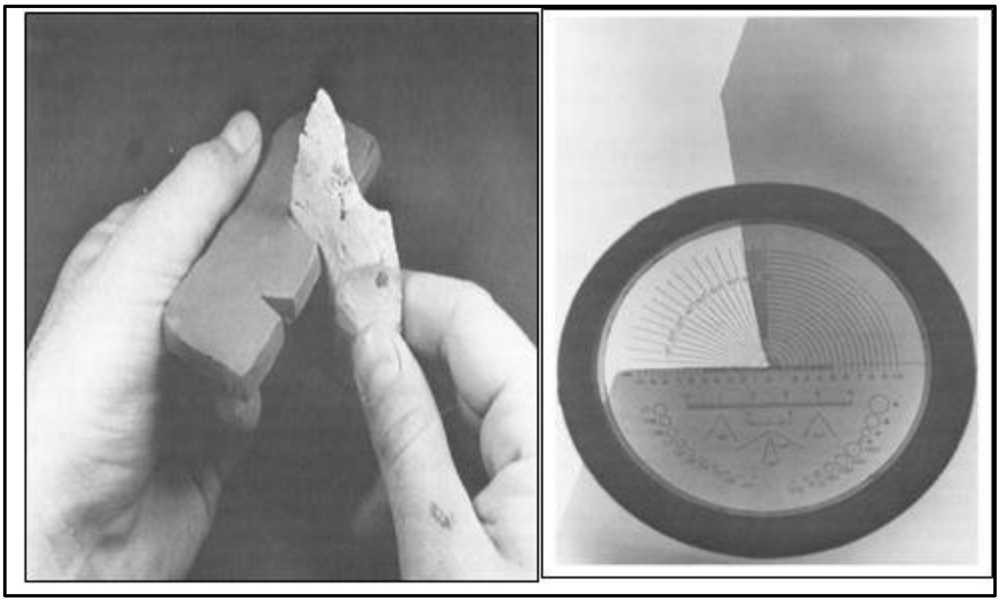

Figure 2.11. Incising artefact edges into clay (left) and a comparator (right) used to measure the edge incised on the clay (from Burgess & Kvamme 1978: 483,485).

Calliper method

Dibble & Bernard (1980) developed the calliper method whereby a thickness measurement is taken by a modified set of callipers which has a bar attached at a set distance behind the calliper needle to standardise the medial measurement. The resulting thickness measurement is substituted into a trigonometric formula to calculate the edge angle. This method once again does not account for highly irregular edges. See Figure 2.12 (D) for an example.

Goniometer method

The most widely used method for edge angle measurement is the goniometer, Labelled 'c' in Figure 2.12, commonly referred to as a swing arm protractor whereby an angle can be taken at any point. An artefact's surface is positioned horizontally on the scale, a movable arm is aligned with the opposite surface, and the measurement can be read directly off the scale. This method has difficulty measuring smaller edge angles, and the alignment of the arm with consistent surfaces or the alignment of the arm itself can prove to be inaccurate (Burgess & Kvamme 1978; Dibble & Bernard 1980; Patterson 1980).

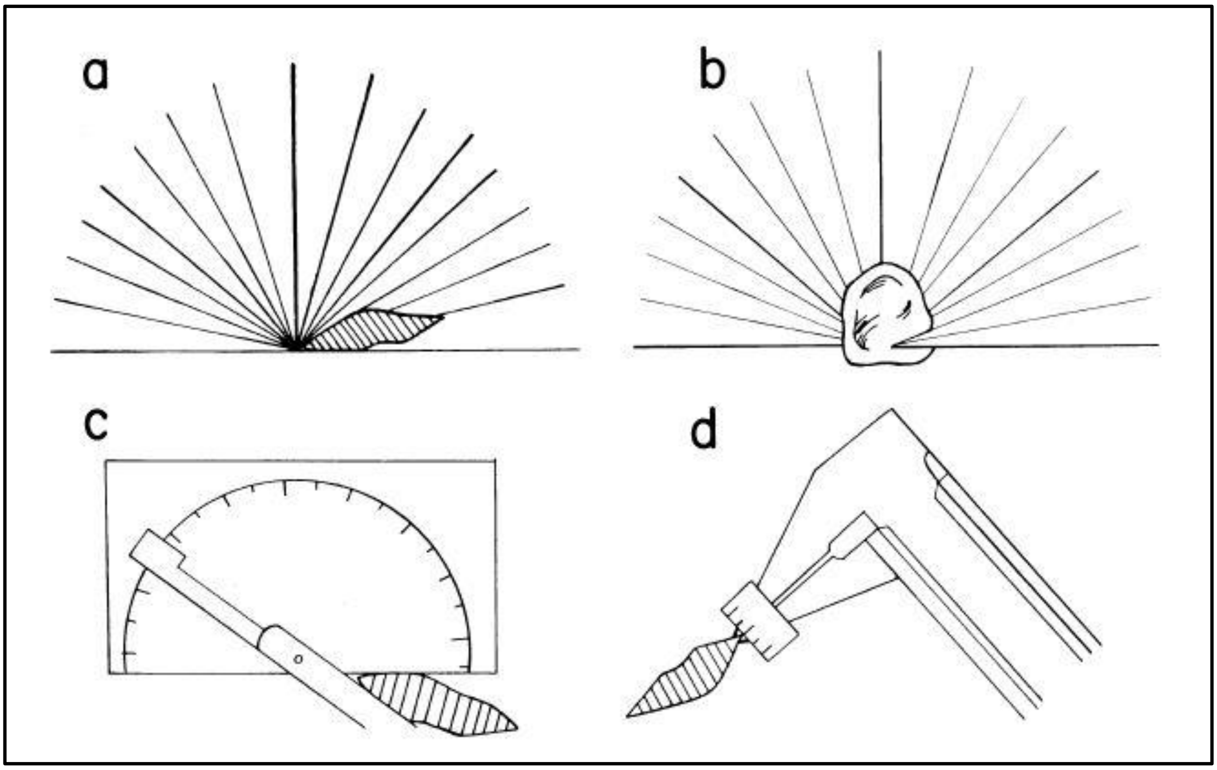

Figure 2.12. a) Polar Co-ordinate Graph Method, b) Clay Method, c) Goniometer, d) Calliper Method (from Dibble & Bernard 1980: 885).

2.9 Edge angle research problems

Past research into edge angles has been explored in depth above. However, some of the main problems in measuring edge angles, beyond those of observation bias and debates on terminology, are fundamentally geometric in nature (Patterson 1980; Hiscock 1982; McPherron & Dibble 1999; Grosman *et al.* 2008). The angular intersections of planes measured by archaeologists can be curved or irregular rather than even. It is very difficult to define non-linear angles or to compile precise data without excluding a portion of the irregular surface of the angle being measured. Light retouch also makes it hard to accurately measure edge angles using some of the older methods described above (Patterson 1980).
A quantitative study was conducted by Siegel (1985) on 67 well-defined end scrapers in order to check whether edge angles could be directly attributed to function. The measurements were performed with the goniometer method and a one-way Analysis of Variance (ANOVA) was used to test the data. A lack of statistically significant results led Siegel to conclude that edge angle was an inconclusive measure of function and he thus suggested a more intensive use-wear analysis to describe functionality. Few studies that actually give meaningful

correlation of edge angle to function are present in recent literature, and even fewer exist regarding the question of abrasion explained in this study.

Abrasion analysis can also be considered as the blunting of an edge. For example, Sonnenfeld (1962) proposed a very early bluntness index (BI) that creates a template for measuring the taper radius of an axe or hoe edge and divided the edge angle by this amount. A smaller BI resulted in a sharper more tapered edge and a larger BI in a much blunter or less tapering edge (Sonnenfeld 1962). The next section considers advances in edge measurements using scans.

2.10 Micro-CT scanning and its importance to archaeology

The modern use of scanning equipment is becoming ubiquitous in the way research is conducted today. With the ever-rising popularity of online communication, it is not surprising that archaeological research is also going digital. Techniques such as laser scanning and photogrammetry are well documented as tools which can be used to proficiently engage with archaeological material to create online galleries and international co-operation (Sumner 2008; Abel *et al.* 2011).

CT scanning is one of the most flexible and affordable techniques available to researchers because, unlike many laser scanners, it can scan highly reflective or translucent surfaces with ease and produce many more 3D images in a single scan than most photogrammetric or laser scanners (Abel *et al.* 2011). The resulting scans from a Micro-CT scanner can show the inner structure of an artefact and the object can be manipulated, rotated and assessed in virtual space. Abel *et al.* (2011) reproduced a refitting study of flint flakes in 3D and managed to use the cavities left on flakes to reproduce missing flake profiles that never could have been produced by traditional techniques. Their study also allows one to see inside each part of a refitted matrix in 3D, something that photogrammetry cannot achieve.

Scans produced by Micro-CT can be of extremely high resolution, yet they take up very little hard-drive space and can be easily disseminated or 3D-printed. Perhaps of most importance is the fact that this technique is wholly non-invasive and no contact with or modification to the sample needs to be made. A specimen could be fully encased by breccia and a trained user would be able to separate the artefact *in situ* digitally and fairly quickly depending on the nature of the material.

Previous geometric morphometric (GM) and 3D studies (digital archaeology studies)

In earlier methods of analysing lithics, researchers reduced artefact wholes to a set of linear measurements consisting of ratios which could only describe certain sections of a tool at a very basic level (Figure 2.13; Roe 1964; McPherron & Dibble 1999; Grosman *et al.* 2008). Roe's indices are examples of this approach using ratios such as thickness divided by width (Roughness or refinement) (Roe 1964; Saragusti *et al.* 2005). More recently archaeology has started to shift into the digital realm. Artefacts can now be either digitised or 3D laser or Micro-CT scanned into a computer system very accurately, whereby GM methods can be applied to artefacts allowing researchers to control selected variables and create very accurate information about artefacts as a whole (Bookstein 1997; McPherron & Dibble 1999; Grosman *et al.* 2008, 2010, 2011a, 2011b; Saragusti *et al.* 2005; Lin *et al.* 2010; Abel *et al*. 2011; Richardson *et al.* 2013; Morales *et al.* 2013; Shott & Trail 2010; Archer & Braun 2010; Archer *et al.* 2017; Lin 2010; Abel *et al.* 2011; Couzens 2012; Zaidner & Grosman 2015; Grosman 2016; Herzlinger *et al.* 2017; Herzlinger & Grosman 2019; Viallet 2019; Valletta *et al.* 2020).

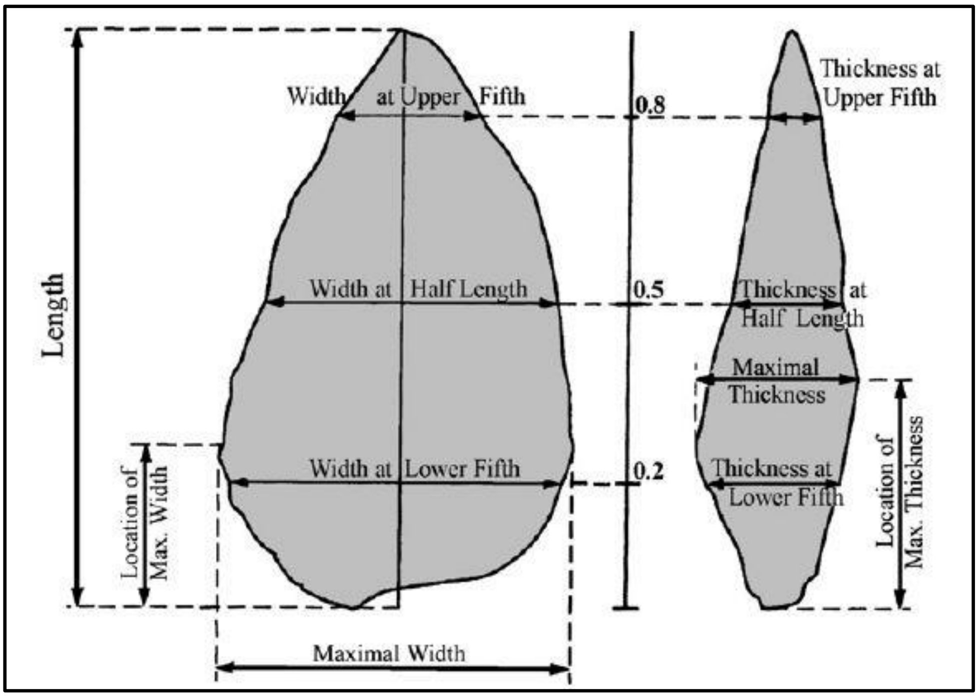

Figure 2.13. Measurement system for ratio analysis on bifaces devised by Roe 1964 (from Grosman *et al.* 2008: 3103).

Various studies have been undertaken to help move away from purely descriptive and metric ways of defining lithics, although many of these deal with larger tool forms such as cores and large cutting tools (LCTs), and not with SFD. The reason for this could be because research questions regarding SFD often attract very little interest. Larger lithics are much easier to study, and thus they make comparable surface differences with 3D and the naked eye more favourable.

Over the years, researchers have developed numerous methods such as the ones described above to explain lithic style, form and function. Many such methods only capture very basic measurements and often reduce complex wholes to simplified models devoid of detailed surface data or attributes (Shott & Trail 2010; Grosman 2016). Various studies in the last decade have tried to improve on what has become termed as 'traditional morphometrics' (Slice 2007) in order to study whole artefacts using polar co-ordinates coupled with a form of statistical shape analysis called Procrustes analysis (Slice 2007). Crompton (2007) explains that much of the traditional linear measurement method reduces important shape information into incorporeal singular values, which serve to only estimate artefact morphology, rather than accurately account for it. Furthermore he states in cases when bivariate or multivariate statistics are applied to linear data yielding no more than a co-variant relationship, "Shape is a multivariate phenomenon and should be analysed as such" (Crompton 2007: 148). A loss of quantifiable evidence when examining 3D wholes with linear measurements and expecting 3D results seems likely.

In the early 1990s, biological anthropologists interested in questions concerning shape and patterns of variation cohesively engaged with anthropologists and statisticians to create "geometric morphometrics (GM)," a term first coined in 1993 by Marco Corti (Corti 1993; Slice 2007; Shott & Trail 2010). GM acts on the application of landmark and semi-landmark points to an object (Lycett & Chauhan 2010). These landmarks contain metadata (a grouping of deeply embedded and essential data) with which one can recreate a whole representation of geometric form in 3D space without any points of interest having to fall along predefined and confining axes (Slice 2007; Shott & Trail 2010). Put simply, a whole object of any form can be replicated in detail along with accurate co-ordinate data, which in turn contains geometric information for each part of that whole. The first landmarks were defined by Bookstein (1997), who also coined the term 'semi-landmarks' in 1997. Semi-landmarks are arbitrary points (defined by any GM user) that are constrained only by the morphology of the material being studied (Lycett & Chauhan 2010).

The main benefits of geometric morphometrics include the conservation of 3D form, outline form, some characteristics of cross-sectional form, and other innate geometrical data. In comparison to more traditional techniques, GM actually stores dimensional information which can be correlated to the points along it within 3D space (Crompton 2007; Shott & Trail 2010; Grosman *et al.* 2008; 2016). GM is additionally beneficial because it has the ability to control for size variability by scaling pieces to a constant. This is advantageous for the analysis of various aspects including typology (Shott & Trail 2010). Many authors have described variation in artefact size to account for variation in shape (Bookstein 1997; Crompton 2007; Shott & Trail 2010; Charlin & González-José 2012).

Geometric morphometrics and 3D analysis are the pivotal types of studies in the modern age that could prove useful in the case of abrasion studies because they are so malleable in their functionality. Geometric morphometrics form the modern basis for analysing shapes in scientific space and can be used to make predictions about overall shape and stone tool characteristics (Lycett & Chauhan 2010).

Grosman (2016) explains that studies, such as those by Saragusti *et al.* (2005) on the symmetry of handaxes from the Levant, have improved the facets by which we describe artefacts by using 3D techniques coupled with 3D technology to detect what is not visible to the naked eye. For example, the study of lithics can now allow for the accurate projection of surface contours, angles, measures of concavity or convexity, volume or surface area and Center of Mass (CM) co-ordinates. All of these measures lead us to better predictions about how lithic shape changed over time within specific sites. Saragusti *et al.* (2005) were able to create an accurate record of symmetry and roughness for many types of artefacts such as: ceramics, handaxes and phytoliths using the information made available through digitization.

The Center of Mass is an important value because it better defines the predetermined purpose of the artefact and the will of its maker. A study by Grosman *et al.* (2014) on Neolithic masks was able to show that the masks were indeed for wearing, not merely display, as was previously thought. In lithic studies, the CM is a commonly recorded trait and important when analysing the *chaîne opératoire* or the sequence of stone tool production (Grosman 2016).

Digitization methods and studies using geometric morphometrics

Some of the earliest studies to use a digitization technique, even though they were never necessarily considered geometric morphometrics, included Montet-White (1973), Dibble & Chase (1981), and Gero & Mazzullo (1984). More recently, a method by Wynn & Tierson (1990) involved creating 22 polar co-ordinates originating radially from the midpoint of the long axes to the outer reaches of the object using a digitizer. Their method was deemed problematic by Shannon McPherron (2000) and David Underhill (2007), but it aided in explaining typological variations of form according to Couzens (2012).

Some examples of types of technology for digitising include: flatbed scanners which can only merge photographs or flat objects, digitizing scribes which record accurate outline landmarks, digital cameras that can replicate a whole 3D surface through a process called photogrammetry, laser scanners which accurately capture and render 3D surfaces, and finally Micro-CT scanners that are extremely powerful and can create 3D surfaces as well as internal structures. Lycett *et al.* (2006) made use of 3D GM to evaluate the shape of Pleistocene cores, combining their study with a biological phylogenetic approach. By using multivariate

statistical analysis, they were then able to search for larger trends pertaining to asymmetry, amongst other variables (Cardillo 2010; Couzens 2012; Lycett *et al.* 2006). Sumner & Riddle (2008) used photogrammetry to recreate an exact 3D replica of an Acheulean hand axe, as well as reconstruct the surfaces of refitted Middle Palaeolithic cores from Egypt in 3D to examine the core reduction strategy. The authors noted that although the turnover rate for a single artefact at the time was about 10 hours, the benefits of having a purely digital platform which could easily be shared across the World Wide Web were of great importance.
Archer and Braun (2010) drew on Lycett and his partners' work by applying a geometric morphometric method to the handaxes from the Acheulean site of Elandsfontein. In order to show that handaxe variability could be related to a specific reduction strategy based on raw material availability or selectivity, they used a 3D digitizer and produced various models (Archer & Braun 2010). Another recent study by Lin *et al.* (2010) used 3D scanning to assess whether 3D measures were more precise for cortex areas than mechanically averaged measurements. Their study showed that 3D measures were more accurate when sample sizes were larger. This also highlighted the fact that 3D techniques are applied better in quantitative case studies. Many studies are produced each year to compare which methods of 3D are most effective.

Grosman *et al.* (2010) among others have implicitly stated that during the lifetime of a stone tool, from its production until its discovery by archaeologists, it is likely to go through many changes based on the context in which it is discarded and the many other environmental processes such as trampling by animals, sedimentary movement, fluvial and even aeolian movement that have an impact upon it. More classical studies regard lithics visually and subjectively as either "fresh" or "weathered". After subjecting tool forms to various experimental rolling/trampling/fluvial processes and then 3D scanning them at every step before super-positioning their initial and final outlines atop one other, Grosman *et al.* (2010) were able to measure to what degree and in which location wear occurred on archaeological tools. A method with substantial accuracy was that of Richardson *et al.* (2013), who performed a morphological study to analyse and record LCT scars and ridges in more detail using a 3D technique coupled with an algorithm that detects surface features and then compares their outcomes to classical hand drawings. Herzlinger & Goren-Inbar (2019) most recently performed a comparison between what they call a 3D homologous landmarks-based geometric morphometric shape analysis (3DGM) and a typo-technological attribute analysis on LCTs from Israel. By using Principal Components Analysis (PCA), they were able to suggest that not only did cleavers and handaxes exhibit variability within their sample, but they were also able to make some speculative claims regarding functionality and suggest some symbolical meaning for handaxes.

Three-Dimensional digitization is also used for many other applications according to Grosman (2016), not only for lithic studies. Many technologies have been re-programmed or optimized by archaeologists to work automatically and specifically target heritage functions such as those of Reflective Transforming Imagery or RTI (Lerma *et al.* 2014). RTI is also called Polynomial Texture Mapping and is a technique whereby an interactive surface is mapped using directional lighting (Coules *et al.* 2019). Laser-structured light for analysing micro-fractures within wood or bone are used as a type of use-trace analysis method (Bradfield 2016; Niven *et al.* 2009), and the use of Light Detection and Ranging (LiDAR) has even been equipped in drone technology in order to better map the contours of sites and landscapes that are covered by heavy vegetation or where features are not immediately visible to the naked eye or recordable through traditional means (Chase *et al.* 2011; Rajani *et al.* 2009). LiDAR was used to help map Stonehenge and ultimately find additional sites in the area (Bewley *et al.* 2005; Grosman 2016).

Digitization of rock art and engravings by way of non-invasive techniques such as laser scanning and photogrammetry are a very good way of preserving art (in colour) that is prone to degradation (Grosman 2016; Lerma *et al.* 2014). It is clear that 3D excavation recording can give access to accurate two-dimensional data, as was the case with the GIS portion of this study, and Grosman (2016) states that a combination of highly accurate 2D and 3D data is a frequent result in modern studies. More recently Zaidner & Grosman (2015) used 3D analytics to study retouch on side scrapers from Israel by looking at edge angles and discerning that raw cutting edges were preferential to retouched ones. In France, Viallet (2019) proposed a method that used 3D scanning and Avizo (as used in this study) to measure the edge angle of bifacial tools by using a variation of Tringham's edge angle measurement and including a depth measurement to isolate the cutting edge portion of the tool. They deduced that bifaces had undergone a process of re-sharpening at their site and that the cutting edge was most likely along the longitudinal edge with the depth of the cut being of some importance. Similarly Valletta *et al.* (2020) proposed a study of Epipalaeolithic microliths to measure edge angles. Their analysis involves mapping each side of an edge of a digitized tool by a series of points and then applying a complex algorithm that measures an angle of intersection between the slopes of each side to give an accurate edge angle. Their analysis is interesting in that it targets the edges in a very accurate way and makes automatic adjustments to capture irregular edges. Their method, when compared to Dibble & Bernard's (1980) manual study, proved extremely accurate and helped provide new information for edge-related functionality in the southern Levant in Israel. Bustoz-Peréz *et al.* (2019) performed an analysis on an experimental assemblage using an extremely fine-tuned microscope and accurate photograph comparisons of edge widths to simulate and analyse the continuous rounding on the edges of quartzite and flint artefacts in fluvial environments. In their analysis they created a tabularised index for rounding of edges in sequential stages of damage. Galland *et al.* (2019) used confocal microscopy and 3D scanning coupled with statistical techniques to quantitatively measure roughness on different types of flint artefacts. Although they did not measure edge angles or rounding, their study was able to provide information about reworked contexts by comparing surface patinas of experimental and archaeological materials.

Macro and micro-fracture analysis of quartz

Quartz is described as a raw material very frequently present at archaeological sites worldwide. It is defined by authors such as Spry *et al.* (2019) and De Lombre-Hermida *et al.* (2015) as a rock type (with hardness of 7 on the Mohs scale) that can be either automorphic (where larger crystals are present and are formed in specific contexts such as silica-rich or magmatic quartz formed over a long period of time) or xenomorphic quartz (where a large substrate is composed of a collective of differentially sized microcrystals). Quartz is an extremely variable material, and many internal impurities and fractures can exist. Thus it is frequently cited in archaeological contexts as shatter-prone, commonly producing small, sharp pieces as a result of the bipolar technique (Barham 1987). Quartz components from sites largely go understudied by researchers because of their technicalities, especially in 2D contexts. In the last decade, there have been many attempts to study quartz lithics through experimental reproductions and most recently Micro-CT scanning see: (Field 1999; Kuman & Field 2009; Kuman *et al.* 2018; Tallavaara *et al.* 2010; Pargeter *et al.* 2017; Spry *et al.* 2019).

Studies in recent years have set out to differentiate natural breakage and fracturing within archaeological material. There has been some consensus that quartz-knapping patterns are not entirely random, and that in fact in most cases, a distinct shape is produced that relates to either freehand or bipolar technique (Spry *et al.* 2019).

Pargeter *et al.'s* (2017) study of small experimental backed tools in quartz, similar to those thought to have been used for bow hunting, represents one of the most recent applications of Micro-CT scanning to quartz assemblages. It must be noted that quartz is not often laser/light scanned because of the high reflectivity of its surfaces, which makes Micro-CT scanning preferential. Pargeter *et al.'s* (2017) study was able to analyse diagnostic impact fractures (DIFs) at both a macro and micro level, which is difficult for the latter, and the authors thus suggest that the application of Micro-CT scanning to quartz-dominated archaeological assemblages could prove highly beneficial in the future.

2.11 Problems in three-dimensional (3D) scanning

Three-dimensional studies are not without problems. Many procedures must be achieved properly in order to either create or extract information from a scan or from photogrammetry. McPherron & Dibble (1999) explain that the equipment and associated programmes can have problems when generating a model. Examples of this include lens distortion in the case of photogrammetry, damage to an artefact using a digital micro-scribe (Abel *et al.* 2011), and loss of image quality associated with poor aspect ratio (or pixel density decline). The material being scanned can also cause reflectivity problems (especially when using a light-based laser scanner and scanning a pale-coloured material), and noise can intrude on scans (Abel *et al.* 2011). One of the most difficult challenges to circumnavigate is how one chooses to align tools when analysing them. This problem has been studied in depth by Grosman *et al.* (2008), and they explain it to be a fundamentally intrinsic problem in modern lithic studies.
The methodology presented in the next section aims to solve many of these problems through the use of Micro-CT scanning. Abel *et al*. (2011) also suggested that Micro-CT scanning has a variety of benefits, many of which have been beneficial in my own study and which I will briefly summarise here. To address the problem of poor image quality, the Micro-CT can scan at an extremely high resolution and its final images are unwavering in their conception, as all noise and sections of an image that are unwanted can be easily accounted for and removed within ten minutes or less. The problem of reflectivity is absent in all cases because

X-rays penetrate an object to create both a surface and internal model and are not influenced by reflectivity to the degree to which some 3-D scanners are. Lastly, Micro-CT scans have a high turnover for an experienced user. For example, in my 2012 study of handaxes (Couzens 2012), I was able to scan 80 LCTs in a number of months, and in the current study I was able to both scan and process over 200 small flakes within about six hours at a fairly low cost. It is thus clear that Micro-CT scanning of small to medium lithics is incredibly useful to modern archaeological studies. The next section will cover the methodology I produced and executed for the SFD and other artefact types of the Oldowan within M5.

2.12 Literature Review: Summary

This chapter has provided an overview of the Sterkfontein Caves, its stratigraphic sequence, and the complexities of those deposits affected by reworking. Particular attention is paid to the artefacts and stratigraphic interpretations of Members 4, 5 and the Name Chamber which were the primary locales of this study. A discussion of the stratigraphic complexity of the StW 53 infill and Lincoln Cave were also covered. Member 4 is roughly dated between 3.3 and 2.14 Ma (Clarke 2013) and yielded many hominid fossils yet no *in situ* stone tools. Member 5 consists of two archaeological subdivisions: the Oldowan and the Acheulean. The Oldowan deposit is dated to ca. 2.18 Ma (Granger *et al*. 2015) and is found in the eastern section of M5 (M5E) below a depth of 22 feet. It includes some fossils of *Paranthropus robustus* within a faunal assemblage accumulated through a narrow opening to the surface that is interpreted as a deathtrap. Although the Oldowan assemblage from M5E is largely intact and accumulated from a catchment area that was relatively stable during deposition, it is important to study the artefacts at a high resolution in order to investigate minor influences during site formation. Doing so will allow me to comment on the details of assemblage integrity for this early Oldowan deposit, which is only one of two large Oldowan assemblages in South Africa. The Oldowan in M5E, as in all of the Gauteng Cradle sites, has accumulated from the surface and is re-deposited in an underground context (Kuman & Field 2009). Hence site formation analysis is critical to understanding its integrity.

In addition, a connection between the lowest part of the M5E deposit and the Name Chamber has been well established by Stratford *et al.* (2012). This research suggested that smaller artefacts from M5E had winnowed through a shaft that had opened and connected the two chambers, depositing some of the Oldowan in M5E into the Name Chamber. The Name

Chamber artefacts thus allow for comparison of M5E artefacts with material known to be re-worked within the site, allowing for even more detail to be assessed in terms of site transformation.

As this thesis focuses on site formation, the theoretical history of geoarchaeology, from its conception in the early 1970s, was reviewed. There has been a marked shift toward more progressive analysis. C- and N-transforms relating to overall site analysis from the standpoint of *cultural* and *natural* processes are discussed in detail. A newer unit of study ('the deposit') was explained and an explanation of this theoretical and practical transformation presented (Schiffer 1983). The rise of geoarchaeology is presented and its importance to studies of cave and open-air site environments is highlighted. The different types of accumulation processes; anthropogenic, biogenic and geogenic which are frequently studied by geoarchaologists are discussed with examples Geoarchaeology adds an additional layer of research at a multi-scale level from macro- to micro- and greatly helps with site interpretations. This review of site formation is important for Sterkfontein where a complicated stratigraphy has accumulated and offers some ideas about possible features that could have affected the Sterkfontein sequence.

Additionally this chapter has discussed a history of micro-wear studies and the various non-digital methods that have been applied to lithics over the years in order to study lithic abrasion, such as the polar co-ordinate, clay, calliper and goniometer methods of measurement. Following this a discussion of modern technological studies in Geometric Morphometrics (GM), making use of photogrammetry, digitization and laser scanning, was presented, along with the benefits and problems that accompany them. Finally some information is provided about the effectiveness of Micro-CT to analyse patterns of edge wear when coupled with powerful and focused 3D software programs. The next chapter will provide more detail about the methods that were selected and applied to the site in order to study the complex relationship between the stratigraphy and the lithics contained therein through the use of high resolution software.

Chapter 3

3. Methodology

The methodology used in this study is intended to provide a more accurate plan of M5 at Sterkfontein Caves, and especially to address the site formation of the M5E Oldowan deposit and reworking of Oldowan lithics into an underlying cavern. Detailed mapping and high resolution MicroCT analysis of artefacts for abrasion are the focus. The methods outlined here are driven by advanced technologies that provide the advantage of interpreting the stratigraphy, formation and transformation data in the highest resolution by current research standards. Section 3.1 addresses the use of EDM and Geographic Information Systems (GIS) to record details of the site that were not interpreted during excavation in prior years. Section 3.2-3.9 concerns the analysis of artefacts from the Oldowan and underlying Name Chamber deposits with the aim of assessing abrasion states through different levels in the deposit. This is done by explaining how Micro-CT scanning was carried out and then interpreted by the use of comparison with artificially user-generated models to search for patterns consistent with abrasion or its absence.

3.1 Three-dimensional (3D) spatial modelling

The importance of specific feature modelling of Sterkfontein deposits

Until this study, the exact boundary of the M4 and M5 deposits has not been recorded in 3D georeferenced space but has only been shown schematically in Kuman and Clarke (2000). This study will therefore be important in plotting the M4/5 boundary path in order to enhance our overall understanding of the site. The boundary is drawn down to the millimetre where the breccias remain, but in cases where those contact areas have been excavated away, it is drawn as the presumed boundary based on those squares with artefacts (M5E) versus those without them (M4). Accurate mapping of several other features within the site were carried out, such as outlines of solution pockets within M5, the StW 53 infill as a deposit distinct from M5, the location of fallen dolomite roof blocks, a capping flowstone and a layer of speleothem drapery separating M4 south from M5. A specific capture of some thick botryoidal flowstone indicating formation under water was also mapped within the aforementioned flowstone.

The main aim of this methodology is to create a comprehensive high-resolution understanding of the M5E Oldowan assemblage that overlies the Name Chamber deposits. Thus, the position of the hole connecting M5E to the Name Chamber was also mapped although it is now buried under fallen roof blocks. The large goal is intended to build on the knowledge about the site and its complex stratigraphy by detailed mapping of areas that were considered re-worked or mixed, as previously described by Kuman & Clarke (2000), Ogola (2009) and Stratford (2012).

Surveying points

The Nikon Nivo (5) C series Total Station was the equipment used to produce the point clouds or geographically referenced co-ordinates (Stratford *et al.* 2016) for individually labelled features and deposit contacts within the M5 area (up to the M4 boundary). The Total Station pictured below (Figure 3.1) is an important piece of equipment to any researcher for accurately plotting sites; it works ideally in low light conditions and is easily transportable. The Total Station comes with an extendable prism reflector but was used without one in this study because it is faster for working alone and more accurate because it can get into smaller crevices than a person carrying a bulky prism rod. The benefit of being able to plot without a prism reflector means a researcher can plot points independently, quickly and highly accurately using just the viewing scope.

The equipment pictured in Figure 3.1 was set up using a tripod attachment which was then positioned and levelled over one of six main datum points or two sub-datum points positioned around the open-air part of the cave and its deposits (Stratford *et al.* 2016). The Primary Control Datums (PCDs) and Secondary Control Datums (SCDs) were globally positioned by Optron in 2012. Their purpose was to situate the Total Station in relative space so that all the points shot could be geographically recalled in real space/position.

Before surveying any points, exposures were cleaned with a mild acid (hydrochloric acid 7%) to make sure all features were adequately visible for recording. To acquire the highest resolution for the site, I decided to survey individual features such as depositional boundaries which were clearly visible in sediment colour or rock type. I shot at intervals of about 2cm along uneven contours and up to 5cm along straight contours. In total, I acquired about 10 000 points. Other features that I shot included: the outline of fallen roof blocks *in situ* in

M5, the remnant of M6 in the northern excavation wall, solution pockets, flowstone and flowstone drapery, the exposed boundary between M4 and M5 or any other deposits that could add extra information to the plan. I primarily shot from the position of SCD 1 because I could see and plot 90% of the M5 features mentioned above from this location.

Figure 3.1. The control unit of Nikon Nivo (5) C series Total Station.

Geographic Information Systems (GIS)

I used Qgis version 2.10.1 (available at https://qgis.org/en/site/forusers/download.html) to compile my digital model of the site in detail. The Coordinate Reference System (CRS) for the site and excavation grid was based on the specifications previously used by Stratford *et al.* (2016).

3.2 Micro CT scanning: materials and methods

The high resolution Micro-CT study of the Oldowan assemblage provides new data to explain the transformation of lithics and furthers our knowledge for understanding abrasion features at a microscopic level. Little literature currently exists for quantifying abrasion over an entire 3D surface and this multi-scalar study seeks to provide a method with which to do this.

The Sterkfontein M5E Oldowan Infill has yielded a large assemblage with upwards of 3000 artefacts, of which 84.17% is SFD and 93.6% of the assemblage is vein quartz (Kuman & Field 2009). Two thirds of this material was initially classed as fresh (Field 1999), which attests to knapping activities occurring near cave entrances and its rapid preservation in the M5E infill through a narrow shaft like opening (Kuman & Clarke 2000; Kuman 2003). As the landscape around the cave entrance was considered stable, the large proportion of SFD provided an opportunity to investigate artefact abrasion, which I hoped would shed some light on details of how the material accumulated and was re-worked within the site. In addition to the smallest SFD being under-represented in the Oldowan assemblage, Stratford's (2012) excavation of the Lower Name Chamber, located directly below the M5E Oldowan deposits and connected by a thin feeding shaft (Clarke 1994), showed that intermixing and movement of deposits can occur within a site. Stratford (2012) has shown that prior to the calcification of the upper M5 deposits, some material shifted into the lower gallery from M5E and was deposited there. An over-represented amount of 84.17 % SFD consisting of 72.4% in the 10-19 mm category and 9.9% below 10 mm was excavated from the M5E deposits, and an even larger sample of SFD (91.2%) was excavated by Stratford *et al.* (2012) in the Name Chamber. Due to the inferred linkage between these sediments, I thought it would be best to study them further.

The winnowing of SFD from the upper M5E all the way through the Oldowan sediments to the lower reaches of the Name Chamber Gallery suggests a period of erosion or movement within the deposits, which could have caused abrasion. For this study, I selected a variety of lithic types for analysis, although the largest focus was on SFD in quartz because of its dominance.

Previously it has been difficult to analyse such small pieces such as the SFD and such material was often ignored, but by using very high resolution scanning equipment I was able to do so both for tool types from the main M5E assemblage, as well as some redeposited in the Name Chamber. The way I did this is discussed below. The equipment employed was the Nikon Metrology XTH 225/320 LC Dual source Micro-CT scanner (shown in Figure 3. 2) and was purchased by the University of the Witwatersrand in 2012, where it is housed in the Evolutionary Studies Institute (ESI). At the forefront of engineering, this machinery has up to one hundred times the pixel resolution of any medical CT scanner and proved exceptional for scanning the Oldowan artefacts. The scanner uses X-rays to take cross-sectional photographs of the subject which is positioned on a self-rotating tray. It then compiles the photographs into a 3D model that can be viewed and/or manipulated using 3D software on a desktop PC. The models can be analysed internally or externally. In this study the external surface was the most relevant and I did not analyse any internal properties.

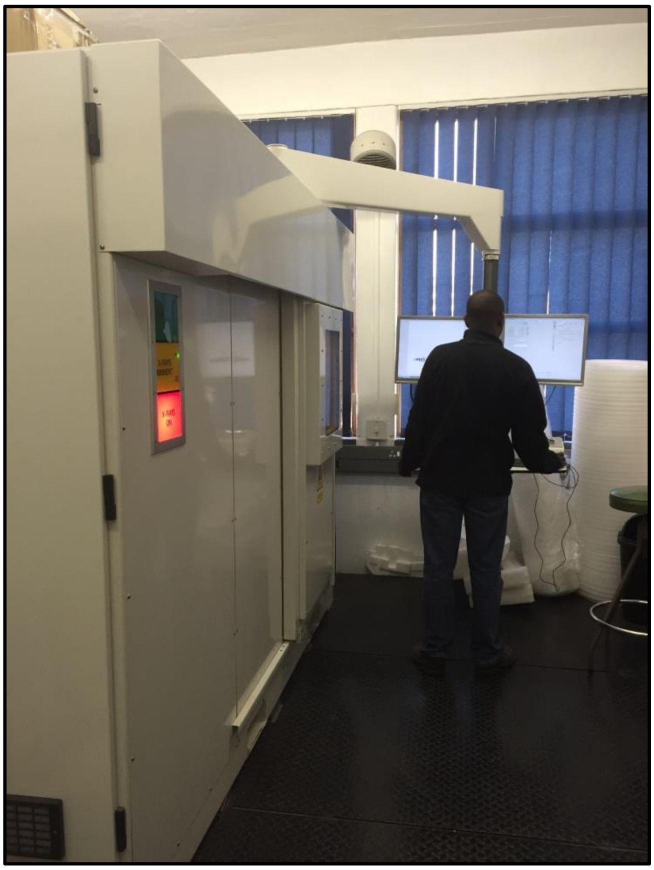

Figure 3.2. Dr. Kudakwashe Jakata working at the Micro-CT scanner.

Sampling materials

The majority of samples analysed in this study came from the Oldowan assemblage in M5E totalling 3513 excavated pieces between lines 49 - 58 at a depth between 22 feet (6.7m) and 36 feet and 10 inches (11.2m) below datum (Kuman & Clarke 2000; Kuman & Field 2009). A second comparative sample of SFD (*n* = 51 pieces) all came from the Name Chamber. Both samples were selected randomly in Excel through a randomization formula, but from varying depth groupings: 9’8’’ (3m), 26’2’’ (8m), 32’8’’ (10m) and 91 feet and 8 inches (28m) below the feeding shaft (R57 area), which lies 41 feet (12.5m) lower than the M5E excavation and connects the two areas together (Stratford *et al.* 2012). The reason pieces were selected at varying depths was to investigate how much more abrasion, if any, had taken place on pieces as they moved deeper into the cave system. The Name Chamber sample consists of only 51 artefacts due to scanning access, time restrictions, and budget, but also because the main focus for this study is the M5E Oldowan assemblage. The Name Chamber data act as an additional subsidiary comparison where movement to a lower cavern is known to have occurred (see Figure 3.3).

According to Stratford (pers. comm.), spit depths were recorded in the Name Chamber but are possibly irrelevant due to the steep nature of the talus and thus the probability of an already uneven distribution. My samples from M5E were chosen using random Excel sampling as explained above. I categorised individual pieces from within the four largest assemblage components: SFD ≤ 20 mm (*n* = 426), and the following material that is all ≥ 20 mm: Complete Flakes (*n* = 59), Incomplete Flakes (*n* = 180) and chunks (*n* = 74). See definitions below. For consistency of raw material, all pieces analysed were quartz, and because it was the most common raw material throughout both the M5E Oldowan and the Name Chamber.

Sample definitions (following Kuman & Field 2009)

Complete Flakes: Complete flakes include pieces ≥ 20 mm struck from cores. They have complete striking platforms, bulbs of percussion, as well as tapered, stepped or hinged terminations.

Incomplete Flakes: Incomplete flakes include: broken flakes ≥ 20 mm which may exhibit a bulb of percussion and/or stepped or hinged terminations; split flakes; and flake fragments that are proximal, lateral, medial or distal portions of flakes (Field 1999).

Chunks: Chunks are angular or blocky pieces ≥ 20 mm in maximum length. They include pieces produced during knapping of a core or flake, but they exclude core fragments.

Small Flaking Debris (SFD): Small flaking debris includes all pieces < 20 mm in maximum dimension, grouped in this category as waste due to their small dimensions.

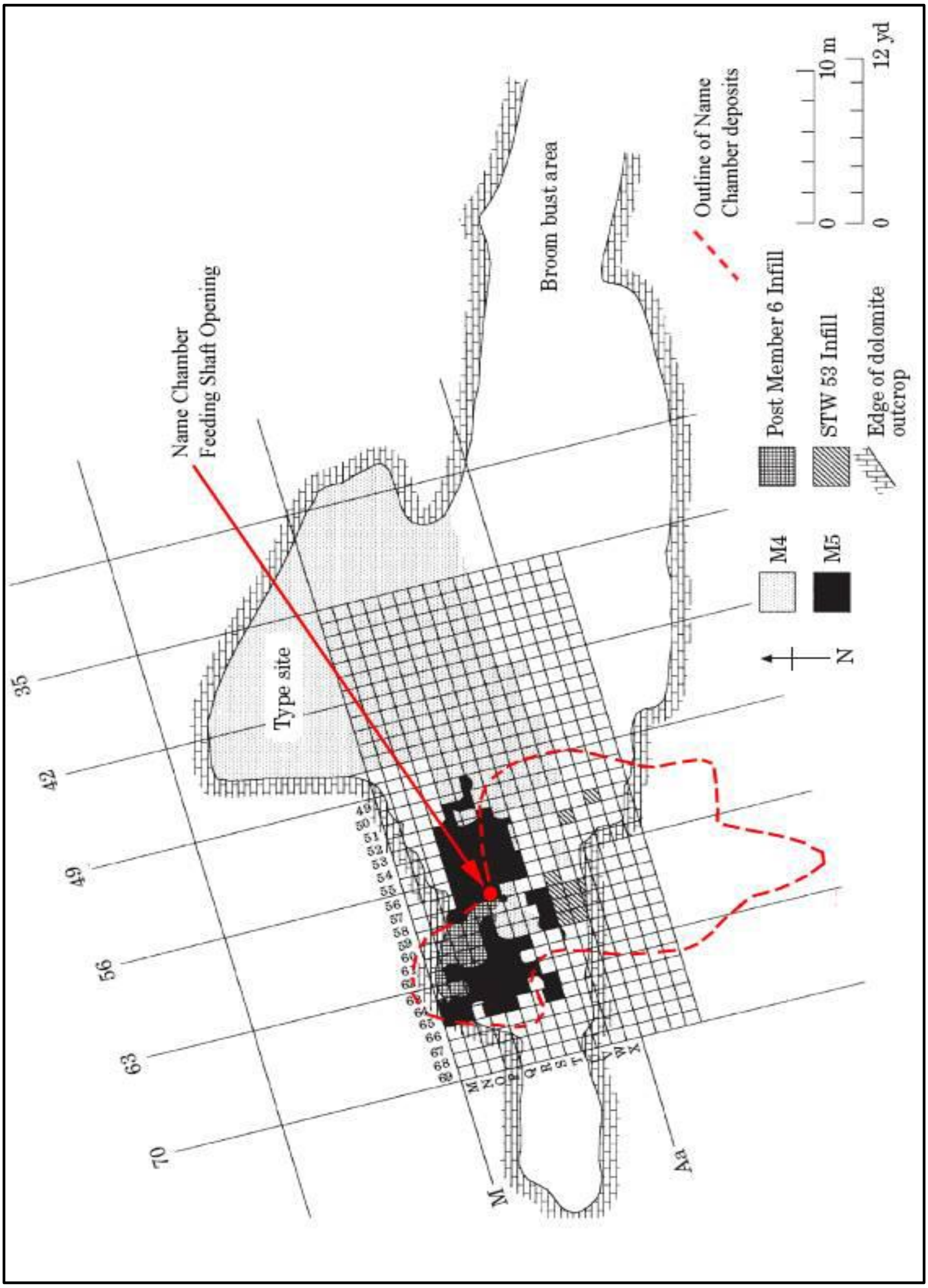

Figure 3.3. Plan of the site showing M5 with the outline of the subterranean Name Chamber in red. The feeding shaft location is indicated in Square R57, and the Oldowan M5E Oldowan area is located between lines 49-58 (from Stratford *et al.* 2012: 166).

Mounting scans and the "Spiral Scanning Method"

The Micro-CT scanner can scan objects that fit into a supporting platform with a radius of 23cm, but larger objects can also be scanned and stitched together, making the scanner a versatile tool for modern research purposes. Since the scanner is very sensitive to the density of the subject it is analysing, the mounting tray had to be very specific. I needed to be able to scan a large number of pieces in the space of a 23cm diameter table primarily for efficiency, and also in accordance with my budget for scanning time. I had considered sponge or suspension of artefacts in liquid, but the former scan operators (Dr. Kudakwashe Jakata and Dr. Kristian Carlson) recommended that a base tray of polystyrene would serve as an appropriate material. In the end, a polystyrene tray with semi-loose grained porosity was the most effective. I used an exact 23cm diameter builder's saw-blade and traced out the outline of the tray with a pencil, and I then used a polystyrene cutter to cut eleven round trays of about 4cm thickness and 23cm diameter for scanning mounts (Figure 3.4 - 3.5).

Most artefacts were easy to place into the polystyrene and I later removed the pieces using tweezers. I had to ensure that there was no contact between pieces above or below each tray or the models would appear merged during visualisation. I scanned 11 individual trays one at a time and I made sure the lithics in each tray were stable by embedding them firmly within the polystyrene. Initially I did a few test scans to figure out the best orientation of the pieces in the trays, and standing the pieces vertically yielded the best results. Scanning pieces in rows did not prove adequate because the final 3D model surfaces needed to be placed in an order that was easy to recall. The best option was a spiral (essentially a straight line that fitted the circular tray; see Figure 3.4). Rows were also not feasible because of the danger of creating beam hardening which is when high and low beams of the scanner do not pass through objects at the same consistency, effectively ruining the resulting image. In other words, scanning through too many specimens at once could complicate the outcome as the beams used to produce an image become irregular.

I scanned eleven trays in total and managed to scan my entire SFD sample in three separate trays (9, 10 and 11). The small size of many pieces <20 mm meant that I could easily fit over 200 in one tray. Separately I recorded each tray and noted any distinguishing features. Each tray was photographed so I could refer back to it and successively re-number the pieces in the visualization phase. See Figures 3.4, 3.5, 3.6, 3.8, 3.9 and 3.10 for examples of the trays.

Figure 3.4. Scanning Tray 1 (incomplete flakes).

Figure 3.5. Scanning Tray 9 (SFD).

Each tray was then placed individually in the scanner by the operator Kudakwashe Jakata. Various specifications were used to prepare the scans (see Table 3.1). All trays were scanned between 75 and 120 kilovolts (kV) and 80-120 microamps (uA), with a voxel size of between 124.2-129.7 microns. The number of the projections done on each tray was 3142 and the angular step between them was 0.11 degrees and at 1 Frame Per Second (FPS). In order to prevent beam hardening from ruining our scans, various pre-sets were differentially set on the scanner according to the tray.

Technical notes: *It is important to note that should any scanning aspects change, it is because scanning was done over a period of time and the Micro-CT scanner had various service maintenances which would make some scans vary minutely in specifications but would not affect the overall scans or their resolutions. It is also important to acknowledge that because all samples analysed in this study are individual in their geometries and in the visualisation step they contain unique triangles, the voxel (a 3D unit that describes a point in space similar to a pixel in 2D) and counts differ scan to scan.*

Table 3.1 A table showing scanned settings per tray.

Tray Number	Voxels X, Y, Z	Voxel Size X, Y, Z (mm)	Projections	Angular step	kV	uA	Beam Hardening Pre-set	Filter Pre-set	Frames Per Second (FPS)
1	1816, 1922, 774	0.1255	3142	0.11	120	120	6	1	1
2	2000, 2000, 754	0.1242	3142	0.11	120	120	3	1	1
3	2000, 2000, 775	0.1242	3142	0.11	120	120	2	1	1
4	2000, 2000, 843	0.1242	3142	0.11	120	120	2	1	1
5	1788, 1763, 921	0.1242	3142	0.11	120	120	2	1	1
6	1896, 1859, 767	0.1242	3142	0.11	120	120	3	1	1
7	1731, 1676, 663	0.1242	3142	0.11	120	120	3	1	1
8	1693, 1860, 745	0.1297	3142	0.11	120	120	2	1	1
9	1997, 1998, 466	0.1297	3142	0.11	80	80	3	1	1
10	2000, 2000, 2000	0.1297	3142	0.11	75	80	3	1	1
11	2000,2000,2000	0.1287	3142	0.11	105	105	3	1	1

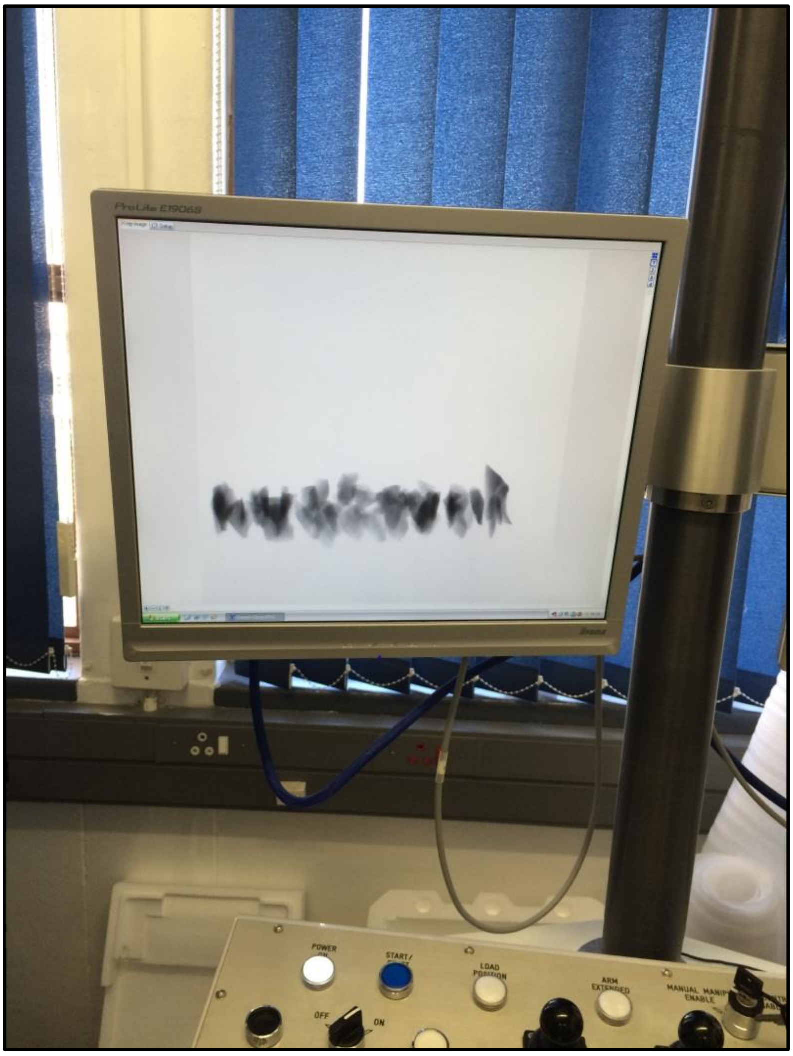

Figure 3.6. Horizontal preview of a tray in X-ray view prior to scanning.

Trays were placed in the scanner atop a larger piece of polystyrene (as shown in Figure 3.8) on the platform and secured with double-sided tape to stop any movement during scan rotations. Bubble wrap was placed on the floor of the scanner in the unlikely case that any pieces dislodged and fell out of the tray. Each scan took approximately one or two hours to run, followed by an extra 20 minutes or so to apply a programme called CT Pro to make sure all the scans were appropriate. CT Pro was used to remove any extra noise that may have entered the scans and reduce anything that could compromise the quality of the scan. See Figure 3.7 for an example of Tray 1, which was scanned in the plastic tubing.

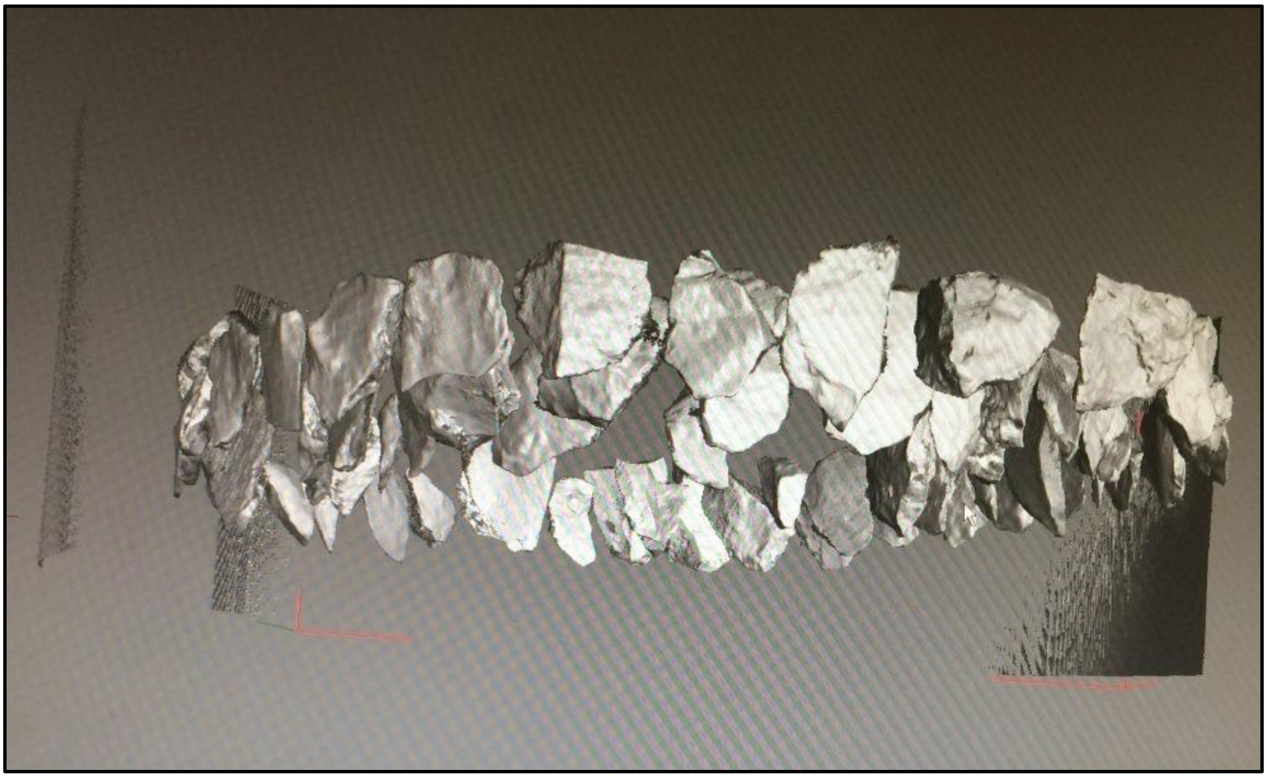

Figure 3.7. Tray 1 showing walls of plastic tubing picked up during a scan.

The walls of the tube are visible and can be removed using this software. The software automatically distinguishes between the different material densities and then can remove these from the scan accordingly. For this study, the tubing was left in for illustration purposes and to show that noise can also be removed in the next step should it not be done automatically in CT Pro.

Figure 3.8. Dr. Kudakwashe Jakata placing SFD scanning tray on scanning podium without plastic tubing.

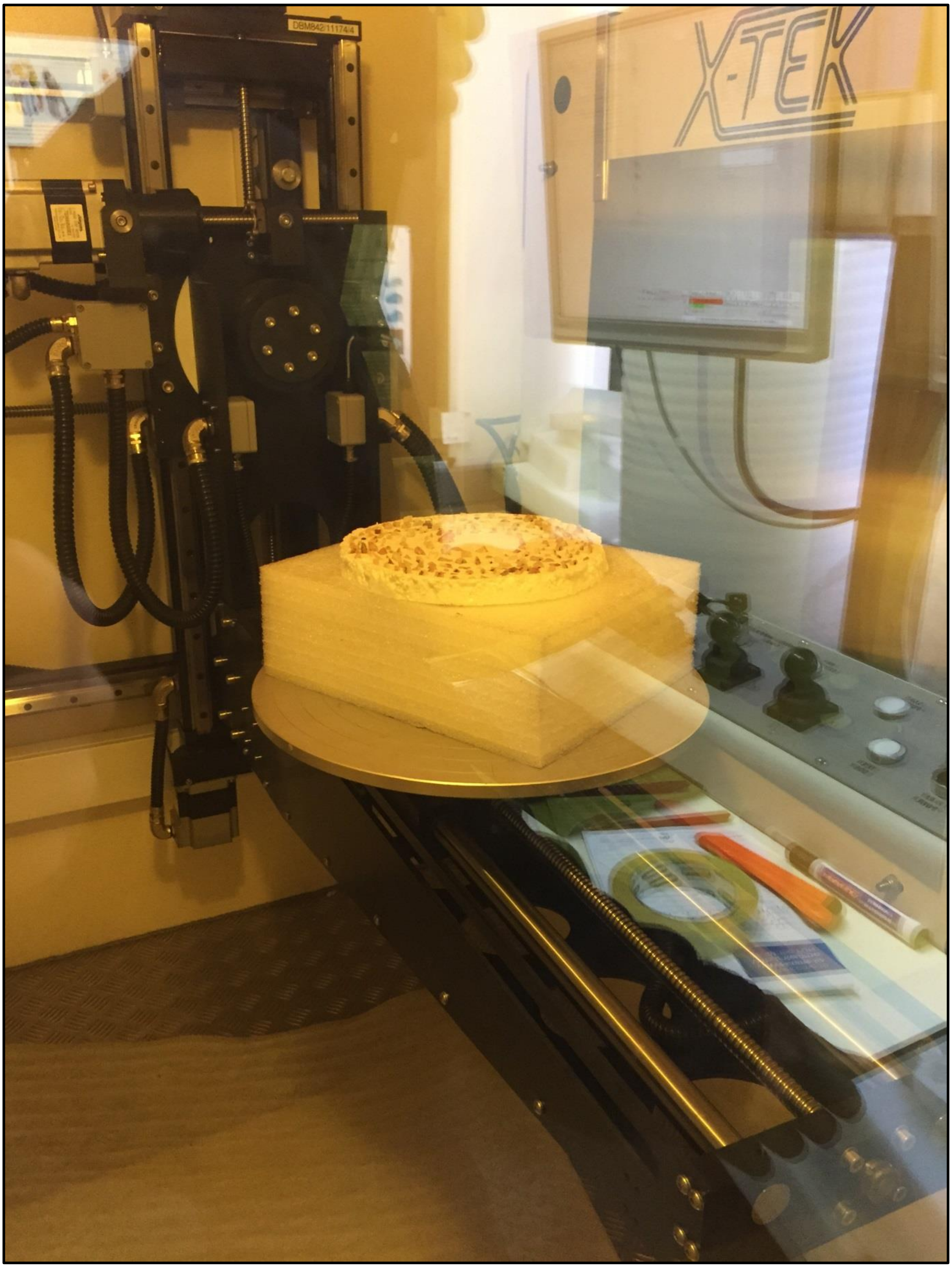

Figure 3.9. Tray 9 atop scanning plate inside Micro-CT. Note the floor is covered by an emergency drop sheet.

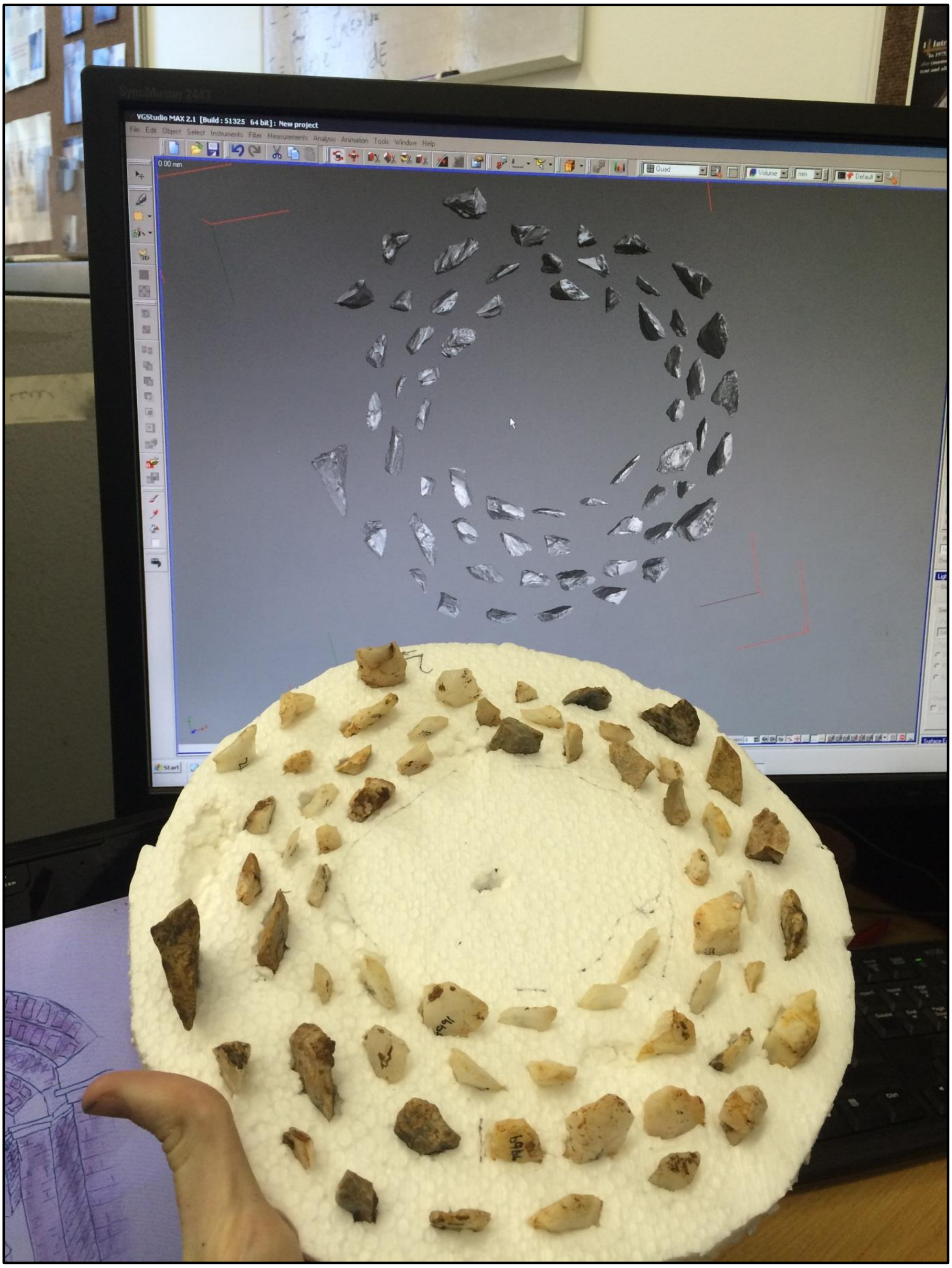

Figure 3.10. Tray 2 and its 3D counterpart in CT Pro after a successful scan.

3.3 Post-processing, iso-surface visualization and transformation

All 11 scan files were saved as reconstructed volume files, each complete with a file that details each tray's metadata. All scans were stored on a single external hard-drive with a total size of less than 50 Gigabytes (20 Gigabytes for the 11 trays and an additional 20 Gigabytes for individual scans) and then exported to the Visual Image Processing (VIP) lab in the Evolutionary Studies Institute (ESI) at the university. There, all 11 scans entered the main stage of post-processing, which included image visualisation, transformation, separation, measurement and recording. The program used to carry out this research is called Avizo 9, provided by FEI Visualization Sciences Group (France), which is a multifunctional 3D tool that is primarily designed to analyse the internal structures of CT-scanned data but can also produce detailed external surface renderings, landmarks and measurements. The programme can be used perfectly within the realm of geometric morphometrics (GM). The programme has a simple user interface and very few hours of training are required to learn to use Avizo. I chose to use primarily Avizo for my research because I have had about five years training in this specific programme (Couzens 2012), and it was suggested at the forefront by my supervisor Kristian Carlson for running the larger file sizes produced by the Micro-CT scanning device. Additionally Avizo is a programme that is orientated to address visualizations of both internal and external structures of a given scan so in that way it can prove advantageous should further research on internal facets wish to be studied in the future. Other 3D programs like Geomagic and 3DS Max exist but these do not account for internal structures like those produced by the Micro-CT scanner used in this study. The computers in the VIP lab were suited for this research because they have high amounts of Raw Active Memory (RAM) which were useful for opening and running each tray (~600 megabytes to 1 gigabyte each) for the entire conversion from real life volume to 3D surface. These computers are highly modified to handle large amounts of 3D processing power and further ratify how high resolution this study is.

Scans of the trays were opened and an "iso-surface" module fixed to each tray. This module made the entire tray visible and open to manipulation. Since this research is based on surfaces only, we needed to convert the 3D volume file to a smaller and more manageable format. To do this, we simply used applied thresholds to remove any unwanted noise that could have been added or subtracted to the surfaces. Figure 3.11 shows Tray 1 represented as an iso-surface. Tray 1 was scanned in the plastic tube, and its edges are still visible. This method was used in order to test the effectiveness of Avizo thresholding (Figure 3.12). A coarse surface indicated by the arrow shows how much material is added or subtracted when trying to phase out noise. Only surfaces that are not affected by over- or under-thresholding are viable for the method detailed here. Such examples were not included in this study and are purely for illustrative purposes.

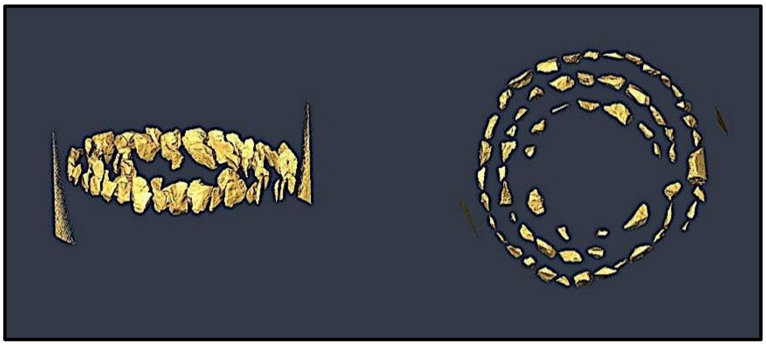

Figure 3.11. Side view and top down view of Tray 1 iso-surface including plastic tubing prior to thresholding in Avizo.

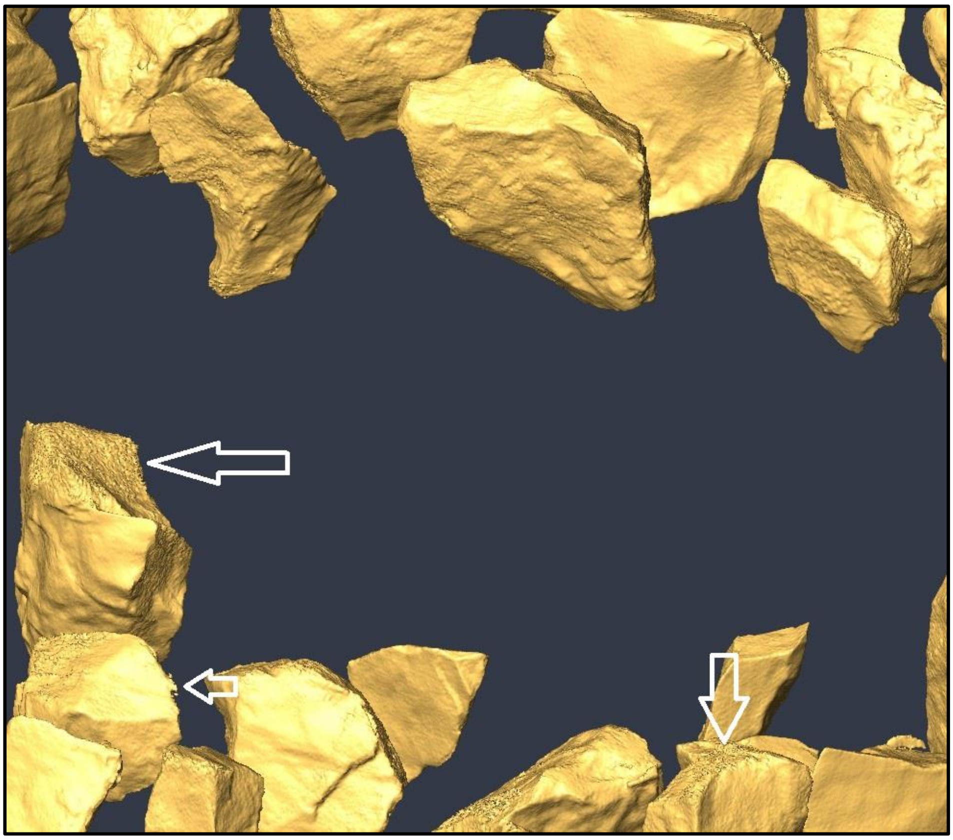

Figure 3.12. A close-up of iso-surface thresholding.

Segmentation

The next step of post-processing was to create an individual Standard Template Library or .STL file (an image or 3D image file) for each stone tool, recording the original number and saving each tool individually. To do this I opened the volume file for each tray and used a tool called 'volume editor' to pencil around individual tools and then cut them out of the larger group. Following this, each was given an iso-surface module (essentially a replica file) from which a new .STL file was created for each artefact and saved before deleting the recently created iso-surface. In this way we were able to keep the original tool's surface and volume in a much more compacted and easily transferrable file.

When pencilling around an artefact, the researcher must be careful to only focus on the area around one tool at a time and avoid any other tools or instances of noise. For trays with smaller spaces between artefacts, the zoom and rotate functions were useful in making sure nothing extra was included. Once a piece was separated and saved, it would be coloured in the tray to serve as a reference position for the next segmentation in the queue (Figure 3.13). Trays were segmented from the outermost spiral inward toward the middle in line with the labelling and placement protocol employed during the setup step, i.e., in order from 1-200.

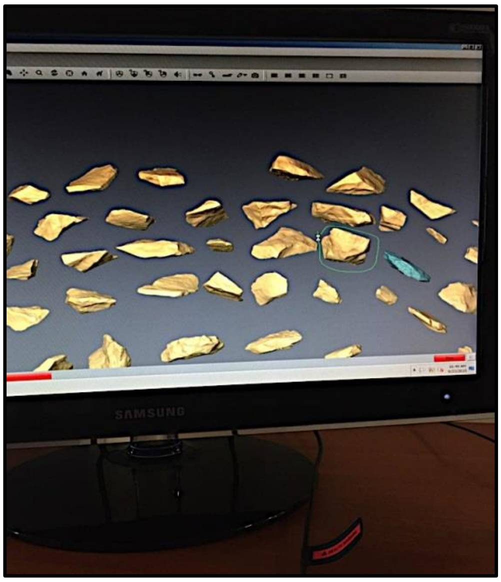

Figure 3.13. An artefact is circled prior to individualisation from the group as a whole. The previously segmented piece is highlighted blue to serve as a placeholder when analysing larger spirals.

To check that all artefacts were separated and saved in their original positions and to eradicate any skipping or mix-ups, the original volume tray (yellow) could be loaded as a whole and each tool selected in sequential order to create an overlay of pieces (blue), as shown correctly in Figure 3.14. It is important to note that by transforming a volume file into a surface rendering, there were no adjustments to the volume/surface areas or any other such variables being measured.

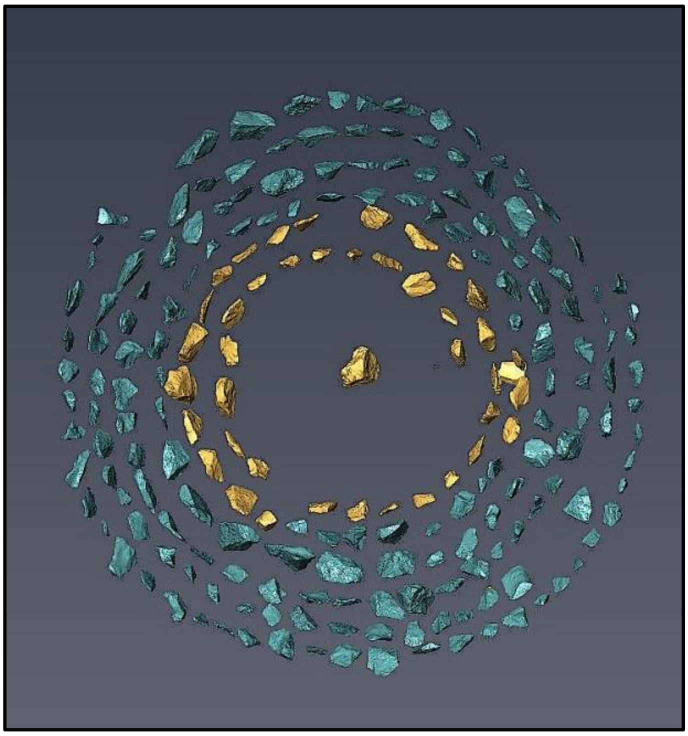

Figure 3.14. Tray 10 individualised artefacts are checked for position post-separation procedure. This is done by overlaying complete, fully separated artefacts (yellow) over yet to be separated artefacts (blue).

3.4 Measurement basis

This research seeks to quantify and analyse the rounding of edges of extremely small or even miniature tools that are in this case quite well distributed in a stratigraphic model. Up until now these tools have been recorded as largely fresh to the naked eye (Field 1999). Our primary concern with this assemblage has been to look closely at the actual surface of the tools in question with the highest resolution we could achieve. Grosman (2016) explains that only by imposing a very specific methodology to a given model can we interpret results from the model we are trying to study. Logically the artefacts cannot speak for themselves so the procedures applied, along with the attributed relationships of the scanned model, are fundamental to our understanding of abrasion in this case. The following sections explain the method.

Triangular mesh

When a surface image is created by Avizo, or any other 3D software, it is usually represented to the viewer as a group of tightly adjacent triangles. These triangles are essentially composed by the scanning process which records a number of points (Figure 3.15) over the entire topographical surface of an object. The points are then transformed into ‘nodes’, (Figure 3.16) which are a series of triangles connecting to one another across the surface of the object (Figure 3.17). These triangles provide the means for us to interpret the degree of rounding across an artefact surface, namely the artefact edge in this case.

Please note: Avizo software smooths surfaces automatically by default. Scanned images are in fact of very high resolution (as per CT scanning procedures) but may not appear as sharp in images where the mesh is set to ‘shaded’ view such as in Figure 3.17.

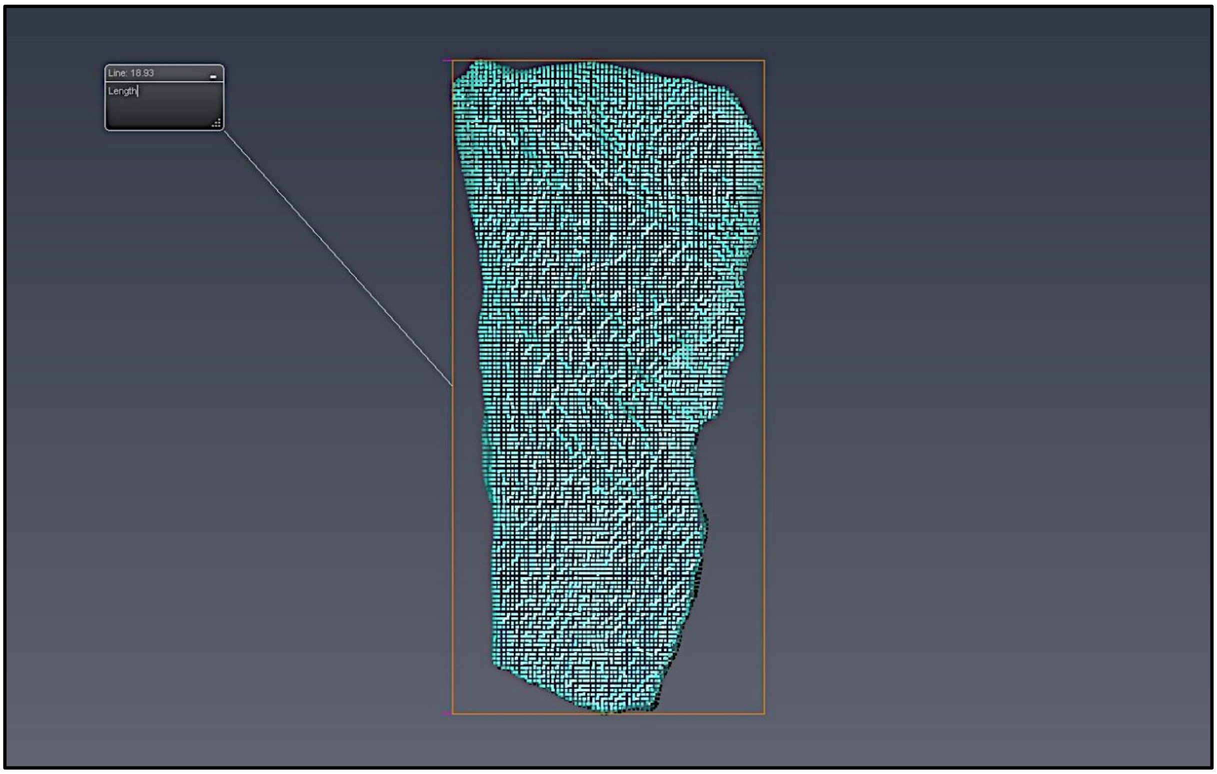

Figure 3.15. An artefact from the SFD component (Maximum Length (XL) = 18.93 mm) as defined by the bounding box (Couzens 2012) and exhibited as points across the surface.

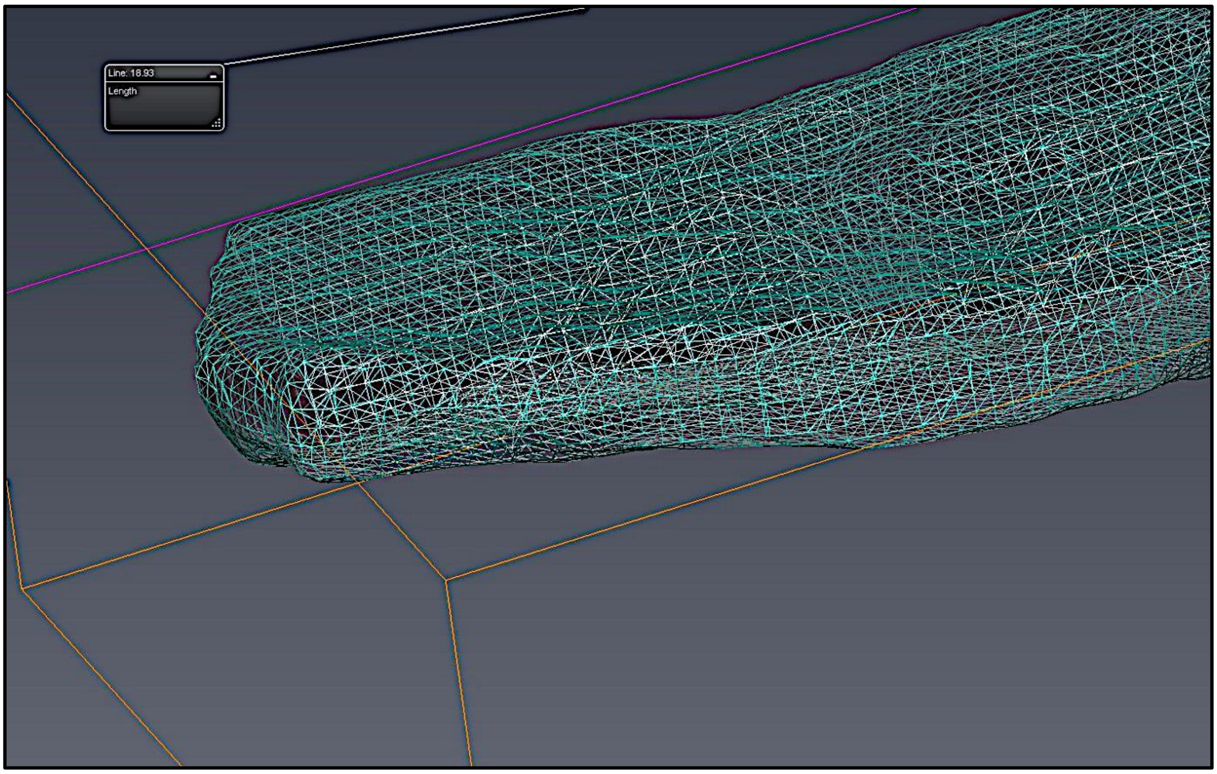

Figure 3.16. Hollow surface mesh as represented by conjoined nodes for an artefact from the SFD component.

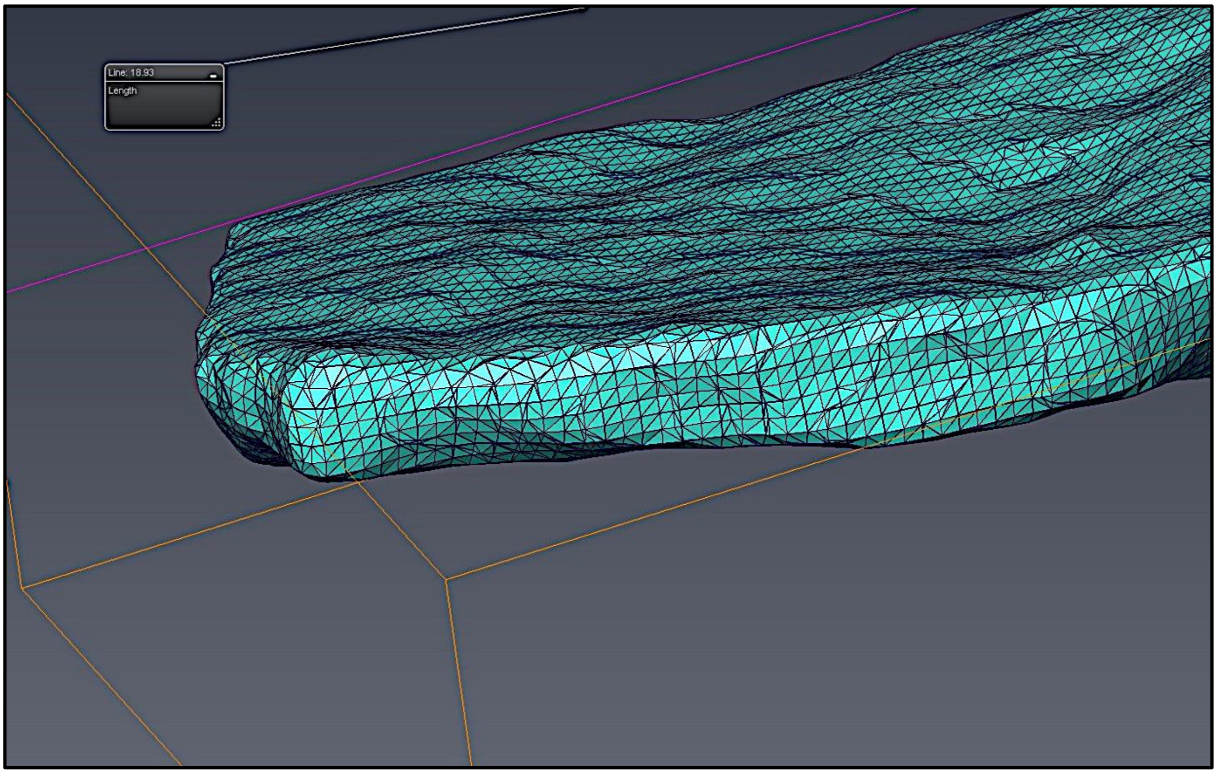

Figure 3.17. Shaded surface mesh complete with angle and relief/topographic data incorporated.

Avizo allows us to measure many variables for each 3D scan; these include details of the mesh and accurate Volume and Surface Area quantities. The surface mesh thus allows the surface geometries of the artefact to be interpreted in a new way. As discussed in Chapter 2, the edges are the parts of an artefact where differential abrasion is most visible, depending on the sedimentary context of the artefact, and thus measureable. The method presented here provides a quantitative analysis of the different tool types, which vary in shape and in some specifics of edge wear. By analysing the data from and between all triangles on a given scan, I aimed to create an index to quantify how much abrasion a given tool had undergone over its entire surface. I also describe a method for measuring more specific regions.

Definitions

Some of the definitions below are used in 3D programs to explain the visuals discussed above and Figure 3.18 visually shows some of these:

Surface: The outside part or uppermost layer of a lithic.

Triangle: A section of a surface defined by three lines and three vertices that connect, also called a face.

Triangular Mesh: A polygon mesh that is comprised of triangles in 3D that are connected by their common edges or corners.

Dihedral Angle (DA): For each tetrahedron edge the dihedral angle is defined as the angle between its adjacent faces. The mathematical definition is based on each plane with equation: $Ax + By + Cz + D = 0$ and $Ex + Fy + Gz + H = 0$ for each plane is then:

$$\theta = cos^{-1}\left(\frac{AE + BF + CG}{\sqrt{A^2 + B^2 + C^2}\ \sqrt{E^2 + F^2 + G^2}}\right)$$

Dihedral Angle Quality: The optimal value obtained for all dihedral angles is defined by the equation: $2\arcsin(1\sqrt{3})$ or (~70.5º).

Vertices: The meeting of two surfaces along an edge.

Edges: Lines between Vertices.

Edge Length: The length in units of the single side of a triangle.

Patch: A group of triangles separating two adjacent regions and having the same boundary identification marker.

Face: A triangle.

Number Faces: Number of triangles on a given surface.

Number Points: Number of vertices should correlate as 3:1 triangles.

CAD: Computer Aided Design: Creation, modification, analysis or optimization of design (Tea Jashishvilli, Pers. Comm. 2014).

Abraded: Scraped or worn away by friction or erosion.

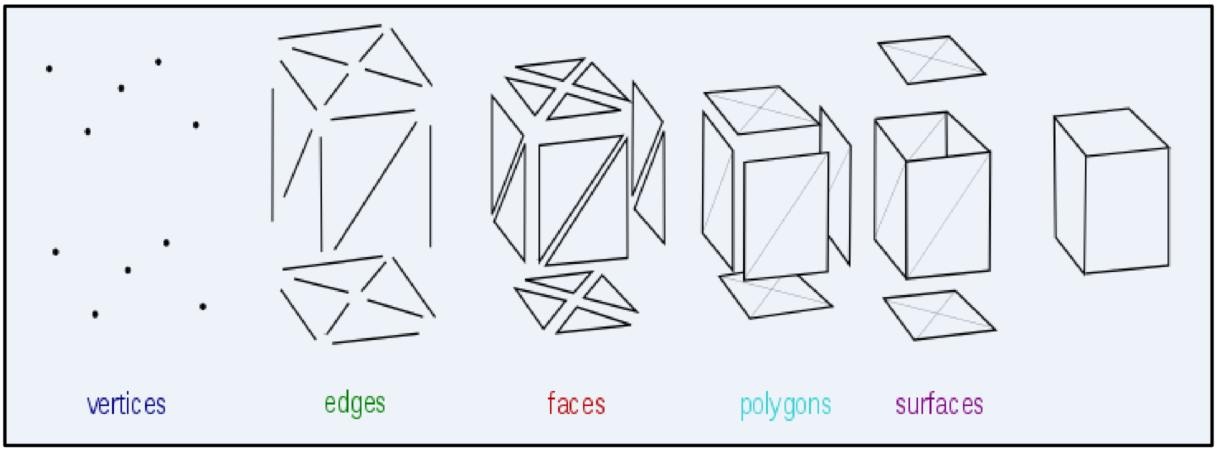

Figure 3.18. The various elements of a 3D polygon mesh (from Avizo Help)

3.5 CAD basis and hypothesis

Since I was looking to analyse form and see which measures a 3D surface can provide, I produced several basic images to compare with my data (Figure 3.19). These consisted of three types of model: a cube, a sphere and a square-base pyramid. Each model was produced at 500 mm^3 and 1000 mm^3. The cube would represent a ‘sharper /more angular/acute/less abraded’ example; the sphere would represent a ‘rounded/less angular/dull/more abraded’ form; and the pyramid would be similar to a cube in angularity but with a tapering end.

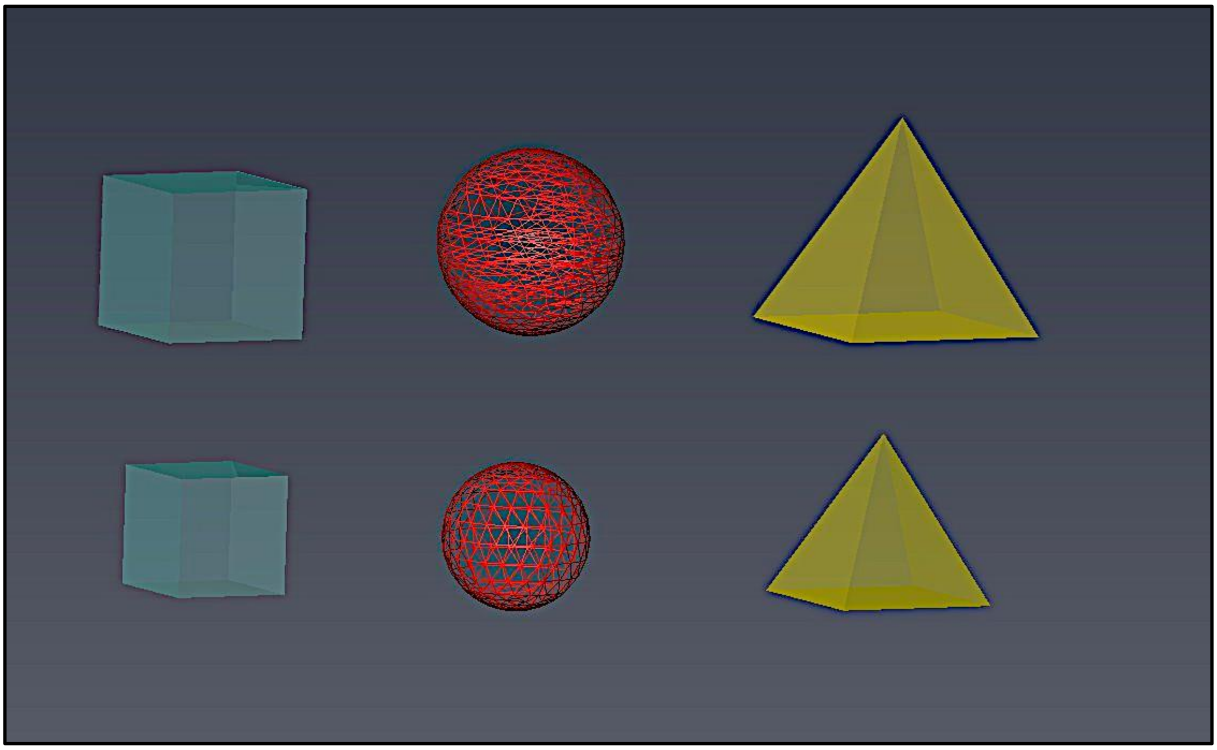

Figure 3.19. Screen capture of user produced CAD surfaces at 1000 mm^3 are shown in the top row of the image and 500 mm^3 examples are shown in the bottom row.

I produced these images using a programme called AutoCAD, usually used for engineering, which can produce 3D shapes at any volume, and then I tested their efficacy in Avizo and Geomagic Studio to confirm that their volumes were portrayed accurately across programme platforms, with each as close to 500 mm^3 and 1000 mm^3 as possible.
(*Technical note: a sphere is harder to produce as exactly 500/1000 in CAD and dihedral angles reflect this. The reason for this is because surface meshes are composed of triangles which are a completely different shape from circles. When a program tries to cover a surface there is always a small loss of volume at the edges.*

I created two of each model category because I wanted to test what impact the variation in volume would have on any other relatable variable (e.g. mean length) for a given shape, which would give this study more accuracy. By analysing the variables associated with each of these shapes, we can compare them across the lithic types: flakes, incomplete flakes, chunks and SFD from the Oldowan of M5E, along with my additional pieces from the Name Chamber.

The primary hypothesis, based on the CAD images and interpretation with surface mathematics, holds that a surface deemed to be more angular or with a flat continuous relief should contain fewer faces/triangles but larger edge lengths. And if we consider something to be more rounded, it would display a larger number of faces with more similar edge lengths. We also expect a piece with a higher value of dihedral angle to be more rounded (169-179º). Dihedral angles can explain much about the shape of an overall surface. This is an entirely new method for analysing and quantifying smaller pieces that are otherwise not viable for analysis. The models (Fig. 3.20) show that both cube and pyramid have a bimodal distribution of angles, 0º (or 180º which is the same as 0º) for the flat faces and 90º and 63.4º respectively between the sides; in contrast, a sphere has a larger range of angles between ~139º and ~170º and would display a more unimodal distribution, statistically because there is more of a distribution across values (Figure 3.20).

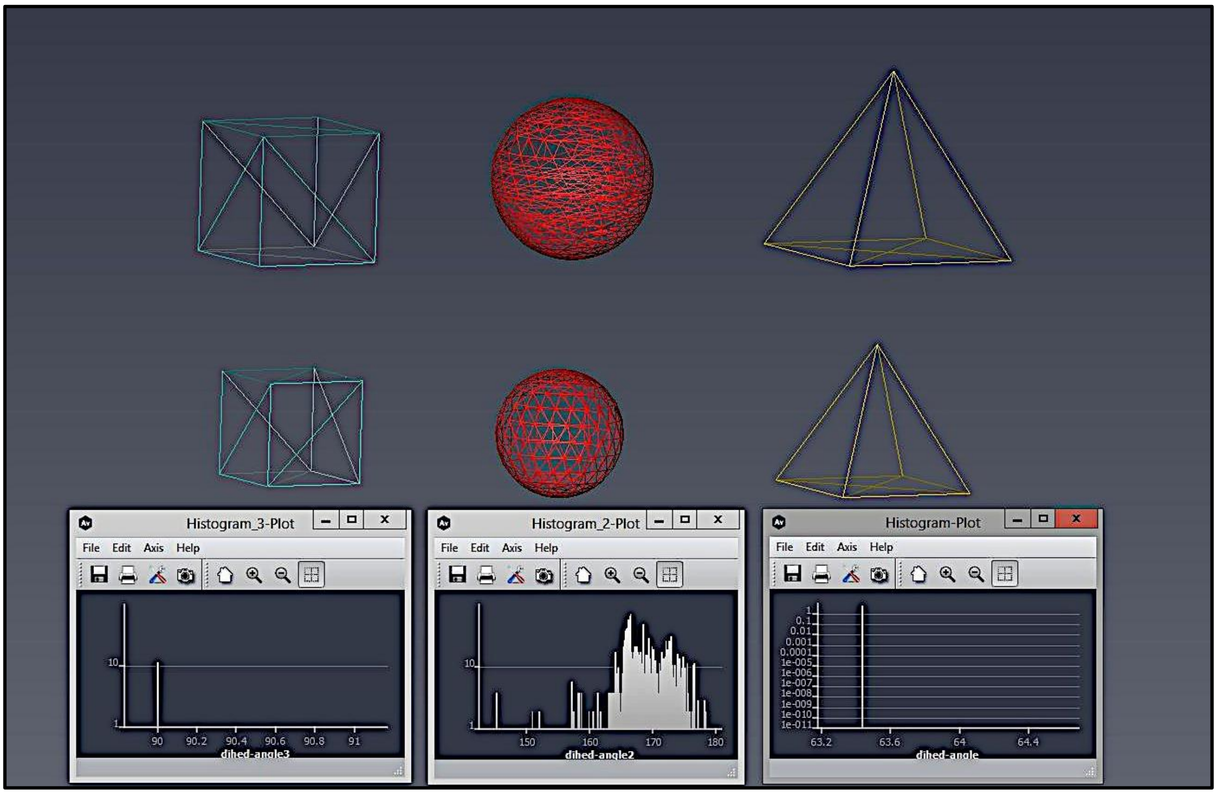

Figure 3.20. Screen Capture showing lined projections with associated histograms showing angle ranges for each model, i.e., Cube (bi-modal), Sphere (uni-modal) and Pyramid (bi-modal).

Table 3.2 details the exact number of faces and values for cube, sphere and pyramid. It is clear that, as hypothesized for the cube and pyramid, the number of faces does not increase as its volume increases, however its mean dihedral edge length does (~2/3 units), while its dihedral angles stay at an expected 90º/63.4º respectively. As a sphere increases in volume, it also increases in number of faces by about double, while its edge length values stay relatively the same (0.02 units difference), and the dihedral angles displayed are much more open at about (~169º). These geometric models create a good picture of how we can describe shape by analysing the dihedral mesh.

Table 3.2. Comparative attributes of CAD basis models.

Type	Number Points	Number Faces (triangles)	Number Edges	Mean Edge Length (units)	Mean Dihedral Angle (º's)
Cube 500 mm^3	8	12	18	9.03	90
Cube 1000 mm^3	8	12	18	11.38	90
Sphere 500 mm^3	353	702	1053	0.97	169.6
Sphere 1000 mm^3	735	1466	2199	0.99	169.4
Pyramid 500 mm^3	6	8	12	10.75	63.4
Pyramid 1000 mm^3	6	8	12	13.68	63.4

Previous research on edge angles focuses on the measurement of a single value in an arbitrary location for defining a piece's edge angle and ultimately its abrasion level. The method proposed here uses an Avizo algorithm to measure every single dihedral angle across an entire artefact surface and for thousands of triangles and contours (up to +50 000). These values can be saved into Excel in a statistical file type called ASCII (.am). The values of all dihedral angles across a surface are then averaged out and applied to each artefact type, which explains its overall abrasion, and then we compare whether the values for a given piece are closer statistically and quantitatively to our "fresh" cube/pyramid or "abraded" sphere basis models. This research produced an extremely large dataset for tools that are usually under-studied due to their tiny size. The measures of dihedral angles provide a very general analysis of total abrasion and a new quantitative method that perhaps, with some refinement, could be used at an even higher resolution.

Bearing this in mind, a preliminary subsample of artefact types was done, followed by a more focused analysis of thinner and thicker edges, and the quantifications were then checked statistically. The results of both the overall abrasion and shape analyses and of the more specific edge analysis are presented in Chapter 4.

3.6 Resample test (a technical note)

I used Avizo to do a base check on how artefact variables change if we simplify the actual triangle mesh so we could better understand the changes in shape of given artefact types to ensure an overall better understanding of what information was being retrieved from our scans. I used an editor tool called "Simplification Editor".

Figures 3.21, 3.22, 3.23 and 3.24 show my CAD images analysed using the Simplification Editor at full faces, 50%, 100 and 20 faces. Table 3.3 depicts the numerical representation of this application at the 50% simplification level. It is clear that changing the surface values of any kind of piece holds obvious problems for analysis, and that simplifying the surface of any kind of piece from its initial scanned surface can lead to a different type of result. Spheres become more angular and angular pieces become more deformed as can be seen in the final image: Figure 3.24. In other words, simplifying any kind of mesh is going to result in a more angular, or in this case a less abraded, representation of the data.
By looking at our models, we can see that the cube deforms instantly because by definition a cube should not have less than 12 faces. Figures 3.22 to 3.24 show examples of how models change as they are simplified.

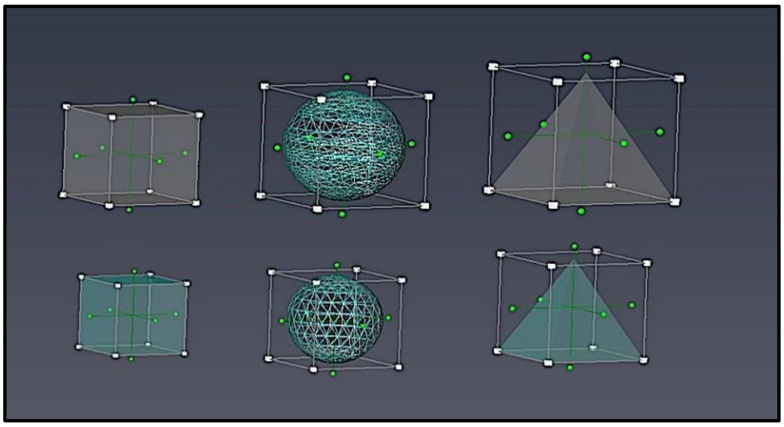

Figure 3.21. Normal basis models at full triangle counts.

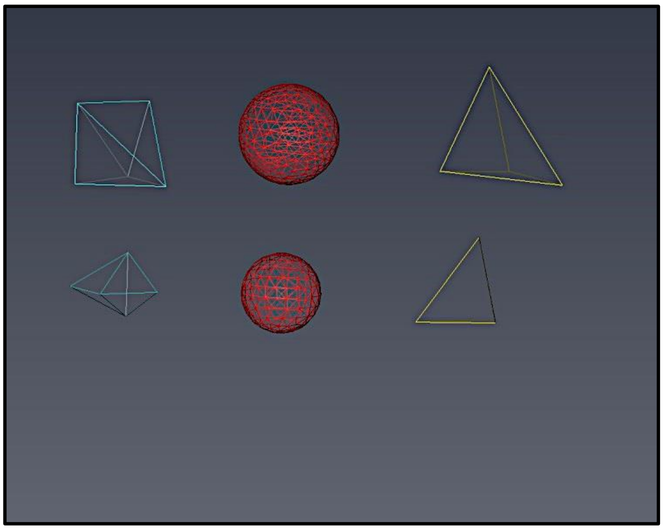

Figure 3.22. CAD models with 50% simplification of triangular faces.

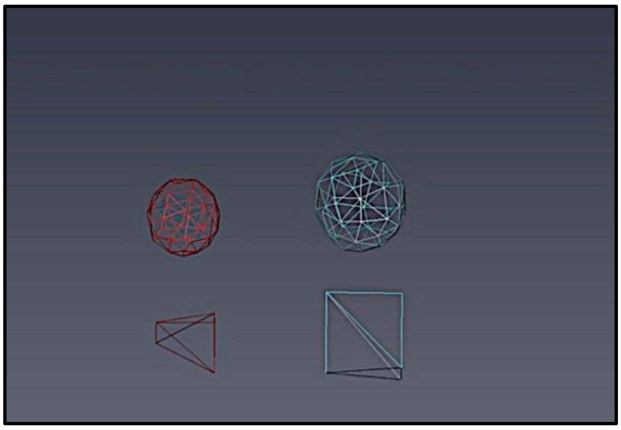

Figure 3.23. CAD models simplified to 100 Triangles.

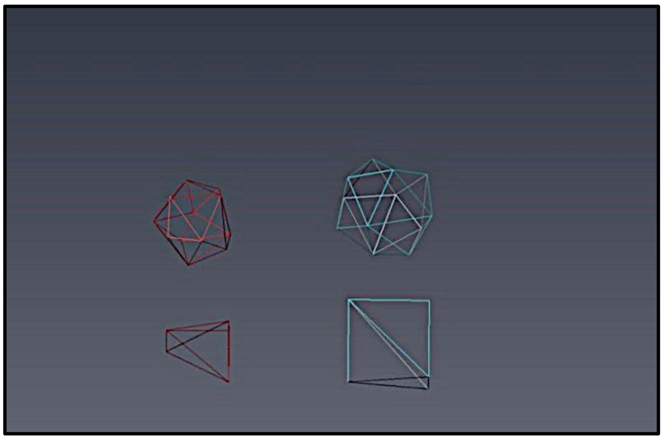
Figure 3.24. CAD images at 20 faces.

Table 3.3. CAD cube, sphere and pyramid statistics compared to 50% resampled data in grey.

Area (mm²)	Volume (mm³)	Mean Dihedral Angle	No. of points	No. of faces	No. of edges	Minimum edge length (mm)	Maximum edge length (mm)	Mean edge length (mm)
Sphere 500 mm³								
300.24	486.59	169.68	353	702	1053	0.05	1.78	0.9
299.82	484.51	166.15	177	350	525	0.76	2.48	1.45
Sphere 1000 mm³								
480.10	983.45	169.42	735	1466	2199	0.058	3.50	0.99
479.56	981.80	168.381	368	732	1098	0.44	3.50	1.30
Cube 500 mm³								
378.26	500.56	90	8	12	18	7.94	11.22	9.03
204.01	166.85	65.42	5	6	9	7.94	11.91	9.23
Cube 1000 mm³								
600	1000	90	8	12	18	10	14.14	11.38
323.607	333.333	65.42	5	6	9	10	15	11.63
Pyramid 500 mm³								
338.3	500.52	63.43	6	8	12	9.89	13.47	10.75
203.01	166.85	58.41	3	4	6	9.89	13.84	11.96
Pyramid 1000 mm³								
668	1000	63.43	6	8	12	7.77	17.1	13.68
336.2	333.33	57.99	3	4	6	7.77	16.9	16.92

Table 3.3 shows various things: the simplification process for a sphere has very little effect on a volume (at 50% anyway), whereas a cube (or pyramid) loses about a third of its volume (we expect this as 3 triangles become 1). The number of faces and points are halved, and we can also see that the mean dihedral angle decreases for all types, which means they are approaching angles that are more acute and thus sharper (i.e., fresher or less abraded). Similarly the mean edge length of pieces increases as we reduce the number of faces. Visually we can see this very clearly and these values quantitatively support these changes.

After observing the changes in our model data, we applied it to a sub-sample of all artefact types, using the first 10 samples from each type in order to easily re-number pieces. This editor allows you to choose how many triangles/faces represent the mesh. The default is set to 18 000, but for this study sub-sample, I decided to reduce it by 50% so I calculated each artefact's face and halved it with the in-house calculator before applying the choice.
Figure 3.25 shows a piece at primary scanned mesh resolution, Figure 3.26 is simplified to Avizo's default of 18 000 faces and finally 100 faces can be seen in Figure 3.27.

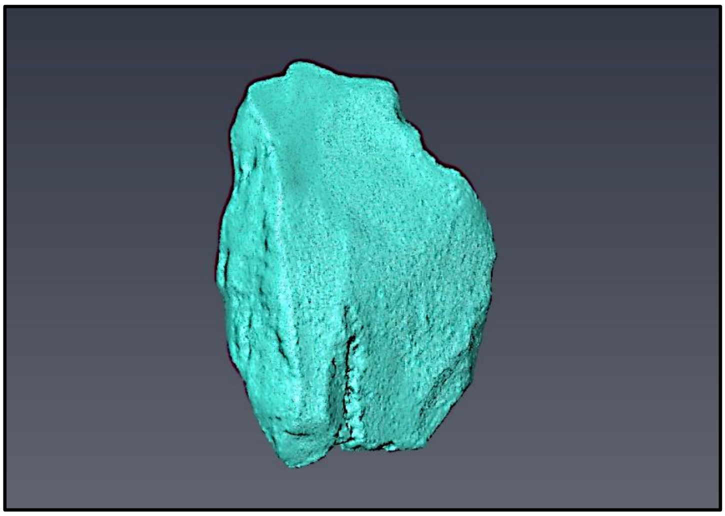

Figure 3.25. A 3D lithic portrayed at regular scanning resolution.

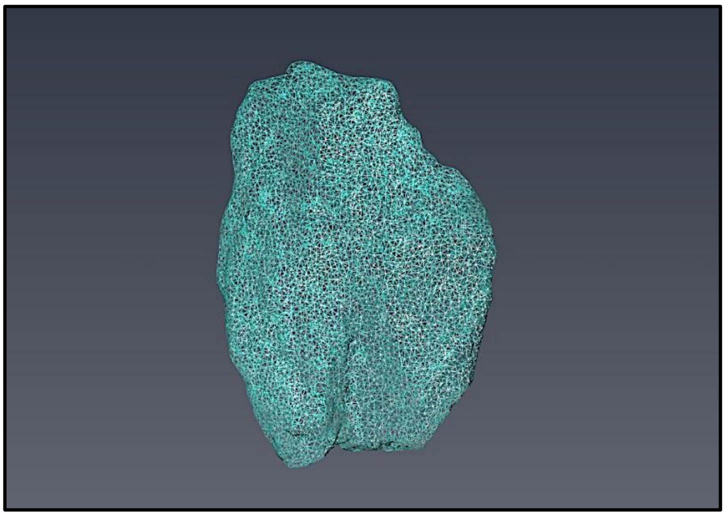

Figure 3.26. A 3D lithic portrayed at the default 18000 faces.

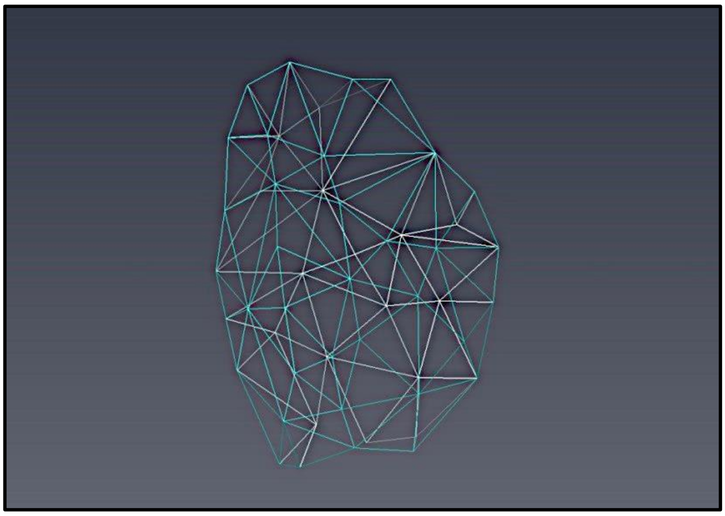

Figure 3.27. A 3D lithic displayed at a much more simplified 100 faces.

I then recorded all the same values which I would later use in my larger scan sample. I attached a volume/surface area module, a statistic module and a triangle quality module to assess dihedral angles for each re-sampled piece. Avizo makes all these measures available and easy to record.

I saved my statistics and volume/surface areas into Microsoft Excel .xml format. Since dihedral angles measure every single angle between faces across a surface (≥50 000 values), this was saved as a statistical file type called an ASCII file (.am) that can be viewed in Excel. By doing some simple Excel macro formatting, I was able to produce a table describing the values for the resampled data (Table 3.3). I used this same technique when I later evaluated my full trays. My simplified data can be found in Table 3.3, which shows that as the number of faces decreases the mean dihedral angles decrease and the mean edge lengths increase (more like a cube).

3.7 Method for analysing specific edges

With Micro-CT scanning, the dihedral angles method can be used in two ways: either the software analyses the entire surface abrasion of a tool and produces a mean dihedral angle value for comparison with other artefacts, or alternatively, a researcher can manually select specific regions to analyse for abrasion to achieve an even higher resolution. I first tested these two methods against one another and found the entire surface abrasion method to be preferable because it analyses everything the specific method can but does not have to account for artefact orientation, a problem which is common in 3D and artefact studies.

The methodology for the study of specific edges is presented here; it is important to note that the segmentation of specific edges is of interest because the blunting or abrasion of edges and arises have traditionally been used as one way to detect abrasion. Many have questioned how we can measure specific edges or ridges using a 3D technique. According to Grosman *et al.* (2008), this is difficult to do because orientating artefacts in a way that encompasses ‘the most useful’ data is hard to standardise. On most pieces there are a number of protrusive ridges and edges, particularly with quartz due to the intrinsic way it fractures. I have no doubt that analysing all specific edges of a given piece could help further our understanding of how artefact abrasion operates. Work of this nature could be useful in the future but was not done macroscopically in this study.

In order to evaluate if the shape of an artefact influences how much abrasion it experiences, I performed an additional smaller sub-study for the edges of five of each of my artefact types. This created a basic method that looks at the classic definition of an artefact’s “lateral edge” or the section that separates one surface from another along a vertical or horizontal plane. This method’s aim was to further prove the efficacy of my dihedral method and quantify some specifics of edges. Technically any edge of any surface can be measured, using the Avizo selection tools, because any portion of triangles can be separated from a given surface (Figure 3.28), but the problem is that there is little or no universally standardized method and user bias could easily become a factor.

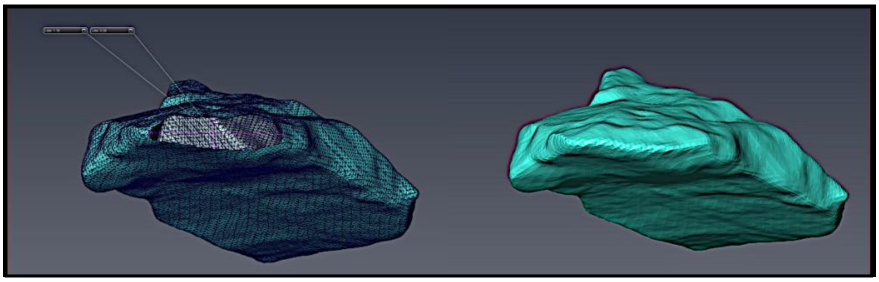

Figure 3.28. Specific edges of a given tool can be separated easily.

My sub-study method which considers a specific region is based on the application of a pre-defined region of interest. It can be applied to any area of a tool, and although many edges can be irregular, it makes adjustments to ensure that all of a given edge and its immediate surrounding areaincluded. Basically the triangles of the angular irregular edge are measured and the flatter relief areas leading up to that edge are included to a set distance, much like the work of Dibble and Bernard’s (1980) caliper method, and more recently that of Valletta *et al.* (2020). The purpose of a width inclusion is to make sure all of an edge can be captured, no matter how irregular. This means that, when one inspects the dihedral angle ranges, one can see a differentiation between the more open flatter parts leading to the edges. Compared to only the more acute angles which display the specific ‘true’ edge.

My overall surface abrasion analysis was more useful for this study because it includes all the measures and information from the entire tool, including all the data described in the sub-study, but it can be performed much faster. Additionally this method circumvents the inherent orientation problems.

Orientation and measurement

Step one is deciding which edge to measure, adding a bounding box, and then transforming the orientation of the edge in Avizo so it is orientated in a vertical fashion (xy), with the bounding box aligned perfectly so that all sides of the box are parallel and can be seen around the artefact. Sometimes I rotated the piece independently within the box to locate the lateral edges of the entire piece so it is upright in virtual space.

Next I measured the bounding box with a 2D measuring tool. The bounding box displays the exact measures of the artefact, so one can actually measure its total maximum length accurately. Following this, I drew a straight line down the approximate centre of the edge I wanted to measure. This line is purely 90º and seeks to fit as much of the edge or ridge as possible (Figure 3.29). Then the maximum length of the bounding box is measured, and using the in-house calculator, this calculation is divided into three. This creates three horizontal landmarks, which further subdivide the tool into 6 sectors. The method presented here draws on Roe’s (1964) division technique for LCTs but primarily focuses on the edges of a tool rather than the entire tool.

Next, in order to standardise the section to be analysed, I drew two straight lines from and on either side of the edge line making sure they are in line with my subdivided “thirds” landmarks, choosing the length of these lines to be one 2D unit or 1cm. This standardisation is an adaptation of Dibble and Bernard's (1980) standardised calliper technique. Finally two lines are drawn down the Y axis that mark from the top of the box through the standard unit measures and are exactly 90º to the bottom of the box. I have termed the resulting upper, mid and bottom sections along the edge (Figure 3.30) the regions of interest or ROI. In future a variation could perhaps be taken at say 10% of total tool length, or 3D units could be used, but this was not done because it makes alignment difficult.

Technical Note: measurements were not drawn freehandedly. All measurements are straight lengths taken according to the vertical orientation of the bounding box (orange in Figures 3.29 - 3.32).

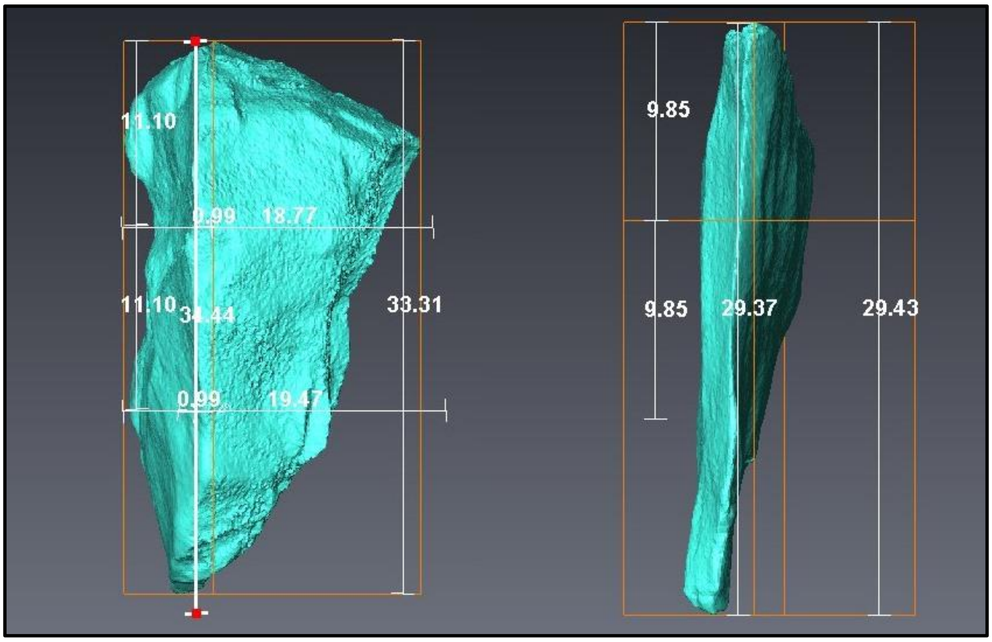

Figure 3.29. The alignment and identification of a ridge on a quartz chunk (left) and the edge of a flake (right). Note that the orange line (bounding box) to the right of the line along the edge line is purely to aid in alignment of all other lines.

After the main divisions are complete, one can then take a measurement on either side of the centre edge point (1 mm). This finally gives us a ROI that lies along an artefact's lateral edge and 1 mm either side of that. In the case where an edge is irregular (i.e., it goes right and then left or vice versa), one can draw two edge lines and two sub-edge lines so as to include all parts of the edge. Because one standardises the amount of edge and its surrounding that are recorded, it does not affect the results to move the middle edge length around so long as the bounding box and the artefact do not shift.

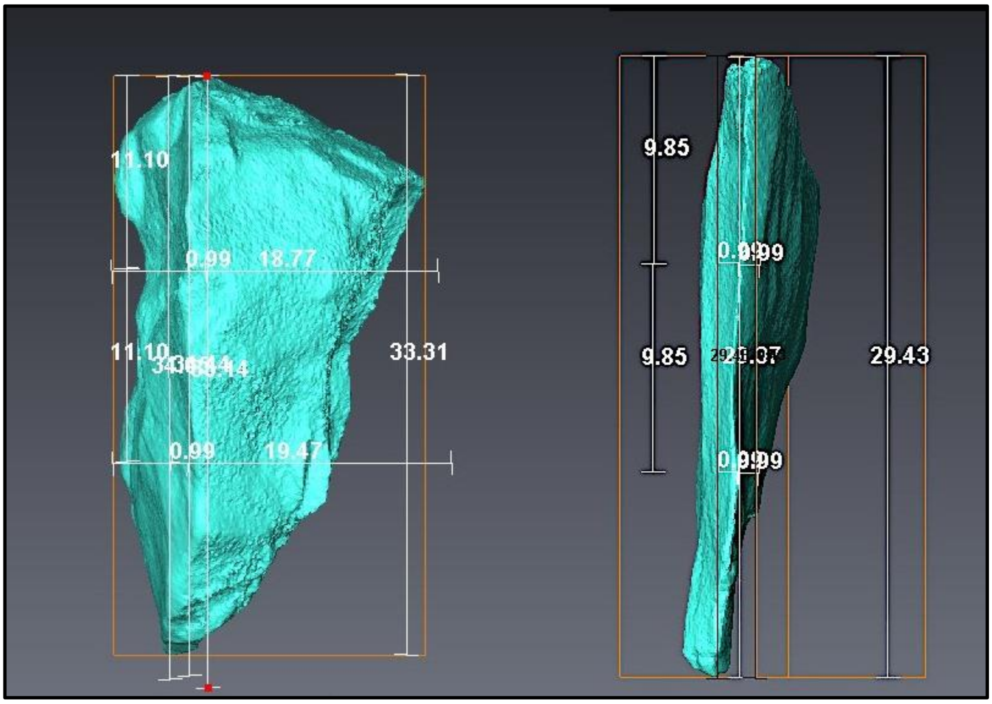

Figure 3.30. The edge line and the lines that define the region of interest at ~0.1 cm difference to 1 cm for a chunk (left) and a flake (right).

After the ROI has been established, it is time to separate the edge into sections. One can use a Wacom touch tablet and stylus to hand-draw in the area with a brush or pencil tool in the surface editor module which when active is indicated by dark blue as seen in Figure 3.31. The triangles selected are only those that are visible, and additional overlapping triangles can be easily added or removed. Often a couple of extra faces are included (because of how a triangle is cut). One can then select and create separate surfaces for each part of the edge and render each section's statistics and dihedral angles separately or together. Figure 3.32 displays the same chunk divided into three by colour.

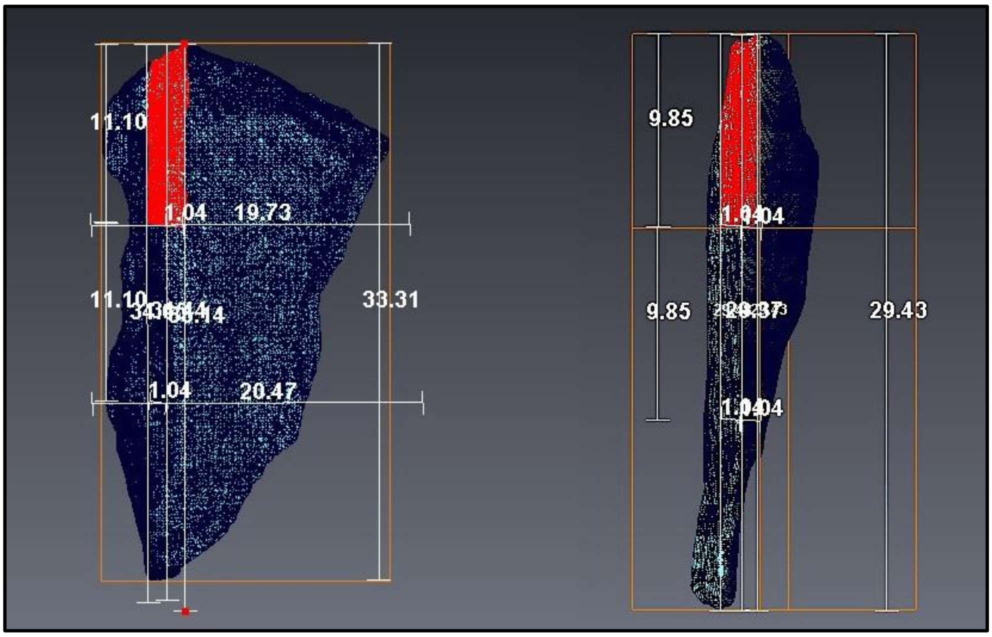

Figure 3.31. The regional selection of the ridge on a chunk (left) and the selection of an edge on a flake (right).

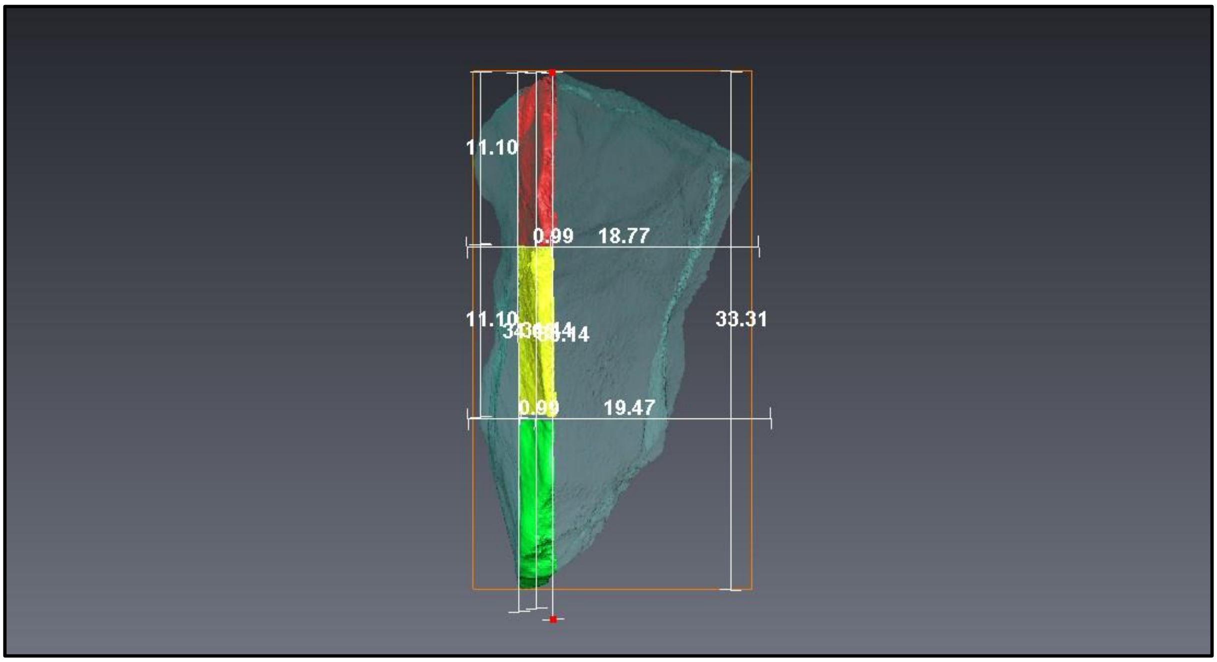

Figure 3.32. The sectoral division of a prominent ridge on a chunk; individual statistics and dihedral angles are available after this step.

Following this, I saved all statistics and dihedral angles for the upper, middle and bottom of five artefacts from each category and analysed these values by averaging the dihedral angles of each ROI sub-section to create a dihedral angle for one edge of each piece. I was confident I would be able to see patterns for the nature of edge angles and the surrounding regions within my ROI. I expected the dihedral angles to display a region of abrasion across an edge and a region of relative openness or flatness moving away from the edge that describe the dorsal or ventral flat plane of an artefact (if it is indeed regular).

3.8 Measuring edge angles using Avizo: problems and ways to circumvent them

My study mainly focuses on the high resolution analyses of edge angles using the dihedral technique; however most traditional early research simply uses the graph, goniometer, caliper or clay method to quantify the edge angles of individual tools. Again a problem that exists is where to measure such angles from (or to) on the artefact. Avizo does provide a tool for analysing angles at a given point in both two and three dimensions, and while useful, I did not use this tool and would like to comment briefly why not. The Avizo angle tool allows you to select three points on a surface in order to calculate an angle. The type of measurement can be done basically and quickly over any portion of a subject, including negative space or actual surface. The more accurate 3D measurement can be done only on the surface of an object and conforms to the surface of the object in order to measure it. In the sub-study of edge specifics, I included a 3D measure for each tool at the crossing point of each horizontal and vertical division, i.e., the lower bound of the top ROI and the upper bound of the lower ROI. I measured this angle horizontally from the left ROI sub-line to the perceived edge middle, and then to the right ROI sub-line. Before deciding on doing this I took my CAD cube (Figure 3.33) and applied the 3D measure first the 90º to angle between sides along the visible lines, and secondly to the 180º angle between the two faces of a given side. Both these measures were done with the cube sides orientated on a flat plane with parallel sides. I noticed, however, that if I rotated the object and then tried to select what I thought was a 90º angle this was not as easy as doing it when it was in its uniform standing position. This is another reason I chose to orientate my pieces the way I have just described. Also, sometimes when I rotated the object to select an angle, the last point ended up further away than I anticipated. This said, the 3D angle tool is quite accurate and may be of some use in future studies.

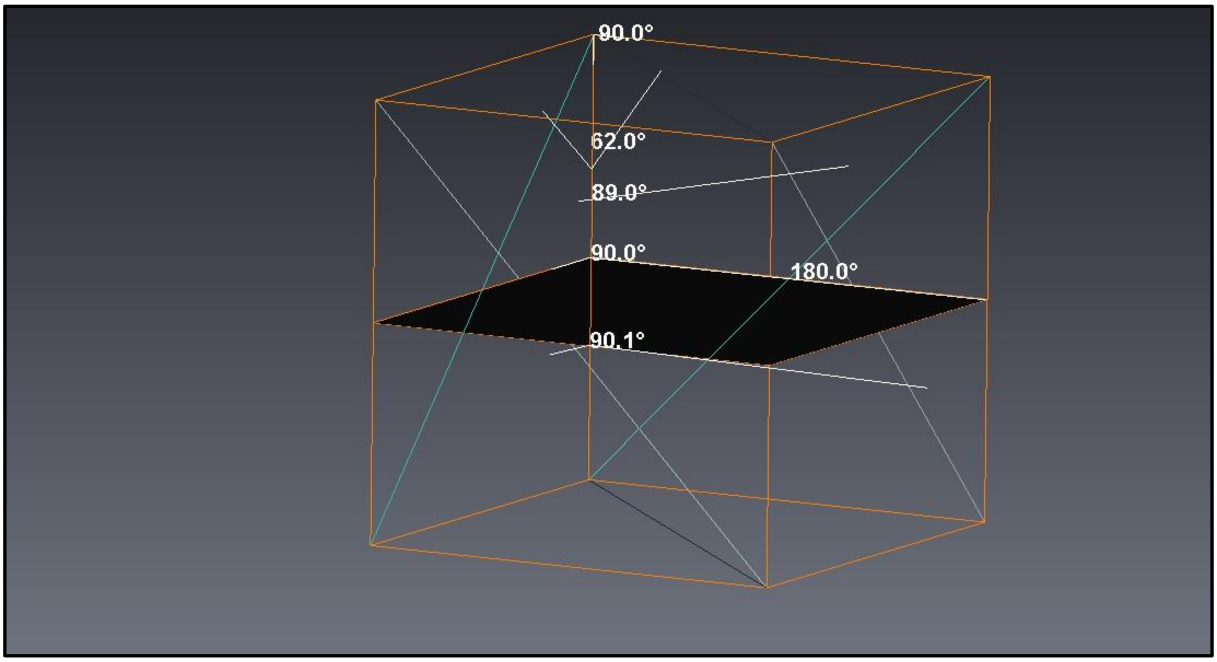

Figure 3.33. The range of angles across a cube. Having a set reference point helps in maintaining reliability of measures.

From my experiments with the 3D angle measurements, I have learnt that in the case of highly variable surfaces such as those of lithics, results can be skewed based on the orientation of the object being visualised or the inability to standardise the point from which a given angle measurement is placed. Thus my dihedral angle method is more accurate because it records the absolute intrinsic value of each dihedral angle and is not subject to user bias beyond the alignment process, which has its own complications (Grosman *et al.* 2008).

3.9 Statistical recording and theory

All of my statistical results were produced using SPSS 24, a licenced statistical software package acquired from the University of the Witwatersrand. I used a combination of descriptive Excel tables along with non-parametric Spearman's Rho and Kruskal-Wallis tests, and the specifics and explanations of these tests are presented in Chapter 4.

3.10 Methodology: Summary

The methodology presented in the first section of this chapter addresses the need for more precise mapping in GIS in order to clarify the following detail for the site: 1) the reconstruction of the sedimentary boundary between M4 and M5; 2) the mapping of existing stratigraphic features that relate to complexities, such as thesolution pockets of M5 that have obscured the original extent of the StW 53 infill in M5; 3) the location of a large flowstone curtain which separates M5 from M4; 4) the more precise distribution of the M5E Oldowan and M5W Acheulean deposits; 5) the location of a capping flowstone that signifies the upper limit of the M5W breccia; and 6) the location of the entrance to the Name Chamber at the base of M5E. Prior to this study, these details for Sterkfontein had only been presented in schematic figures, but they are now integrated within an accurate GIS framework .

The second section on methodology addresses how best to perform a high-resolution analysis of the degree of abrasion experienced by artefacts in the main Oldowan deposit, which is then compared to those lithics re-worked into the underlying Name Chamber deposits. These methods use a combination of Micro-CT scanning and 3D software. A substantial quartz sample (n = 739) was selected, consisting of: complete flakes (n = 59), incomplete flakes (n = 180), chunks (n = 74), SFD ≤ 20 mm (n = 426); and for comparison with the Name Chamber, an additional (n = 51) SFD pieces from the Name Chamber were scanned using a spiral scanning method which was created for efficiency. The 3D images of each artefact are separated individually using a program called Avizo 9. For this study I decided on a method that analyses the dihedral angles for a given artefact's entire surface. I additionally outline some of the internal tests on the lithics from M5E and the Name Chamber in order to measure their efficacy. One such example is to create a specific edge analysis method to compare to my complete surface mesh analysis method Following this I planned to record the details of each individual surface mesh and the dihedral angles (or the angle between triangles on a given surface) in Excel and later export them to SPSS.

Then six artificially computer-generated models are created with different volumes (two of each at 500 mm^3 and 1000 mm^3) using AutoCAD. The purpose of these models is to provide a comparison of the way in which a surface mesh and the dihedral angles contained therein behave for different shapes, which could be ultimately compared to lithic scans from the M5E and the Name Chamber. These three shapes are defined as: a cube (sharper/more angular/acute, hence less abraded), a sphere (rounded/less angular/dull, hence more abraded) and also a pyramid (similar to a cube but with a tapered end). Results from the Auto CAD models are then statistically compared to the real-world assemblage and these results are illustrated in Chapter 4.

Chapter 4

4. Results

Chapter 4 first describes the GIS spatial models created with the Nikon Total station, illustrated with corresponding photographs of the individual areas that have been detailed in the new plan for the site (section 4.1). It then presents the results of the 3D abrasion study, along with the statistical tests used for their evaluation in comparing the Oldowan assemblage pieces with the user-generated CAD models (section 4.2).

4.1 Results of spatial modelling

Figure 4.1 shows the most recent plan of the western part of the site at surface, which was created schematically by Kuman and Clarke (2000) based on site contents rather than with mapping of the actual breccias. The plan in Figure 4.2 now shows the Sterkfontein (STK) site and breccias exposed at surface in greater spatial detail for areas where features and boundaries had not been removed through excavation and remained to be mapped. In the years following the 2000 study, weathering of the breccias also enhanced the distinctions, and I was able to map them quite clearly in 2013/14; Figure 4.3 provides an enlarged view of the western squares. Using a Nikon Nivo (5) C series Total Station, I was able to record greater detail, down to a few millimetres of accuracy. Although the map is purely a plan view from an aerial perspective, it is now the most accurate plan we have of this part of the site in the last 20 years. The following sections discuss the notable stratigraphic features added to the site plan since 2000: the remnants of the original dolomite roof and walls; speleothem drapery and flowstone curtains; other instances of flowstone (e.g., capping flowstone extending into the Lincoln Cave in the area of Square L/63); boundaries between different breccia infills; and solution pockets. Enlarged plans and sections, along with photographs of the area in question, are provided in this chapter for greater visual representation of these stratigraphic features. All the data is stored online on the Sterkfontein research server and will available for download online through the Wits Wired Space platform in the future.

Please note: the figures in the following section show photographs taken from various directions, but their position on the plan is shown with the corresponding portion of the grid which is either circled or in a rectangle. The key is not repeated but can be referred to in

Figures 4.2. or 4.3. Arrows showing the direction of north are shown in each image. The grid size is 3x3 feet in all cases, following the original recording system for the site.

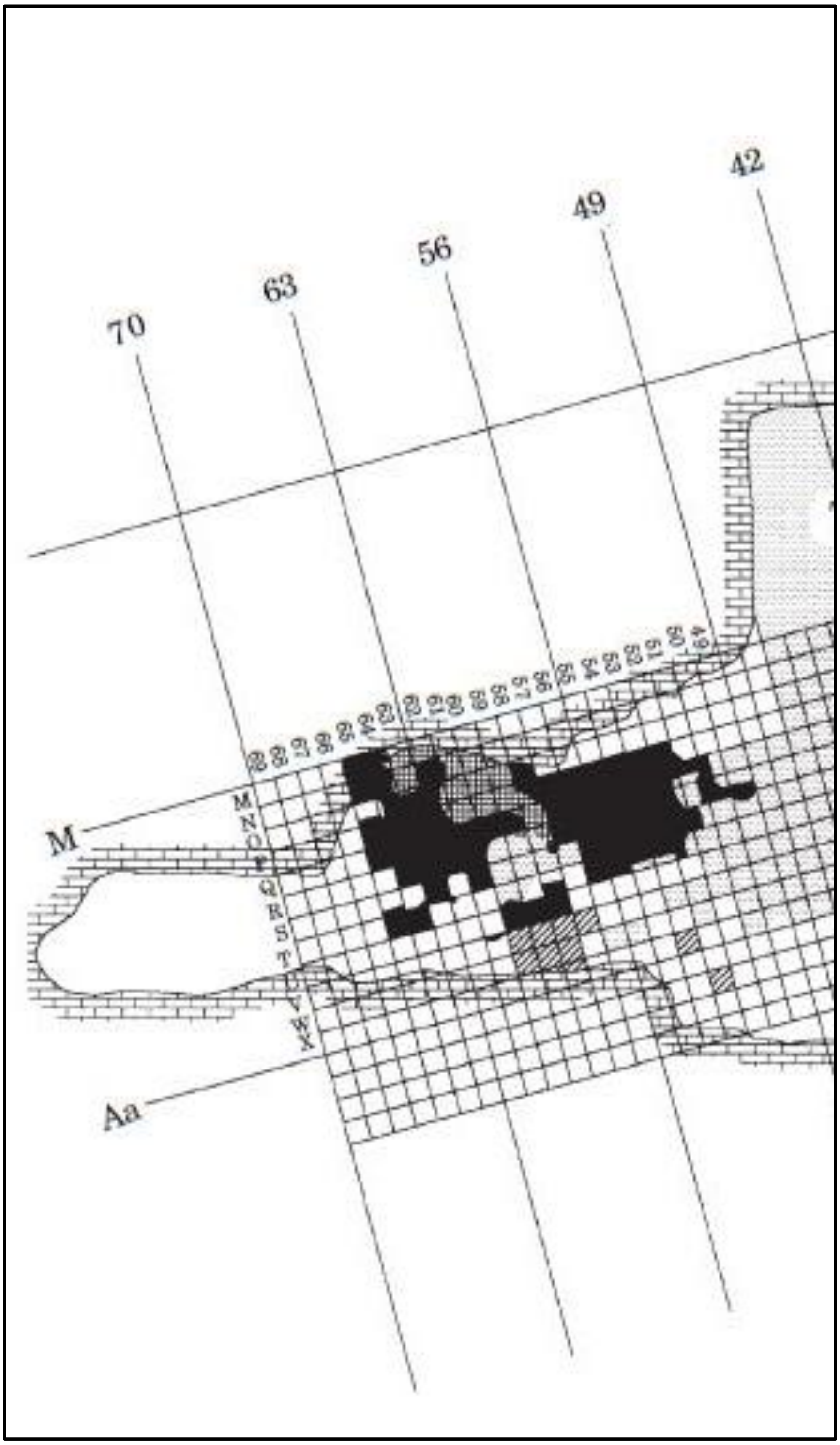

Figure 4.1. Enlargement of the relevant area of Figure 2.6 (from Kuman & Clarke 2000). For the key, refer to that figure, as it is removed here to better show the area of study.

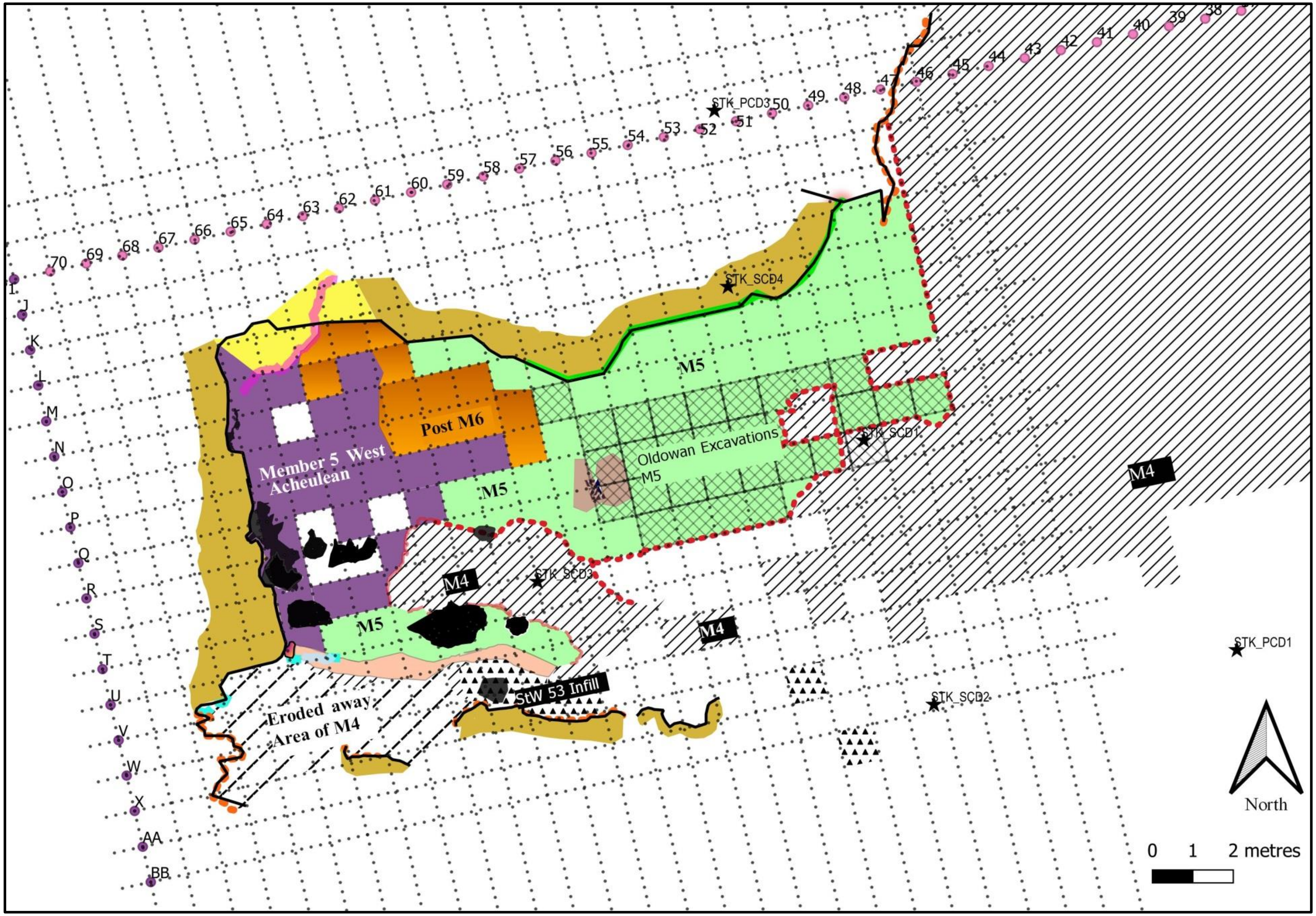
Member 5 West Acheulean
Post M6
M5
Oldowan Excavations M5
M4
StW 53 Infill
Eroded away Area of M4
STK_PCD3
STK_SCD4
STK_SCD1
STK_SCD3
STK_SCD2
STK_PCD1
North
0 1 2 metres

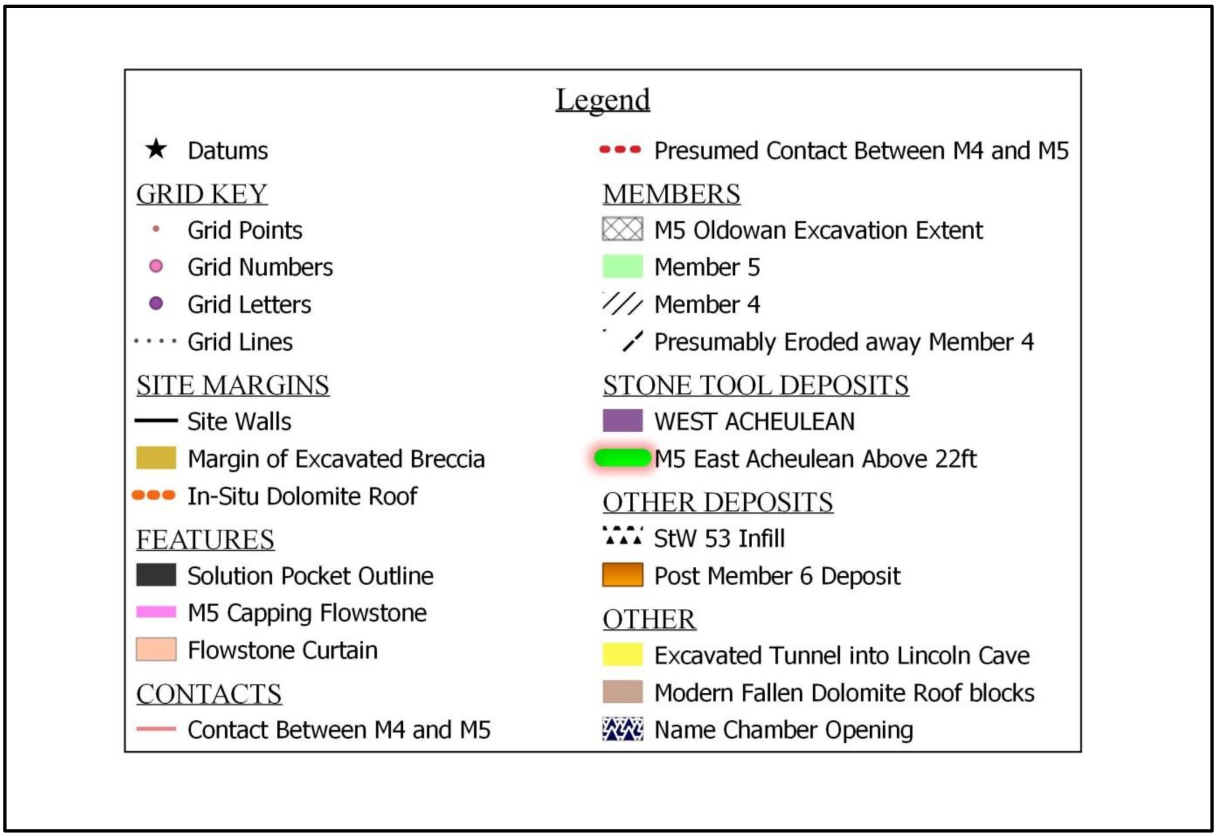

Figure 4.2. Spatial plan of the extent of Sterkfontein (STK) members exposed at the surface in the western part of the site, and associated Legend for GIS map. It provides much greater accuracy for features indicated in the western half of the M5 area, such as flowstones, solution pockets and remnants of older breccia.

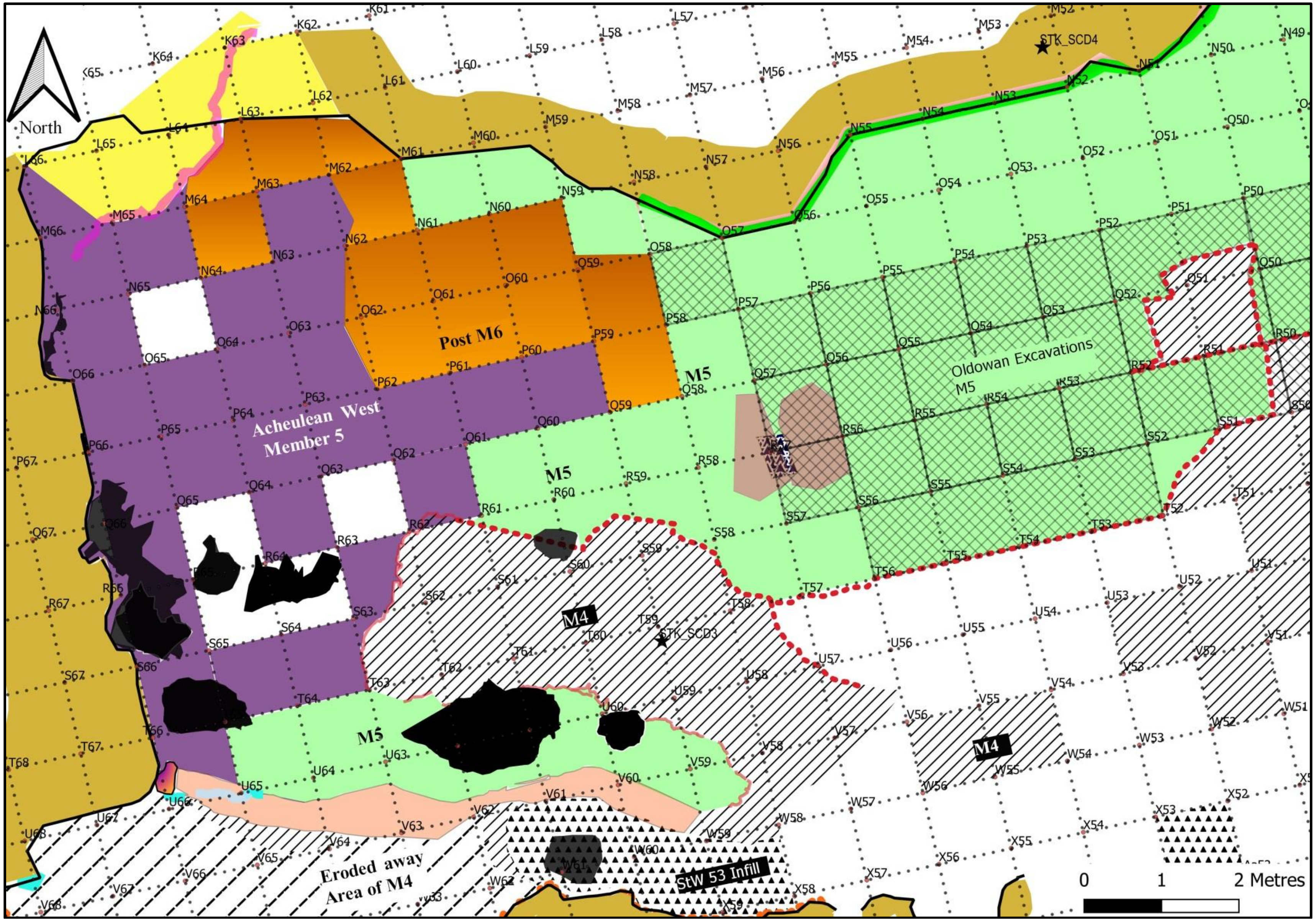
North
Acheulean West
Member 5
Post M6
M5
M5
M5
M5
Oldowan Excavations
M5
M4
M4
STK_SCD4
STK_SCD3
Eroded away
Area of M4
StW 53 Infill
0
1
2 Metres

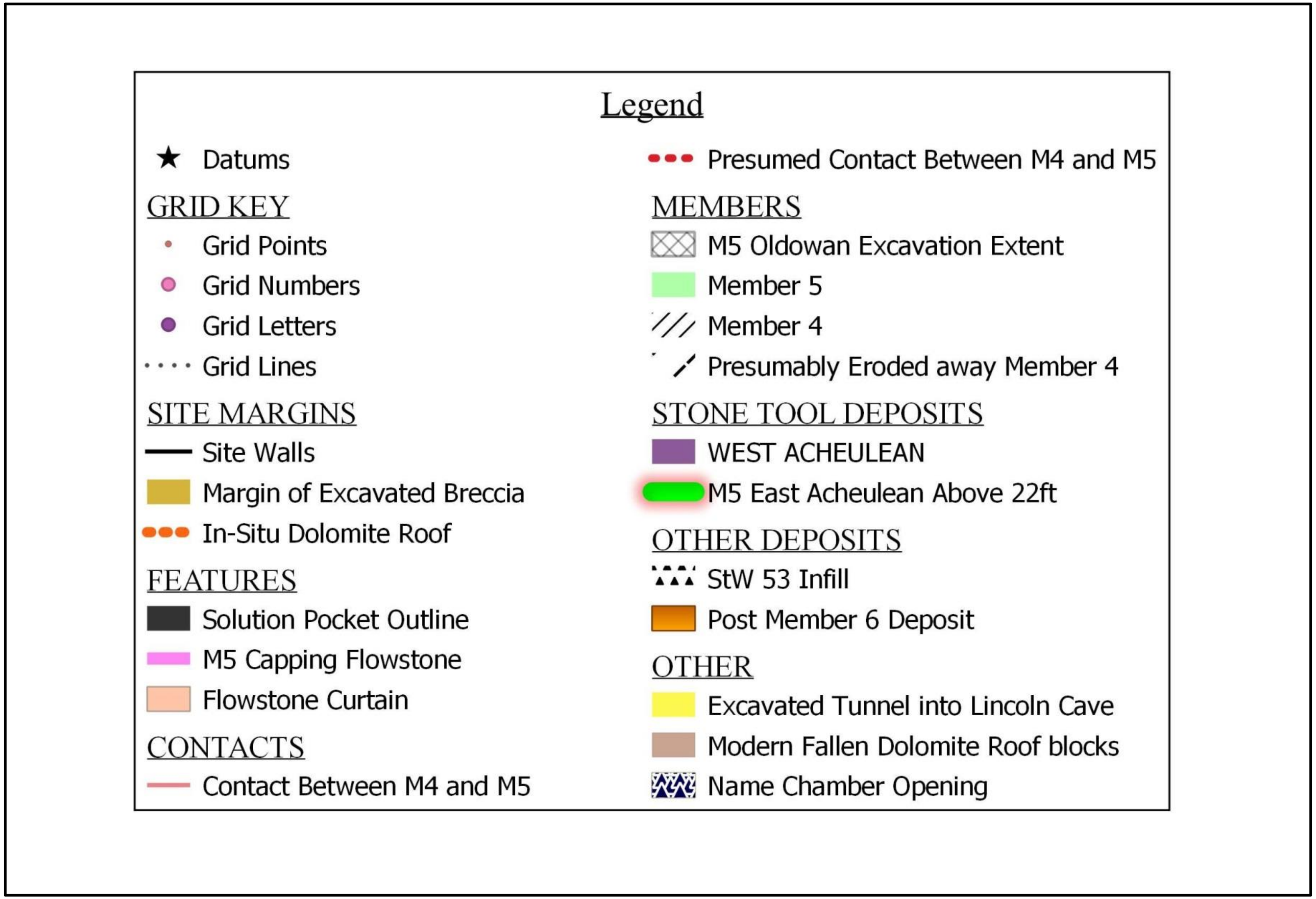

Figure 4.3. Enlargement of Figure 4.2 showing the area of interest, for the western side of the site.

Description of the site

The control datum from which a majority of points were shot is shown in Figure 4.4; the geo-referenced point is called SCD_3 (circled white in photograph and black on the plan). The datum rests on rocky M4 (solid hatched black in plan). The photograph is looking east towards the rest of M4 which is seen in the background. At the very back of the photograph is the wooden tourist walkway outside of the site perimeter, which faces east toward Kromdraai. Figure 4.5 shows the eroded away area of M4 in the southwestern corner of the site. The photograph in Figure 4.6 shows the complex relationship between the stony M4 and less stony, darker M5 breccia in the southern sector of the site. The StW 53 Infill is visible in the top centre of the same photograph, where a plaque indicates the general location of the hominid cranium with the same name. The StW 53 cranium was excavated from both hard breccia and a solution pocket eroded into that breccia, and later joined together (indicating the complexity of such stratigraphic features in the site). At the top right of the photograph, dolomite can be seen where a part of M4 has eroded away (dashed hatched black in plan). Northwards in Figure 4.7, an eastern section of the northern wall and the Acheulean levels in M5E are displayed in both the photograph and the plan. The original dolomite roof is toward the top of the photograph, and collapsed roof blocks below lie within the deposit and follow the slope of the talus. The Oldowan infill (cross-hatch in plan) lies at greater depth. The section shown in the photograph lies between N58-49 in the GIS Projection. The mustard colour in the map shows the extent of the breccias.

Figure 4.8 provides a photograph of a northern portion of the site showing the M5W and Post-M6 infills. The Acheulean calcified breccia is visible in the left third of the photograph as light breccia (purple in the plan). A tunnel has been excavated into the Post-M6 (darker) deposits in the area of L/63 (circled, and shown yellow in the plan), where a connection between the main site and the Lincoln Cave was discovered. The Post-M6 breccia occupies both the tunnel and the sediments to its right, and both contain MSA artefacts. The remnant of the dolomite roof is visible at the top of the photograph. Below this is a thick layer of flowstone (pink in the plan) that caps the M5W breccia, but which broke into fragments during erosion of the Post-M6 channel. In the Post-M6 breccia, fragments of that flowstone and other clasts with horizontal bedding are visible. This deposit filled the eroded channel that now separates M5W (to the left) and M5E (not shown here). Remains of this capping flowstone (already described as pink in the plan) can be seen overlaying M5W (purple in the plan). Figures 4.9 and 4.10 provide closer views. The flowstone continues inside the excavated tunnel (yellow) which is located at L63, connecting the main site with the Lincoln Cave. Lincoln Cave itself cannot be seen from the main site and is accessed through a separate entrance. In the plans, Post-M6 deposits are noted in brown, M5 capping flowstone is shown in pink, and M5W is visible to the left in the photograph (purple in the plan). Looking westward in Figure 4.11, we can see M5W (purple in the plan) and some solution pockets (indicated in black in the plan). The solution pockets were excavated by Alun Hughes prior to the 1990s and found to be sterile (pers. comm. from A. Hughes to K. Kuman). It is evident in this photograph that the M5W Acheulean deposits are more calcified than the M5E Acheulean deposits shown in Figure 4.7.

In the southwestern corner of M5W in the plan, Figure 4.12 depicts a photograph looking westwards with a speleothem drapery that has been described. The drapery is exposed through excavation and circled black on the plan. It is presumed that M5 deposits entered into the cave after these speleothems had already been formed possibly during a wetter period of deposition (Ogola 2009). The white circles in the photograph are part of Ogola's study and show large Acheulean tools. An enlarged photograph of this flowstone drapery is represented from an aerial view in Figure 4.13. The photograph in Figure 4.13 is taken at approximately U66, in the southwestern corner of the site. The black rectangle shows a portion of the flowstone curtain with M5 above and M4 below. The arrow in the photograph points to the inter-digitation of M5 against the flowstone drapery. Figure 4.14 shows a photograph of a white curtain of speleothem drapery (in the U66 area) looking westwards, in the southwestern portion of the site. In the plan, the flowstone is shown as pink and separates M4 breccia (depicted as solid hatching) from M5, which is drawn on the photograph (5). M5 consists of red sandy deposit (in plan shown as purple or green). The portion of M4 on the left of the photograph (dashed hatched black on the plan) is thought to be a part of M4 that has completely eroded away. Figure 4.15 shows a northward orientated view of the flowstone curtain separating M4 from M5, while Figure 4.16 displays a thick calcified botryoidal flowstone which is thought to have formed underwater, once again illustrating the wetter conditions while M5 breccia formed up against the flowstone curtain.

The StW 53 infill is shown from above (triangles in the plan) in Figure 4.17. The plaque on the southern wall is visible in the top left of the photograph. The StW 53 cranium, as previously mentioned, was found partly in the solution pocket (red circle) and partly in solid breccia that formed the right hand wall of the solution pocket.

M4 and M5 are shown aerially in Figure 4.18 (from lines 59 to 66) with south at the top of the photograph. The red line in the photograph shows the contact between M4 and M5. Speleothem drapery (U66) and the flowstone curtain are outlined in black. Figure 4.19 shows the location of the Name Chamber feeding shaft opening, looking east in the photograph. The hole leading to the shaft lies at R57 (circled white in both maps). The large white arrow pointing left denotes the direction of the M5E northernmost wall (bold green line in map, also see Figure 4.7). In the left of the photograph, M4 wall collapse has resulted in large dolomite boulders falling into the site. The M4/5 contact boundary is once again shown as a red line in the photograph.

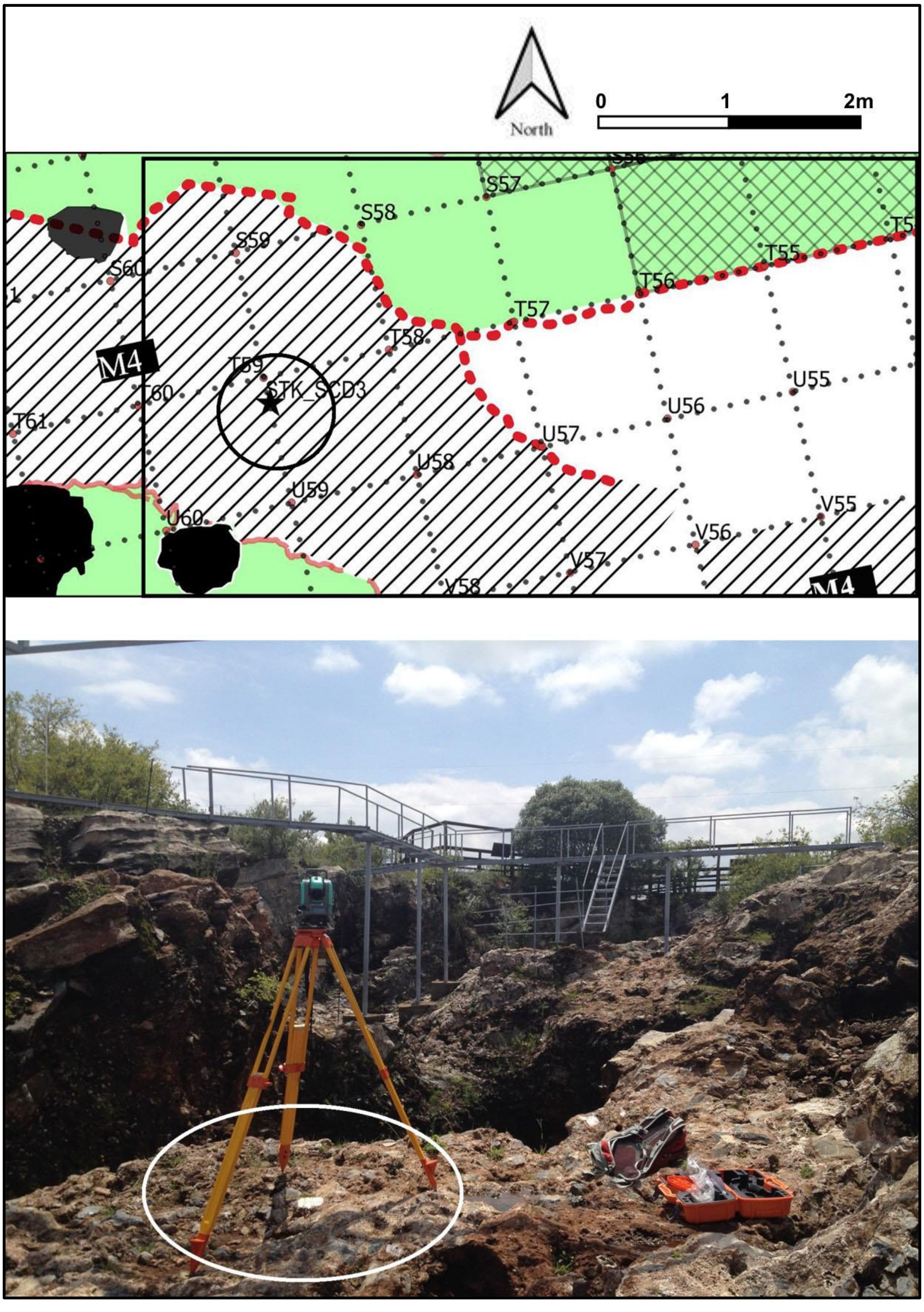

Figure 4.4. Location of the primary Total Station for this study (circled white). The black rectangle in the plan denotes the current view.

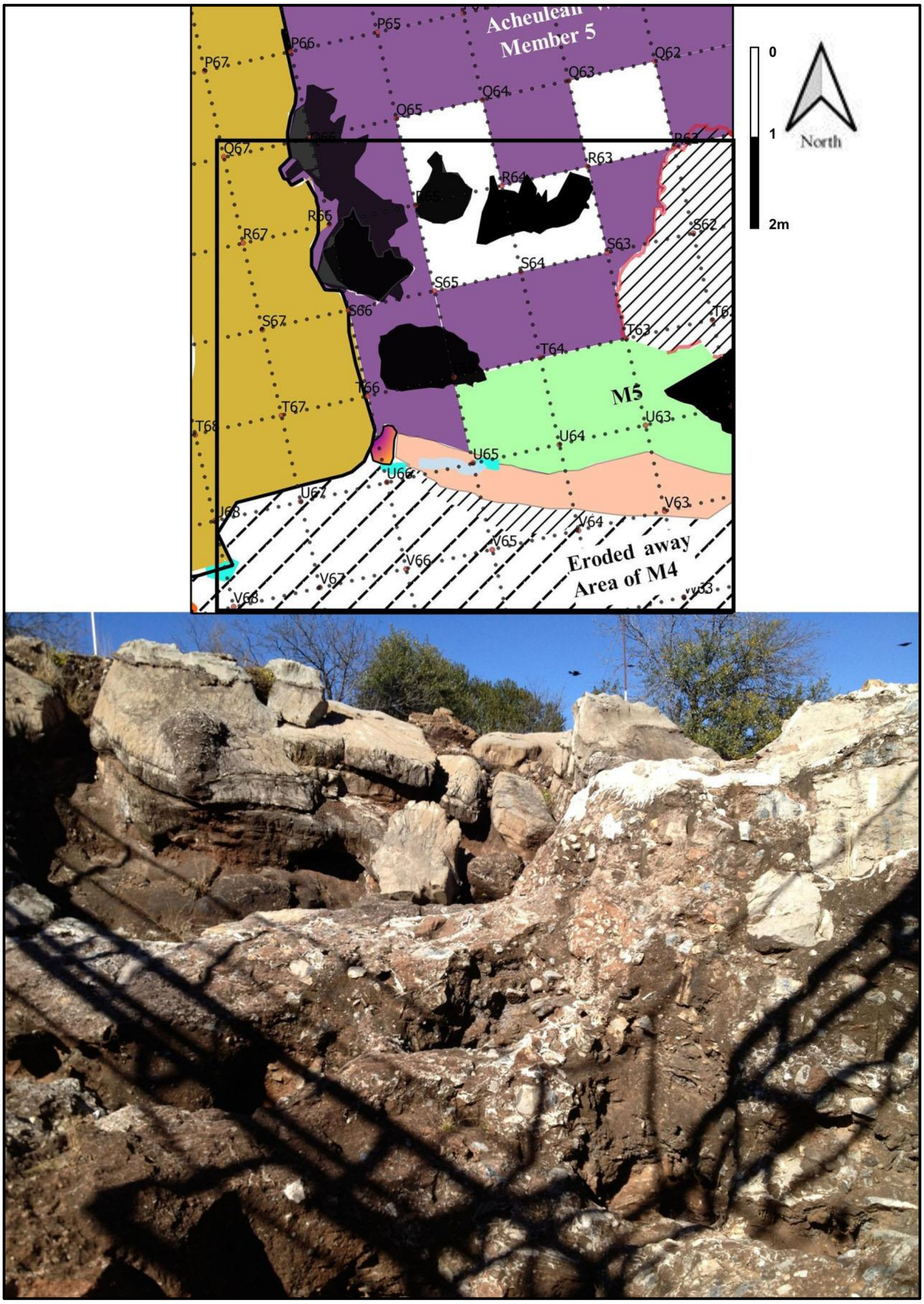

Figure 4.5. Enlarged portion of the southwestern section of the site, with a photograph of this area looking southwest toward the eroded area of M4. The black rectangle in the plan denotes the current view.

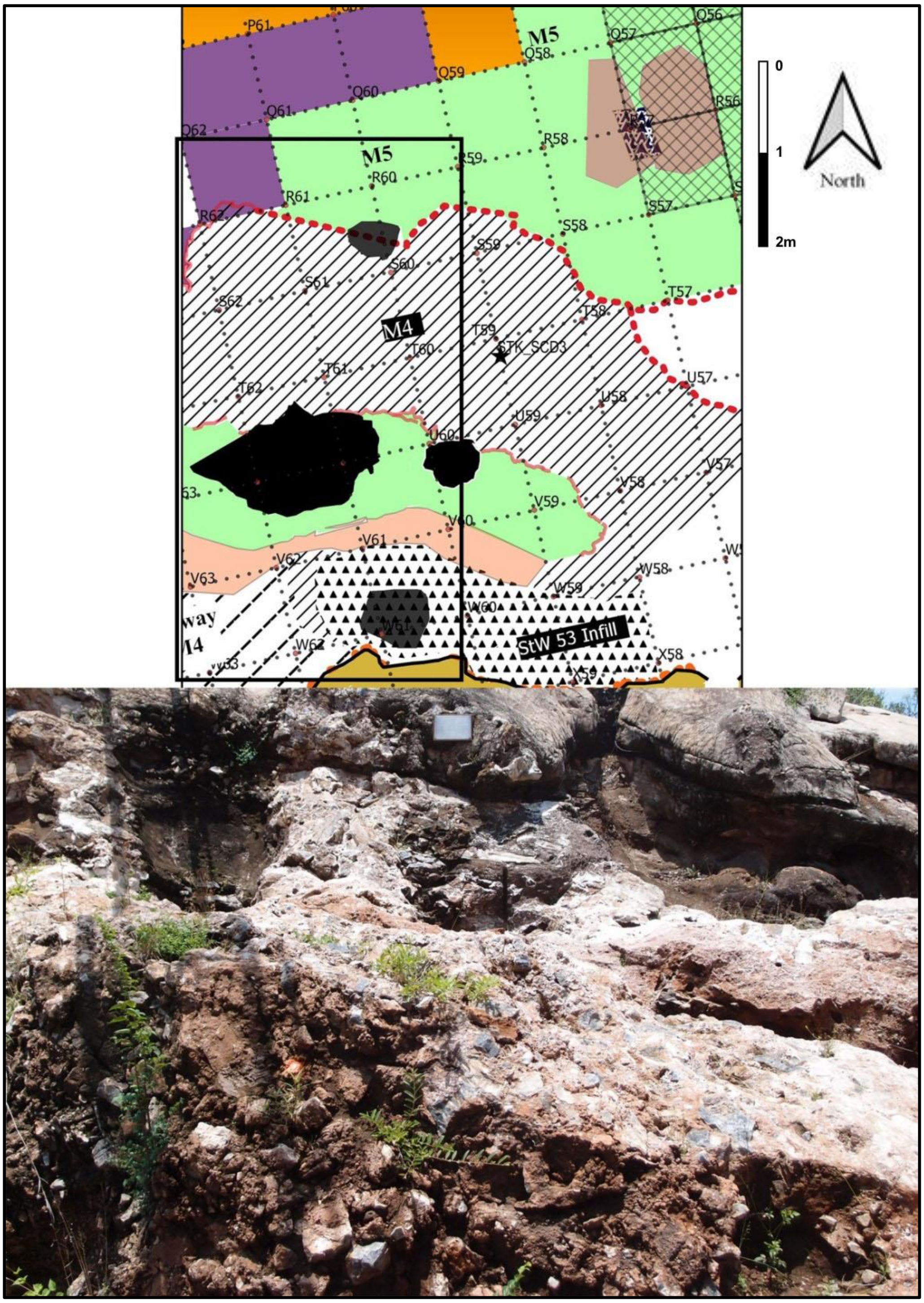

Figure 4.6. A view of the southwestern part of the site, with the photograph looking toward the StW 53 infill (delimited with the black rectangle).

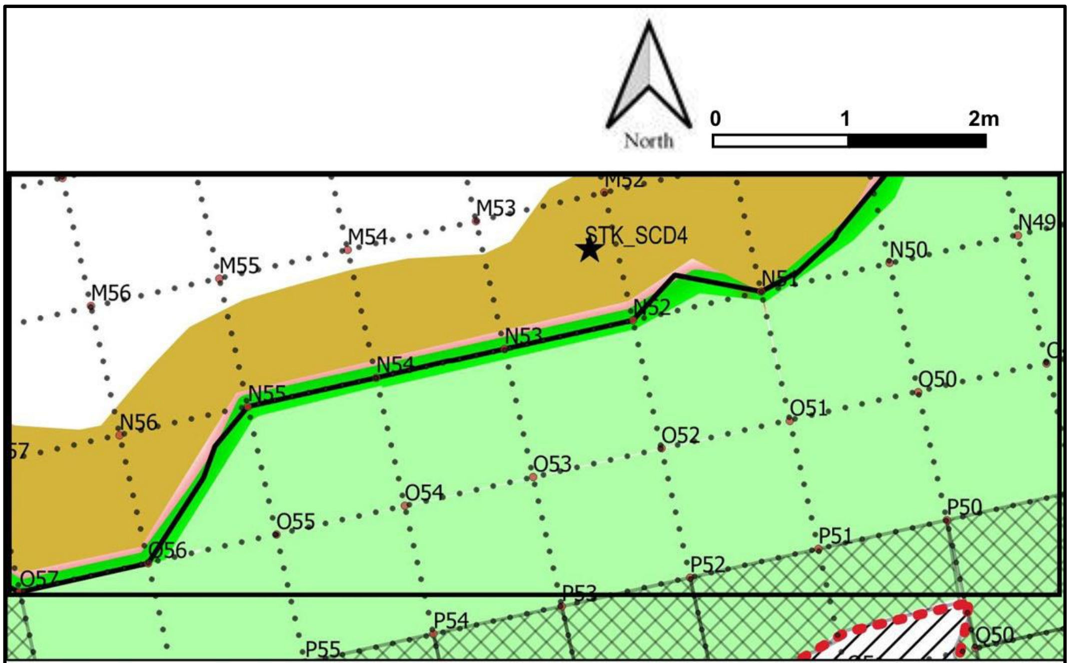

Figure 4.7. An eastern section of the northern wall, showing the Acheulean levels in M5E, looking north. The black rectangle in the plan denotes the current view.

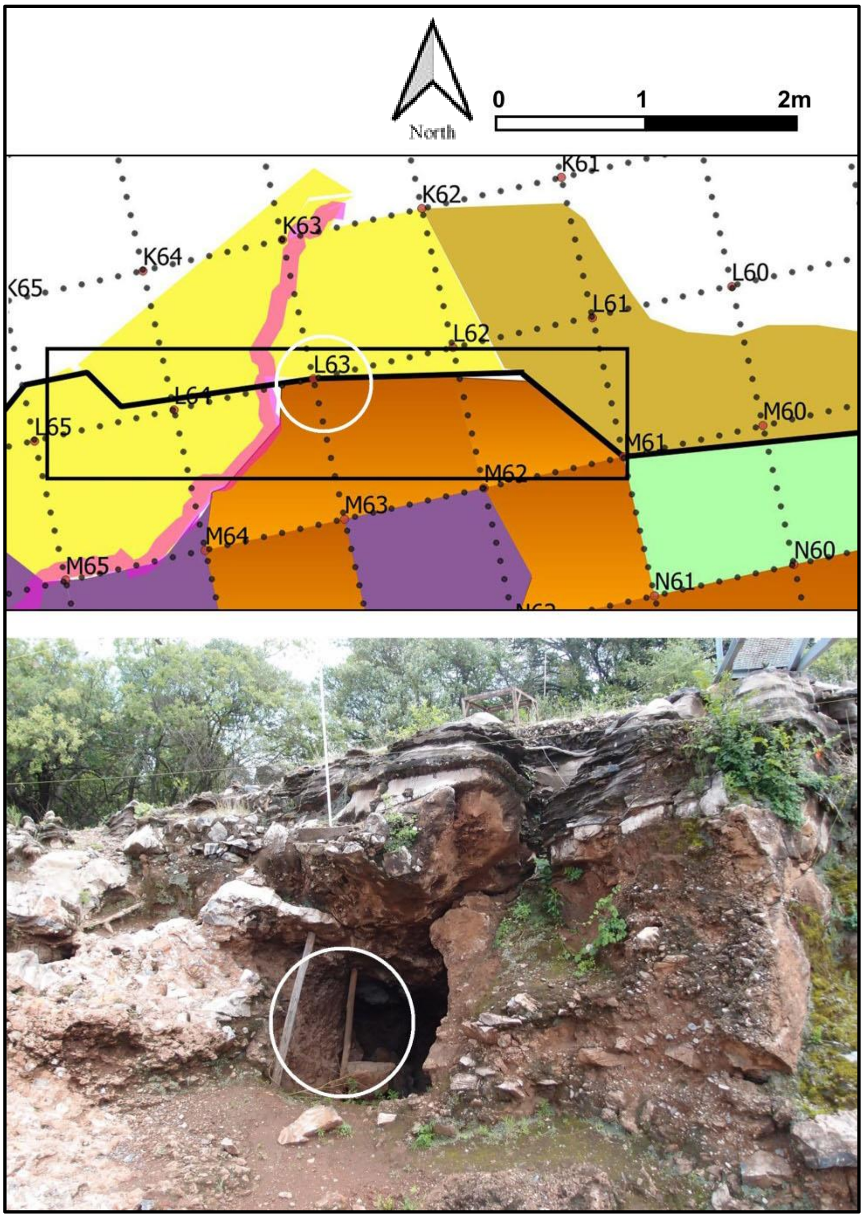

Figure 4.8. A northern portion, showing the M5W (left) and Post-M6 (right) infills, and the tunnel excavated in the latter infill toward the connection with the Lincoln Cave (circled white at L63).

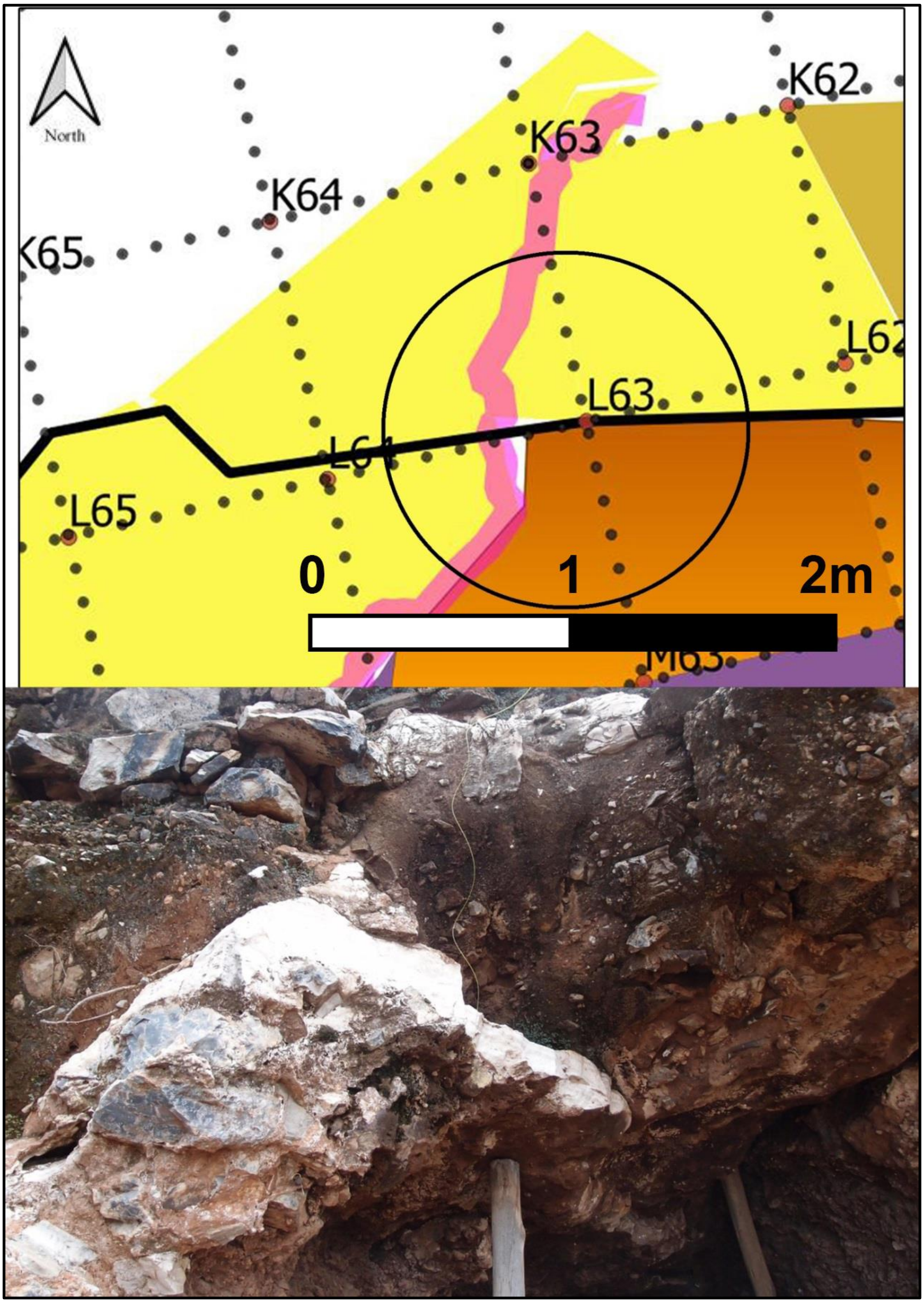

Figure 4.9. Remains of the capping flowstone (pink in the plan) over M5W (purple in the plan). The black circle in the plan shows the location of the excavated tunnel opening at L63.

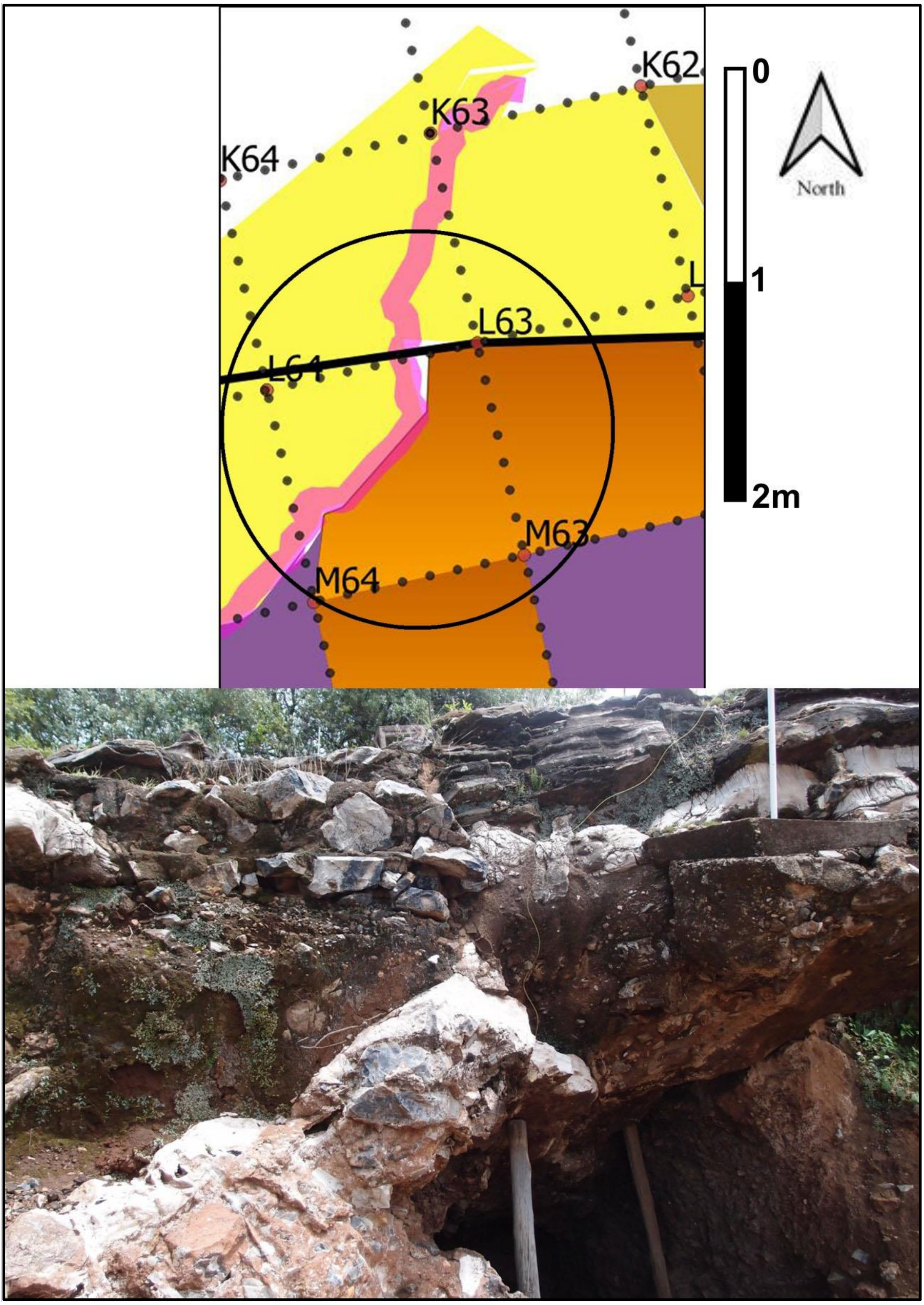

Figure 4.10. A closer view of the excavated tunnel excavated in toward the Lincoln Cave at L63, shown in yellow in the plan. The black circle in the plan shows the location of the excavated opening at L63.

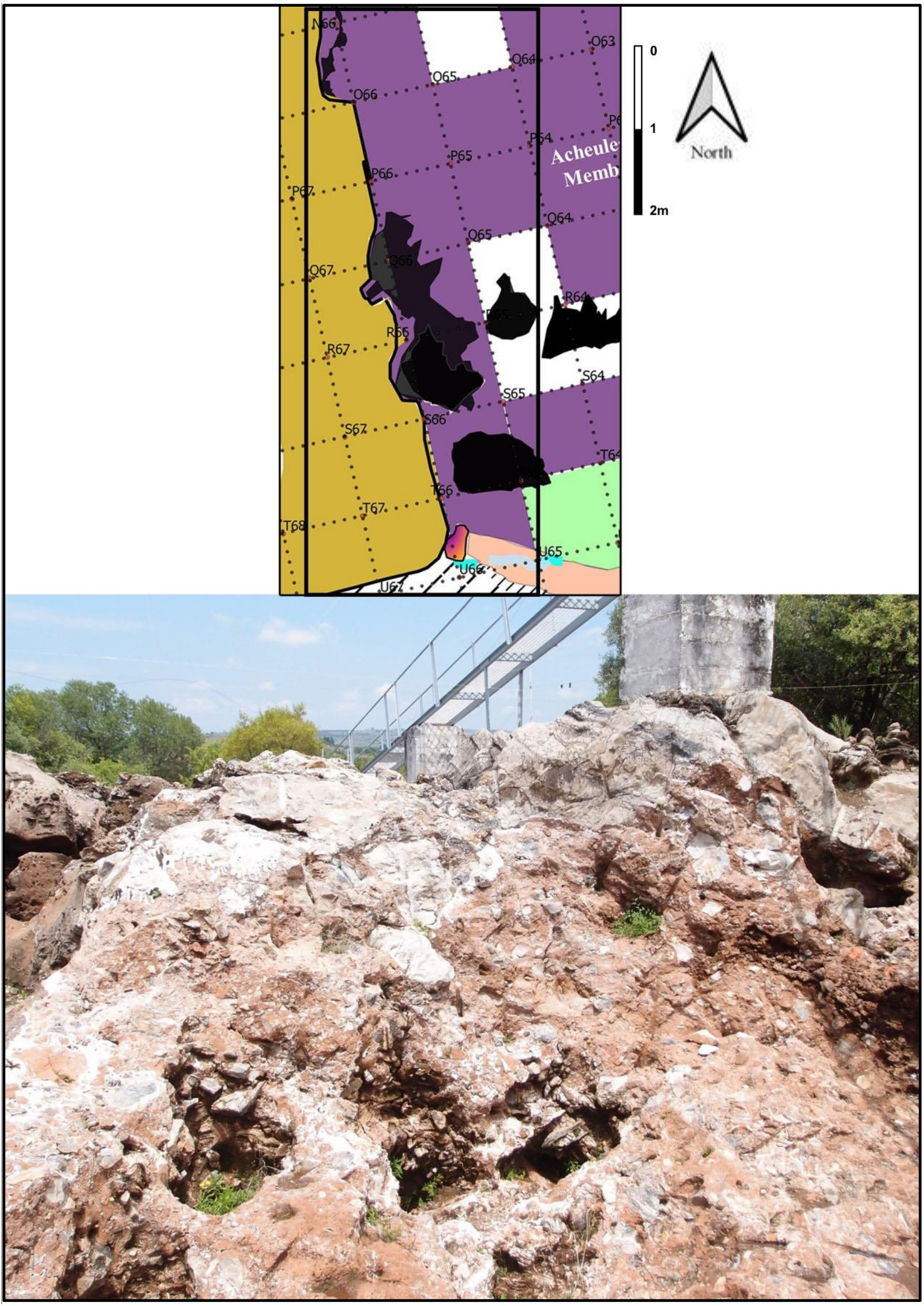

Figure 4.11. A view of M5W looking westwards in the photograph. The black rectangle in the plan denotes the current view.

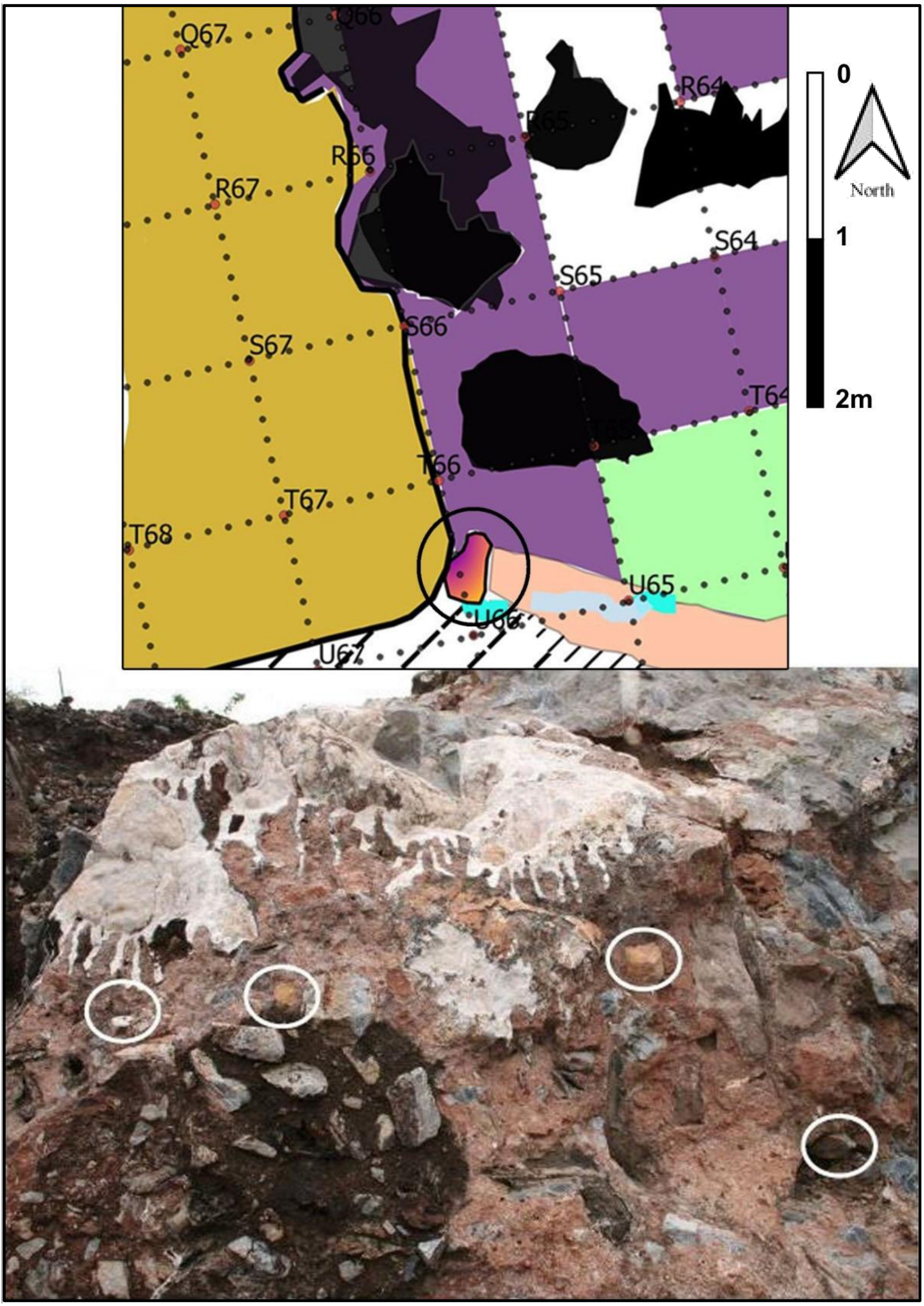

Figure 4.12. Speleothem drapery in the southwestern corner of M5W which is circled black in the plan (from Ogola 2009: 48). The white circles in the photograph depict *in situ* artifacts plotted by Ogola (2009).

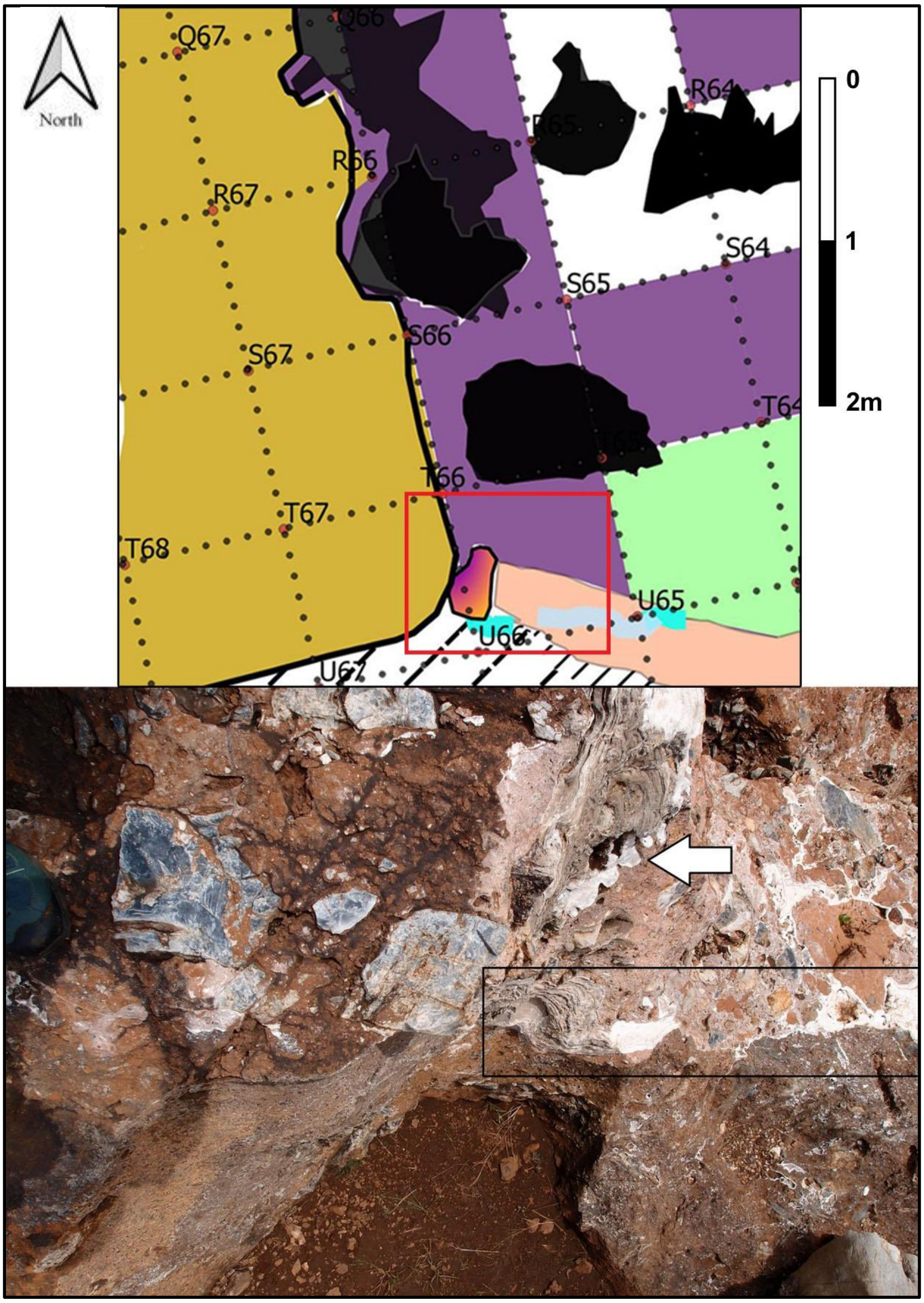

Figure 4.13. A close-up of speleothem drapery in the southwestern corner of M5W. The red rectangle in the plan shows the current view and the black rectangle in the photograph illustrates the continuation of the flowstone eastwards.

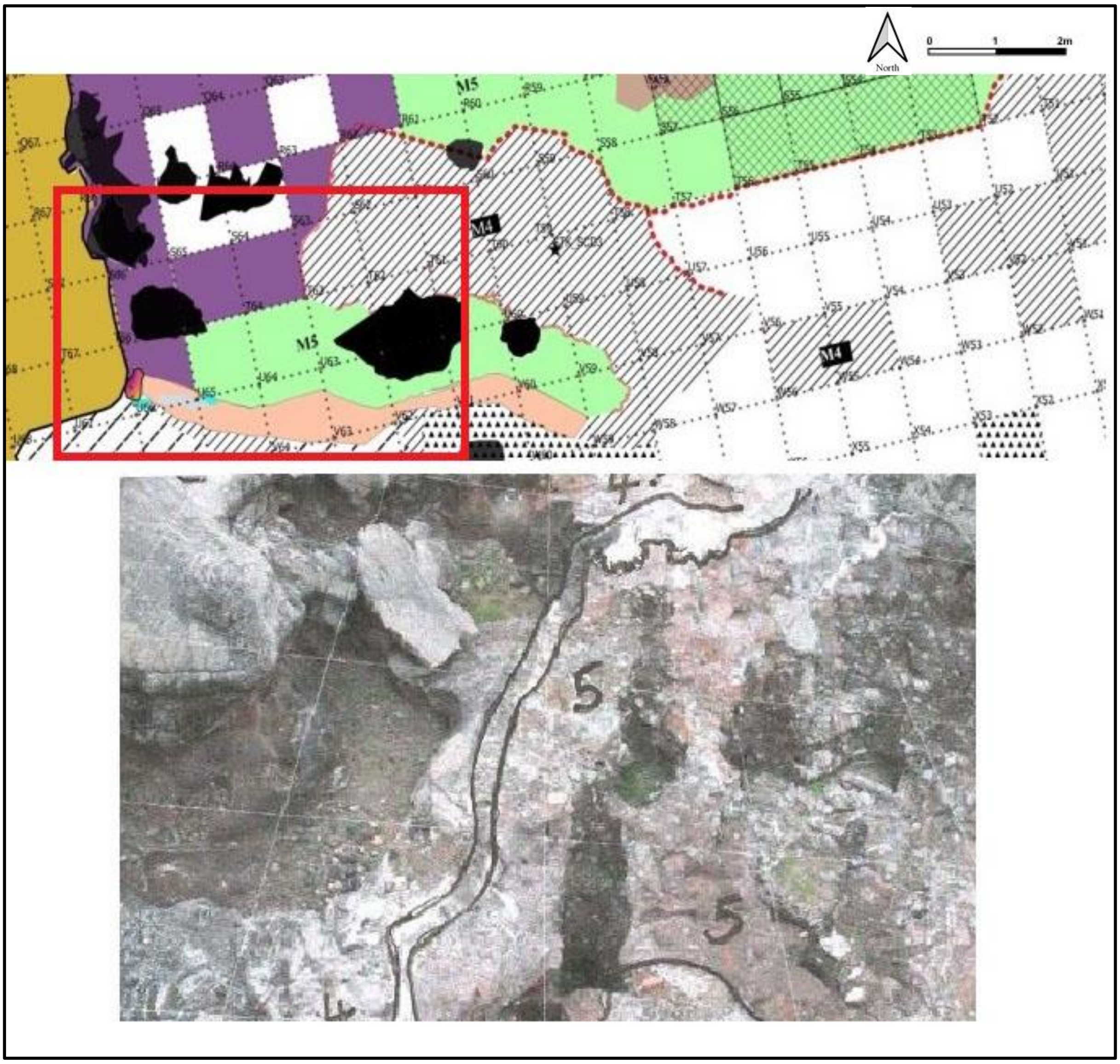

Figure 4.14. A photograph of white speleothem drapery (in the U66 area) looking westwards, in the southwestern portion of the site (from Ogola (2009: 46, based on a photograph provided by R. J. Clarke). The red rectangle in the plan denotes the current view.

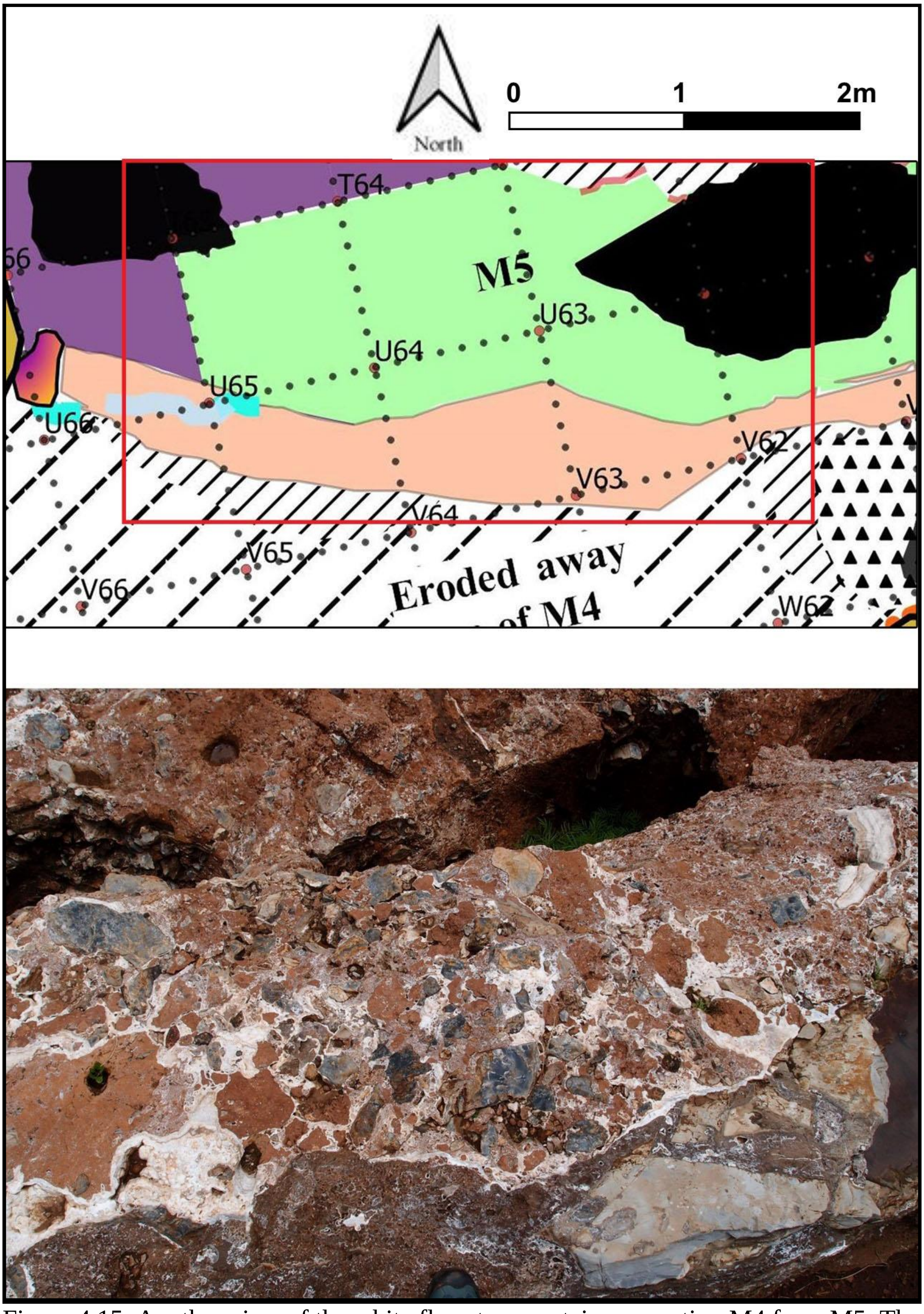

Figure 4.15. Another view of the white flowstone curtain, separating M4 from M5. The red rectangle in the plan denotes the current view. A large portion of M4 south, behind the flowstone curtain, is eroded away and only a few remnants cling to the curtain.

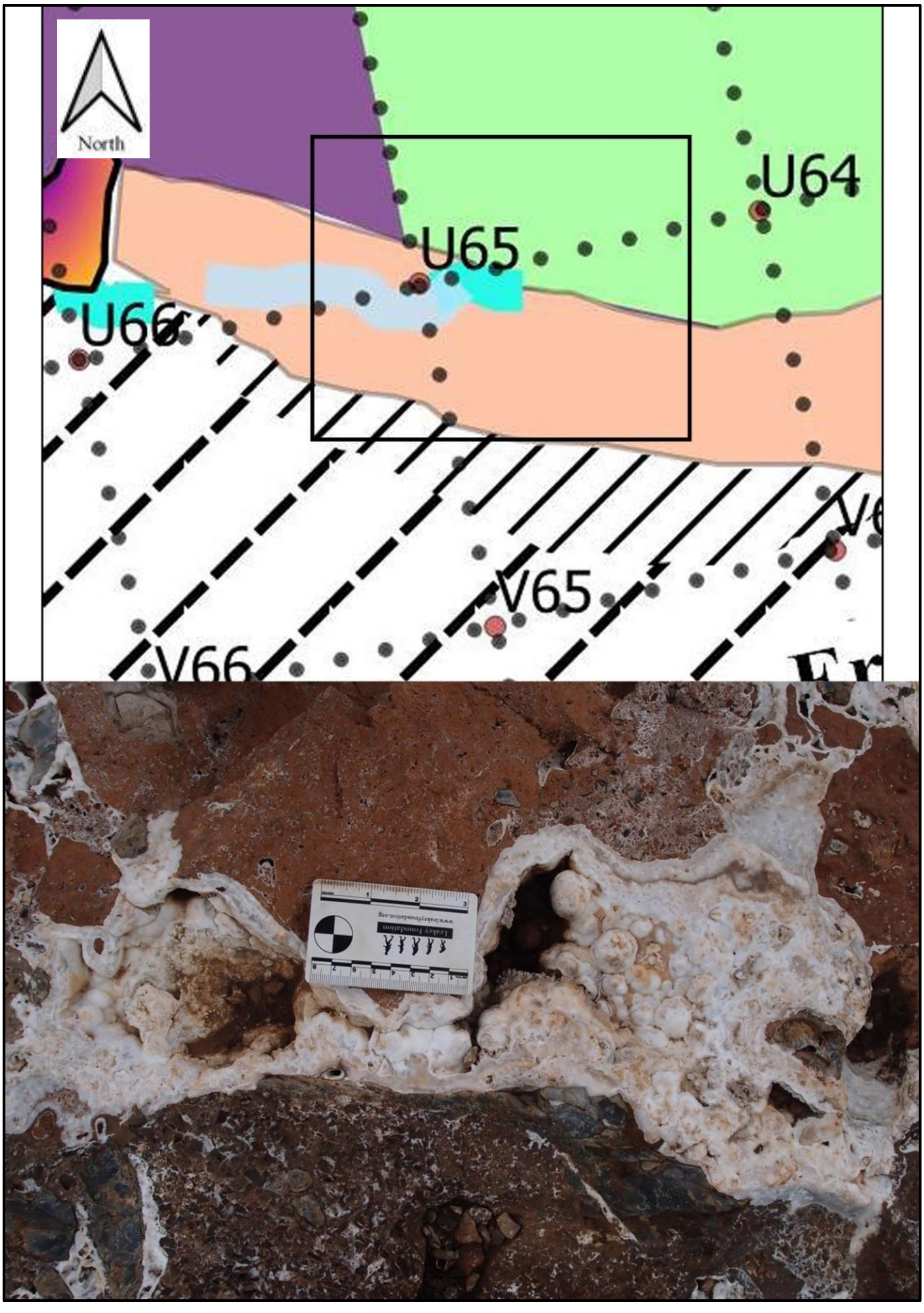

Figure 4.16. A close-up photograph of a thick portion of botryoidal flowstone, formed underwater (coloured bright blue-green in the plan). The black rectangle in the plan denotes the current view.

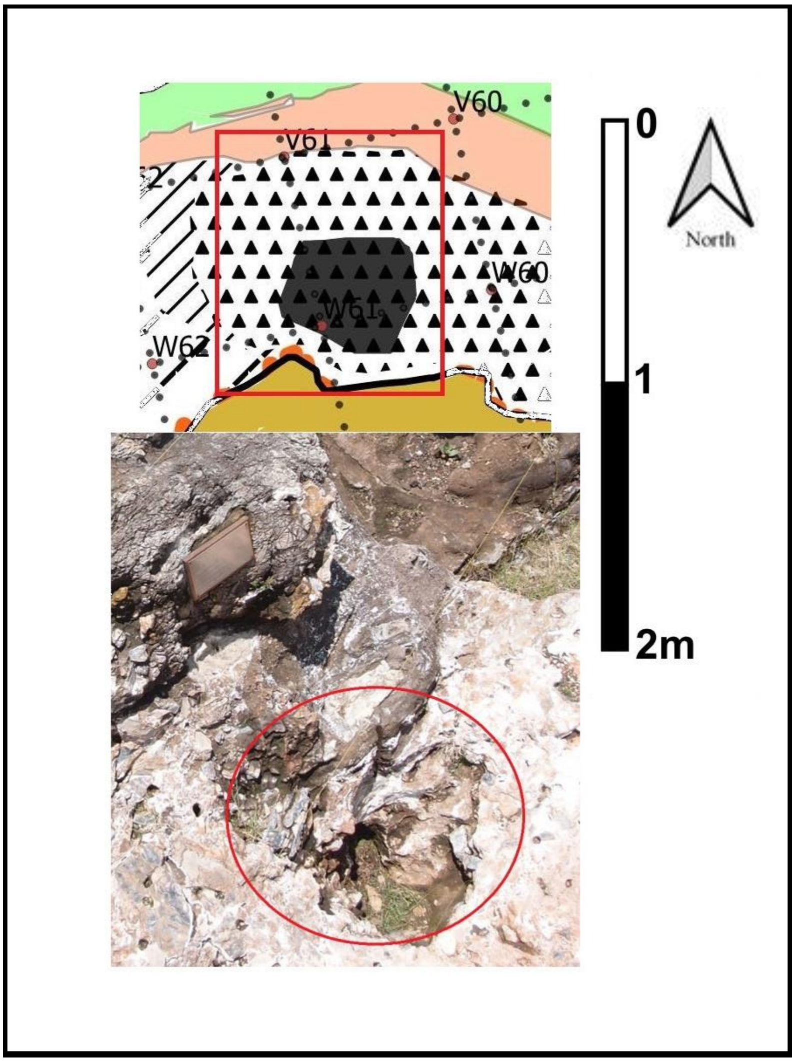

Figure 4.17. A view from above of part of the StW 53 infill (shown as triangles in the plan). The StW 53 cranium was found partly in the solution pocket (red circle) and partly in solid breccia on the right. The red rectangle in the plan denotes the current view.

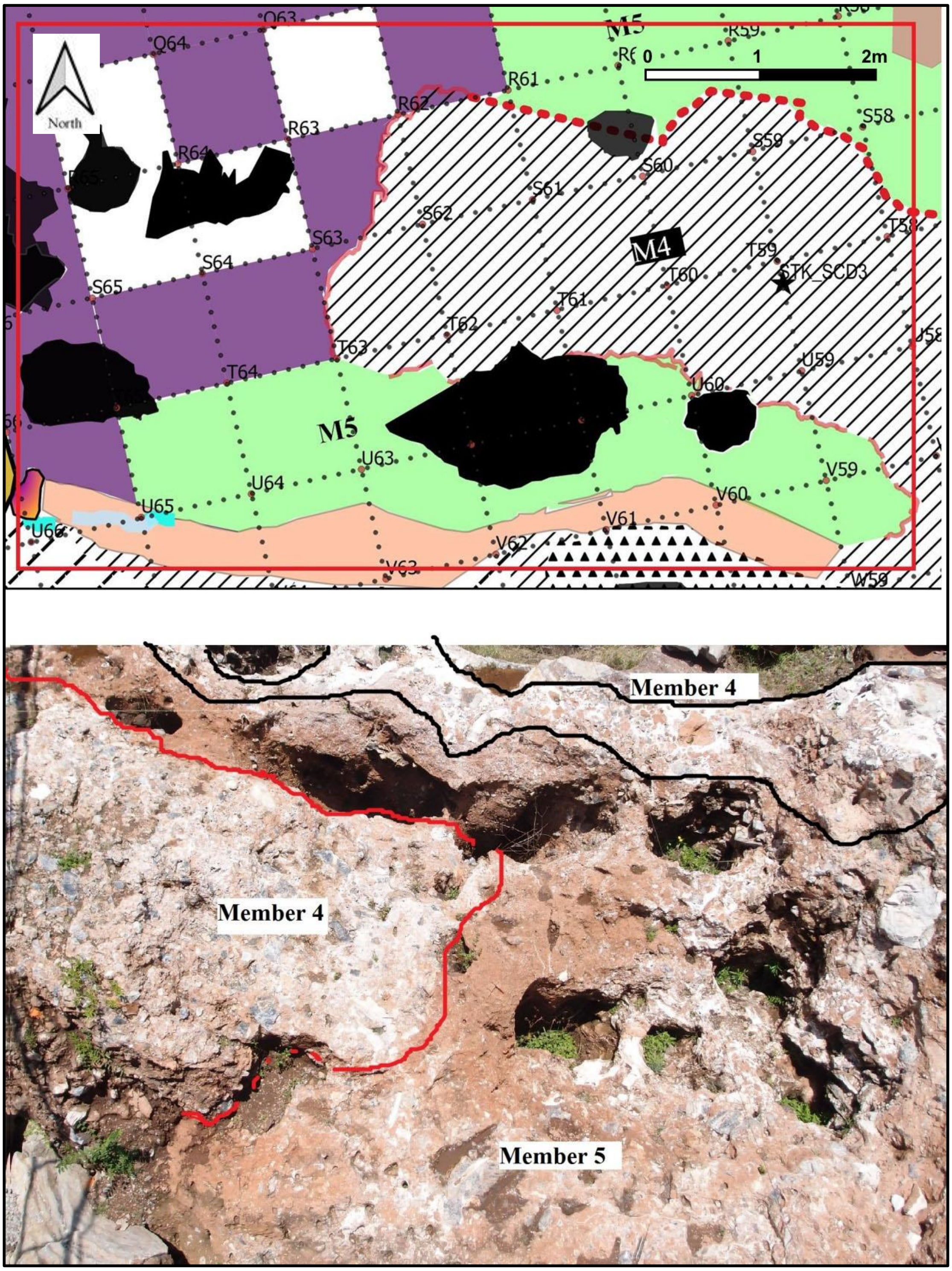

Figure 4.18. An aerial view from lines 59 to 66, with south at the top of the photograph. The red line shows the contact between M4 and M5. Speleothem drapery (U66) and flowstone curtain are outlined in black. The red rectangle in the plan denotes the current view.

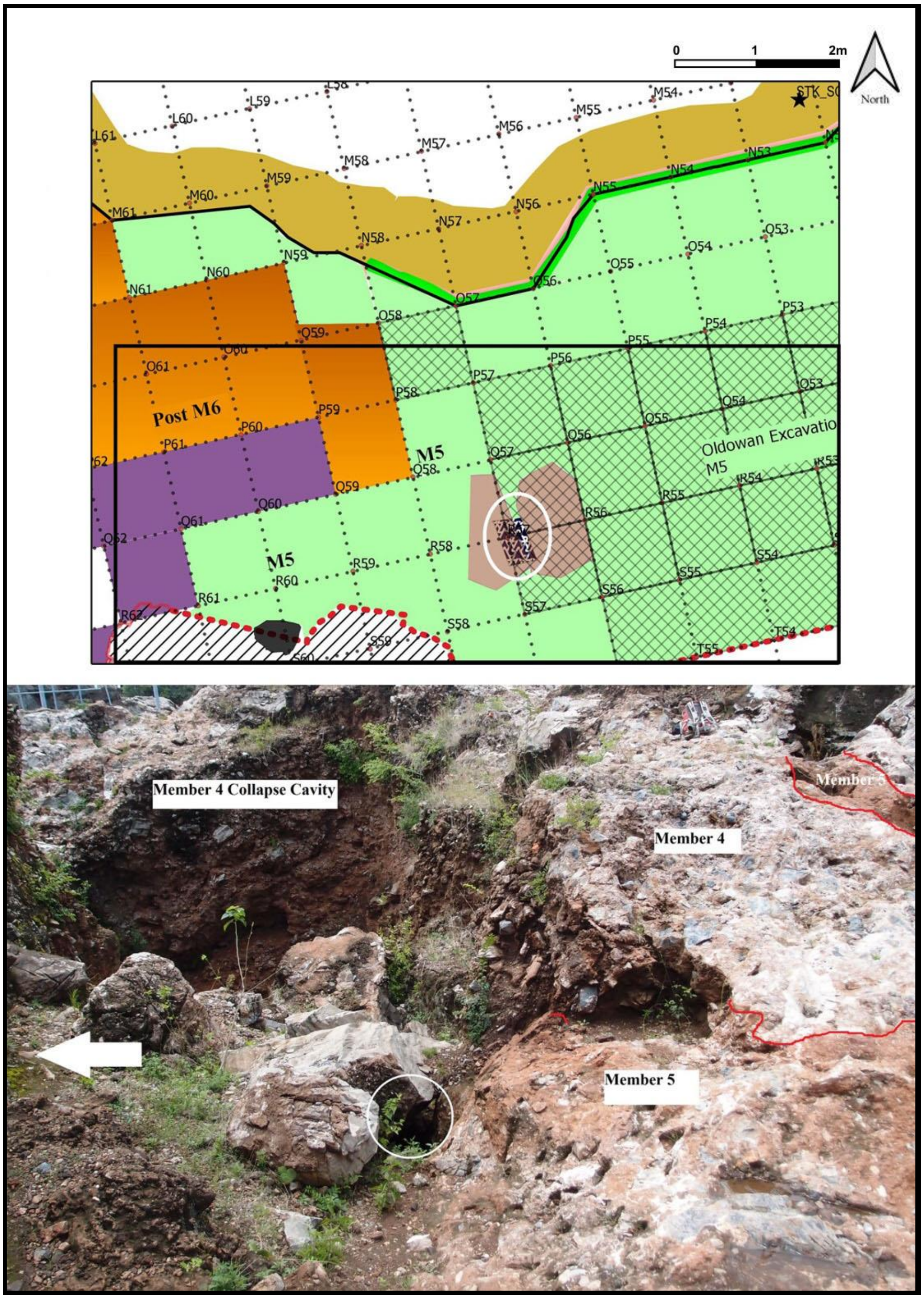

Figure 4.19. The location of the Name Chamber feeding shaft, looking east in the photograph. The shaft hole lies at R57 as (circled white in both maps). The large white arrow pointing left denotes the direction of the M5E northernmost wall (bold green line in map). In the top left of the photo M4 collapse has resulted in large dolomite boulders falling into the site. The M4/5 contact boundary is shown in red. The current view is delimited by the black rectangle in the plan.

4.2 Results of abrasion analysis

Introduction and general notes

My geometric CAD models consisted of two cubes each with volumes of 500 mm^3 and 1000 mm^3, two spheres and two pyramids. Their respective attributes are listed below and serve as a basic comparative model for our real world assemblage study.

Table 4.1. The Geometric standard model data for sphere, cube and pyramid (500 mm^3 and 1000 mm^3 respectively). Abbreviations: Num = number; min = minimum; max = maximum. Linear measurements are in mm.

Type	Area (mm^2)	Volume (mm^3)	Mean Dihedral Angle	Num points	Num faces	Num patches	Num edges	Min edge length	Max edge length	Mean edge length
S500	300.247	486.59	169.7	353	702	1	1053	0.05	1.78	0.97
S1000	480.101	983.456	169.4	735	1466	1	2199	0.05	3.50	0.99
Cu500	378.262	500.566	90	8	12	1	18	7.941	11.22	9.03
Cu1000	600	1000	90	8	12	1	18	10	14.14	11.38
P500	338.3	500	63.4	6	8	1	12	9.89	13.47	10.75
P1000	333.3	1000	63.4	6	8	1	12	7.77	17.1	13.68

My geometric CAD models display unique dihedral angle distributions, unimodal for spheres and bi-modal for cubes and pyramids, and these data were represented graphically in Figure 3.20.

The Coefficient of Variation (CV)

The Coefficient of Variation (CV) statistically is a normalized measure of dispersion that proved useful to this study for analysing the data. The CV is defined as the ratio of the standard deviation to the mean. Larger CVs indicate more dispersion around the mean (i.e. lots of variability in the sample), while lower CVs indicate less dispersion around the mean (i.e. less variability in the sample). Tables 4.2 through 4.6 represent descriptive values and highlight mean dihedral angles (DA) and Coefficient of Variation (CV) for each type of tool component.

Descriptive results of tool type surface analysis

With reference to my analysis of the tool types at Sterkfontein, it was interesting to see that chunks presented a DA = of 165.2º and a CV of 2.2%, incomplete flakes (DA = 167.4º & CV = 2.1%), flakes (DA = 168.3º & CV 1.6%), SFD (DA = 171º& CV 0.8%) and finally the Name Chamber (DA = 173.7º & CV 0.4%).

Table 4.2. Descriptive values for entire surface analysis of flakes (n = 59).

Flakes	Max Length (mm)	Volume (mm³)	Area (mm²)	Dihedral Angle (º's)	Faces
Mean	34.6	17367.7	1740.7	**168.3**	330730.6
Standard Deviation (SD)	12.9	17714.8	1485.3	2.7	283194.2
CV (value)	0.372	1.02	0.853	0.016	0.856
CV (%)	**37.2**	**102**	**85.3**	**1.6**	**85.6**
n = 59					

Table 4.3. Descriptive values for entire surface analysis of chunks (*n* = 74).

Chunks	Max Length (mm)	Volume (mm^3)	Area (mm^2)	Dihedral Angle (º's)	Faces
Mean	32	15405.5	1673.1	**165.2**	318016.7
SD	11.9	18573.6	1370.7	3.7	269918.4
CV (value)	0.373	1.206	0.819	0.022	0.849
CV (%)	**37.3**	**120.6**	**81.9**	**2.2**	**84.9**
n = 74					

Table 4.4. Descriptive values for entire surface analysis of incomplete flakes (*n* = 180).

Incomplete Flakes	Max Length (mm)	Volume (mm^3)	Area (mm^2)	Dihedral Angle (º's)	Faces
Mean	26.5	13045.3	800.3	**167.4**	151068.7
SD	5.8	11923.4	433.9	3.6	83190.6
CV (value)	0.218	0.914	0.542	0.021	0.551
CV (%)	**21.8**	**91.4**	**54.2**	**2.1**	**55.1**
n = 180					

Table 4.5. Descriptive values for entire surface analysis of SFD (*n* = 426).

SFD	Max Length (mm)	Volume (mm³)	Area (mm²)	Dihedral Angle (º's)	Faces
Mean	14.4	651.5	447.2	**171**	43429.5
SD	3.2	1506.1	100.6	1.3	20025.6
CV (value)	0.220	2.312	0.225	0.008	0.461
CV (%)	**22**	**231.2**	**22.5**	**0.8**	**46.1**
n = 426					

Table 4.6. Descriptive values for entire surface analysis of Name Chamber SFD (*n* = 51).

Name Chamber SFD	Max Length (mm)	Volume (mm³)	Area (mm²)	Dihedral Angle (º's)	Faces
Mean	12.7	189.7	226.6	**173.7**	40120
SD	2.9	160.4	112.1	0.8	20109.9
CV (value)	0.228	0.855	0.495	0.004	0.501
CV (%)	**22.8**	**85.5**	**49.5**	**0.4**	**50.1**
n = 51					

4.3 Specific Edge analysis sub-study

A smaller and much more time-consuming sub-study method that analysed specific edges of pieces was included. The results listed here are useful in providing a comparison to my more general overall surface abrasion model.

The results of this are presented below in Tables 4.7. through 4.10. In most cases the individual scores differ only slightly between the two methods, but larger differences do exist for individual pieces than when they are all encased by a group sample mean.

Table 4.7. Descriptive values for specific edge sections and their attributes for chunks (*n* = 5).

Type	Tray	Specific piece number	Number	XL (mm)	Top DA (º's)	Mid DA (º's)	Lower DA (º's)		Mean DA (º's)	Whole piece method DA (º's)
CH	6	3529	35	29	162	158	163		**161**	**160**
CH	6	3681	40	22.8	157	168	170		**166**	**166**
CH	6	2507	2	21	158	167	159		**161**	**165**
CH	7	6130	2	34	166	168	166		**167**	**162**
CH	7	6168	12	32	170	171	172		**171**	**171**
			Mean	**27.76**	**164**	**166**	**166**		**165**	**165**
			SD	5.7	5.1	4.8	5.0		4.0	4.2
			CV		**3.1**	**2.9**	**3.0**		2.4	2.5

Table 4.8. Descriptive values for specific edge sections and their attributes for flakes (*n* = 5). Abbreviation: XL = maximum length.

Type	Tray	Specific piece number	Number	XL (mm)	Top DA (º's)	Mid DA (º's)	Lower DA (º's)		Mean DA (º's)	Whole piece DA (º's)
F	4	2888	15	21	168	171	171		**170**	**170**
F	4	3239	24	39	169	170	172		**170**	**171**
F	5	3639	1	29	168	171	172		**170**	**169**
F	5	5083	4	21	166	170	171		**169**	**170**
F	5	8520	21	27	166	168	171		**168**	**171**
			Mean	**27.4**	**167**	**170**	**171**		**169**	**170**
			SD	7.4	1.3	1.1	0.5		0.9	0.6
			CV		0.79	0.66	0.00		0.5	0.4

Table 4.9. Descriptive values for specific edge sections and their attributes for incomplete flakes (n = 5).

Type	Tray	Specific piece number	Number	XL (mm)	Top DA (º's)	Mid DA (º's)	Lower DA (º's)		Mean DA (º's)	Whole piece DA (º's)
IF	2	3312	3	31	165	171	171		**169**	**170**
IF	2	3371	10	23	169	171	170		**170**	**170**
IF	2	3381	14	33	170	169	170		**170**	**166**
IF	2	3479	16	33	166	168	163		**166**	**167**
IF	3	3675	1	22	165	169	170		**168**	**168**
			Mean	**28.4**	**167**	**170**	**169**		**169**	**168**
			SD	5.5	2.2	1.5	3.5		1.8	1.9
			CV		1.3	0.9	2.0		1.1	1.2

Table 4.10. Descriptive values for specific edge sections and their attributes for Small Flaking Debris (*n* = 5)

Type	Tray	Specific piece number	Number	XL (mm)	Top DA (º's)	Mid DA (º's)	Lower DA (º's)		Mean DA (º's)	Whole piece DA (º's)
SFD	9	2391	1	18	172	171	168		**170**	**171**
SFD	9	2398	8	8	170	171	170		**170**	**170**
SFD	9	2403	13	11	166	172	167		**168**	**169**
SFD	9	2425	20	14	169	168	163		**167**	**169**
SFD	9	3007	195	11	169	172	171		**171**	**168**
			Mean	**12.4**	**169**	**171**	**168**		**169**	**169**
			SD	3.8	2.0	1.5	3.2		1.7	1.0
			CV		1.2	0.9	1.9		1.0	0.6

4.4 Statistics

Due to the large amounts of data generated in this study, the use of statistical measures was necessary to test degrees of causality and difference between artefact types and groupings. To make sure what statistical measure would be most suitable for this study, I tested my data using the Kolmogorov-Smirnov (K-S) test to assess variable distributions versus normal distributions. I found that in most cases my data were statistically significantly different to a normal distribution, thus leading me to use non-parametric tests such as Spearman's Rho and Kruskal-Wallis (sometimes called one way ANOVA), as opposed to a parametric alternative. Spearman's Rho is a non-parametric test used to measure the strength of association between two variables, where the value $r = 1$ means a perfect positive correlation and the value $r = -1$ means a perfect negative correlation.

An important value for interpreting the tables below is the 'Sig. one/two tailed value'. This value is also known as the P (or α) value, and is a measure of significance. In standard scientific research, the general practise when performing statistical testing is to reject the Null Hypothesis (H_o) when the significance value (P) is below a chosen value. Typically this value is chosen to be equal to/less than 0.05 or 0.01. When Ho is rejected, the alternative hypothesis (H_a) is accepted and the values are deemed statistically significant. When a hypothesis is deemed statistically significant this means that it is highly improbable that factors leading to any relationship have occurred by random chance. All statistical significance in this study was determined by using a significance value (P) of 0.01. The P value was adjusted to reduce the chance of false positives from occurring in testing.

4.5 Spearman's Rho tests results

Table 4.11 compares the volume of the sample to the number of faces. The Null Hypothesis (H_o) is that there is little or no relationship between the two and the alternative hypothesis is that the two are related. The results show that the two are statistically significant because the P value is lower than the α value and highly positively correlated (p = 0.762). This means that as volume increases expectedly so do the number of faces. The descriptive statistics are listed below in Table 4.12.

Table 4.11. Correlation of volume to faces.

Non-Parametric Correlations				
			Volume mm³	Number faces (Triangles)
Spearman's rho	Volume mm³	Correlation Coefficient	1.000	.762**
		Sig. (2-tailed)	.	.000
		n	794	794
	Number faces (Triangles)	Correlation Coefficient	.762**	1.000
		Sig. (2-tailed)	.000	.
		n	794	795
**. Correlation is significant at the 0.01 level (2-tailed).				

Table 4.12. Descriptive statistics for volume and number of faces.

Descriptive Statistics			
	Mean	Std. Deviation	*n*
Volume mm³	6030.0563	11604.29694	794
Number faces (Triangles)	114566.3535	158396.32630	795

The H_o for Table 4.11 is that there is no correlation between volume and number of faces and in this case we have statistical significance $p < 0.05$ so we reject the null hypothesis. The volume and number of faces are strongly and positively correlated with $r(762) = .762$, $p = .0$ (or simply $r_s = 0.762$) so as volume increases so do the number of faces on a surface.
Our H_o for the relationship between volume and mean edge length are that the two are not related. Table 4.13 demonstrates that statistical significance exists, as the two are related and correlate at $r_s = -0.626$ which is a strong correlation coefficient. This is a negative correlation; descriptives are given in Figure 4.14. We can say that as volume decreases, mean edge length increases, which is an expected result.

In Table 4.15, additional correlations between mean edge length and number of triangle faces are displayed. These are also statistically significant. The alternative hypothesis (H_a) helps us conclude a relationship with a strong negative correlation of $r_s = -0.628$. This means that as mean edge length decreases the number of faces increases. Table 4.16 reports the descriptive values for mean edge and number of triangles. Table 4.17 shows $r_s = -0.562$ meaning that there is a moderate negative correlation and mean dihedral angle decreases as volume increases.

Table 4.13. Non-parametric correlations of mean edge length to volume

Non-Parametric Correlations				
			Volume mm³	Mean edge length
Spearman's rho	Volume mm³	Correlation Coefficient	1.000	-.626**
		Sig. (2-tailed)	.	.000
		n	794	794
	Mean edge length	Correlation Coefficient	-.626**	1.000
		Sig. (2-tailed)	.000	.
		n	794	795
**. Correlation is significant at the 0.01 level (2-tailed).				

Table 4.14. Descriptive statistics for volume and mean edge length.

Descriptive Statistics			
	Mean	Std. Deviation	*n*
Volume mm³	6030.0563	11604.29694	794
Mean edge length	.1233	.00306	795

Table 4.15. Non-parametric correlation between mean edge length and number of faces on a surface.

Non-parametric correlations				
			Mean edge length	Number faces (Triangles)
Spearman's rho	Mean edge length	Correlation Coefficient	1.000	-.628**
		Sig. (2-tailed)	.	.000
		n	795	795
	Number faces (Triangles)	Correlation Coefficient	-.628**	1.000
		Sig. (2-tailed)	.000	.
		n	795	795
**. Correlation is significant at the 0.01 level (2-tailed).				

Table 4.16. Descriptive statistics for mean edge length compared to number of surface triangles.

Descriptive Statistics			
	Mean	Std. Deviation	*n*
Mean edge length	.1233	.00306	795
Number faces (Triangles)	114566.3535	158396.32630	795

Table 4.17. Non-parametric correlation between mean dihedral angle and volume.

Correlations				
			Mean Dihedral Angle	Volume mm³
Spearman's rho	Mean Dihedral Angle	Correlation Coefficient	1.000	-.562**
		Sig. (2-tailed)	.	.000
		n	793	792
	Volume mm³	Correlation Coefficient	-.562**	1.000
		Sig. (2-tailed)	.000	.
		n	792	794
**. Correlation is significant at the 0.01 level (2-tailed).				

4.6 Kruskal-Wallis Test

The Kruskal-Wallis test (sometimes called the 'one-way ANOVA on ranks') is a rank-based non-parametric test that can be used to determine if there are statistically significant differences between two or more groups of an independent variable. This test is important in this study because it compares the difference in means across a sample by using location. The ranks of the data values are used in the test rather than the actual data points. The test determines whether the medians of two or more groups are different. The test measures how much variability is accounted for within a range of contexts. For this study, the context is the excavated depth of pieces ranging every foot from 21 feet (6.4 m) to 34 feet (~10.3 m). The Null Hypothesis (H_o) for these tests is that 'groups are homogeneous,' and our alternative hypothesis (H_a) is that 'groups are different'. The effect size refers to a quantitative measure of the strength of a phenomenon by the magnitude of the difference, rather than confounding it with sample size (Coe 2002). The formula for the effect size is the chi square value divided by (n-1)*100. The effect size estimate means that x% of the variability in ranks scores is accounted for by group or location (Coe 2002). In this study, I simply report it in most cases where there is a difference between groups but we cannot be sure where the difference lies.

The α or significance level of these tests were all taken at the 0.05 level because we are testing a larger range of groups.

Flakes n = 59

Table 4.18 shows the correlation coefficient for flakes. We fail to reject the null hypothesis as p = 0.278, and thus there is little or no difference between groups. The frequency statistic shown in Tables 4.30 and 4.31 reinforces this because the p value is 0.230. Table 4.19 displays the ranked groupings for flakes.

Table 4.18. Test statistics for flake variance.

Test Statistics[a,b]	
	Mean Dihedral Angle
Chi-Square	14.371
df	12
Asymp. Sig.	.278
a. Kruskal Wallis Test	
b. Grouping Variable: Depth Group	

Effect size= 24.7%

Table 4.19. Ranked data for flakes.

Ranks			
	Depth Group (feet)	*n*	Mean Rank
Mean Dihedral Angle	21-22	6	40.83
	22-23	5	46.40
	23-24	8	35.50
	24-25	7	28.43
	25-26	5	26.40
	26-27	5	23.40
	27-28	6	24.17
	28-29	2	28.50
	29-30	3	34.67
	30-31	1	10.00
	31-32	1	34.00
	32-33	7	18.43
	33-34	3	27.33
	Total	59	

Chunks n = 74

For Chunks (Table 4.20) we reject the null hypothesis because the *p* value is 0.000, and thus there is a statistically significant difference as groups are different irrespective of chance. Our frequency test statistic (Tables 4.32 and 4.33) H_o is that median values are the same, but this too is rejected because our *p* score is 0.000. The ranked data is represented in Table 4.21.

Table 4.20. Test statistics for chunk variance.

Test Statistics[a,b]	
	Mean Dihedral Angle
Chi-Square	36.665
df	13
Asymp. Sig.	.000
a. Kruskal Wallis Test	
b. Grouping Variable: Depth Group	

Effect size= 50.22%

Table 4.21. Ranked data for chunks.

Ranks			
	Depth Group (feet)	*n*	Mean Rank
Mean Dihedral Angle	21-22	4	35.25
	22-23	10	22.20
	23-24	6	28.00
	24-25	7	17.43
	25-26	9	25.00
	26-27	2	53.00
	27-28	5	37.60
	28-29	9	38.00
	29-30	2	47.00
	30-31	2	67.50
	31-32	3	56.67
	32-33	12	57.25
	33-34	2	51.50
	34-35	1	72.00
	Total	74	

Incomplete flakes n = 180

For incomplete flakes (Table 4.22) we reject the null hypothesis because $p = 0.000$, and thus incomplete flakes are significantly different and are different between groups. The frequency test (Tables 4.34 and 4.35) also suggests that there is statistically significant difference ($p = 0.000$). The ranked scores for incomplete flakes are shown in Table 4.23.

Table 4.22. Test statistics for incomplete flake variance.

Test Statistics[a,b]	
	Mean Dihedral Angle
Chi-Square	83.418
df	12
Asymp. Sig.	.000
a. Kruskal Wallis Test	
b. Grouping Variable: Depth Group	

Effect size= 46.6%

Table 4.23. Ranked data for incomplete flakes.

Ranks			
	Depth Group (feet)	*n*	Mean Rank
Mean Dihedral Angle	21-22	9	93.33
	22-23	25	95.20
	23-24	35	91.09
	24-25	20	31.95
	25-26	22	46.32
	26-27	10	56.50
	27-28	6	110.00
	28-29	4	97.75
	29-30	8	135.75
	30-31	5	109.00
	31-32	2	131.00
	32-33	28	138.68
	33-34	6	138.67
	Total	180	

Small flaking debris (SFD) n = 426

For SFD (Table 4.24) our *p* value is 0.000, and thus I reject the null hypothesis and conclude that there is a statistically significant difference between groups. My frequency table further supports this difference with a *p* statistic of *p* = 0.000 (Table 4.36 and 4.37). Ranked data is shown in Table 4.25.

Table 4.24. Test statistics for SFD variance.

Test Statistics[a,b]	
	Mean Dihedral Angle
Chi-Square	67.154
df	11
Asymp. Sig.	.000
a. Kruskal Wallis Test	
b. Grouping Variable: Depth Group	

Effect size= 15.8%

Table 4.25. Ranked data for SFD

Ranks			
	Depth Group (feet)	*n*	Mean Rank
Mean Dihedral Angle	21-22	35	186.51
	22-23	95	209.87
	23-24	63	203.43
	24-25	34	201.74
	25-26	33	209.76
	26-27	50	125.88
	27-28	27	315.48
	28-29	35	246.86
	29-30	34	263.00
	30-31	12	312.17
	32-33	6	162.33
	34-35	2	387.00
	Total	426	

Name Chamber n = 51

For the Name Chamber (Table 4.26) we fail to reject the null hypothesis because $p > 0.5$. Thus we accept the null hypothesis that groups are homogeneous. What little difference exists can be measured by our low effect size of 6.52%. Our frequency statistic is $p = 0.203$ (Table 4.38 and 4.39). Thus, we can say there is homogeneity between the medians of tools between depths of 9'8'', 26'2'', 32'8'' and the tourist path at 91 feet and 8 inches. These values are also represented in Table 4.27.

Table 4.26. Test statistic for variance of Name Chamber artefacts.

Test Statistics[a,b]	
	Mean Dihedral Angle
Chi-Square	3.256
df	3
Asymp. Sig.	.354
a. Kruskal Wallis Test	
b. Grouping Variable: Depth Group	

Table 4.27. Ranked data for Name Chamber artefacts.

Ranks			
	Depth Group (feet and inches)	*n*	Mean Rank
Mean Dihedral Angle	9'8''	15	20.93
	26'2''	15	25.53
	32'8''	18	29.92
	Tourist Path 91'8''	3	30.17
	Total	51	

4.7 Median Test

All samples n = 739 (excluding Name Chamber)

The *p* value for ranked data from all samples is $p = 0.000$ (Table 4.28) and is the same for the frequency tables (Tables 4.40 and 4.41). Thus, our data is statistically significant and we can reject the null hypothesis. For the entire sample there is a difference between groups (Table

4.29) and our results indicate 9.76% of that difference is accounted for by depth but we cannot tell what else is affecting this difference.

Table 4.28. Test statistic for all samples.

Test Statistics[a,b]	
	Mean Dihedral Angle
Chi-Square	72.096
df	13
Asymp. Sig.	.000
a. Kruskal Wallis Test	
b. Grouping Variable: Depth Group	

Table 4.29. Ranked data for all samples.

Ranks			
	Depth Group (feet)	*n*	Mean Rank
Mean Dihedral Angle	21-22	54	378.83
	22-23	135	406.23
	23-24	112	363.19
	24-25	68	286.47
	25-26	69	287.94
	26-27	67	309.72
	27-28	44	461.77
	28-29	50	426.46
	29-30	47	493.13
	30-31	20	470.45
	31-32	6	243.17
	32-33	53	312.98
	33-34	11	300.18
	34-35	3	593.33
	Total	739	

4.8 Frequency Tables

The tables for each tool component (tables 4.30, 4.32, 4.34, 4.36, 4.38, 4.40) that precede each frequency table display a test for statistical significance. The null hypothesis(H_0) is that frequencies are homogeneous by depth, and the alternate hypothesis (H_a is that frequencies differ by depth. The frequency tables show that chunks, incomplete flakes and SFD are statistically different, whereas both flakes and all Name Chamber lithics are deemed homogeneous.

The frequency tables (tables 4.31, 4.33, 4.35, 4.37, 4.39, 4.41) show how many pieces within a particular tool category exceed or fall below the median dihedral angle value for that particular spit. This is important because we can compare it to our median dihedral angle index and describe what spit depths indicate a more or less abraded component. The pieces with dramatic increase or decrease in frequency are highlighted and emboldened. Using these frequency tables we are able to quantify abrasion states for different components for the first time.

Flakes n = 59

For flakes (Table 4.31), we fail to reject the null hypothesis as $p = 0.230$, and thus there is little or no difference between depths. We thus accept that spits are homogenous, although there is a slight variation above the median in (Table 4.31) for spits 22-23 and 23-24, indicating a relatively larger degree of abrasion for flakes in these regions.

Table 4.30. Frequency test statistic result for flakes.

Test Statistics[a]	
	Mean Dihedral Angle
n	59
Median	168.9023
Chi-Square	15.216[b]
df	12
Asymp. Sig.	.230
a. Grouping Variable: Depth Group	
b. 26 cells (92.9%) have expected frequencies less than 5. The minimum expected cell frequency is .5.	

Table 4.31. A frequency table for flakes showing uniform distribution of median values. Spits showing an increase or decrease in frequency are highlighted and their values emboldened.

Frequencies														
		Depth Group												
		22-23	23-24	24-25	25-26	26-27	27-28	28-29	29-30	30-31	31-32	32-33	33-34	34-35
Mean Dihedral Angle	> Median	**4**	**6**	3	2	1	1	1	2	0	1	2	1	0
	<= Median	**1**	**2**	4	3	4	5	1	1	1	0	5	2	0

Chunks n = 74

For chunks (Table 4.32) we reject the null hypothesis because $p = 0.000$ and thus there is a statistically significant difference as groups are different to chance. Regarding frequencies (Table 4.33), spits 22-25 fall below the median, showing that pieces are less abraded. Conversely spit 32-33 which is lower in depth shows that 12 pieces are more abraded.

Table 4.32. Frequency test statistic for chunks.

Test Statistics[a]	
	Mean Dihedral Angle
n	74
Median	**165.9763**
Chi-Square	38.727[b]
df	13
Asymp. Sig.	.000
a. Grouping Variable: Depth Group	
b. 24 cells (85.7%) have expected frequencies less than 5. The minimum expected cell frequency is .5.	

Table 4.33. Median frequency table for chunks; spits showing a dramatic increase or decrease in frequency are highlighted and their values emboldened.

Frequencies														
		Depth Group												
		22 - 23	23 - 24	24 - 25	25 - 26	26 - 27	27 - 28	28 - 29	29 - 30	30 - 31	31 - 32	32 - 33	33 - 34	34 - 35
Mean Dihedral Angle	> Median	**1**	**1**	**1**	**2**	2	3	5	1	2	3	**12**	2	1
	<= Median	**9**	**5**	**6**	**7**	0	2	4	1	0	0	**0**	0	0

Incomplete flakes n = 180

For incomplete flakes (Table 4.34), we reject the null hypothesis because *p* = 0.000 and thus there is a statistically significant difference as groups are different to chance. Regarding frequencies (Table 4.35) spits 24-26 are ≤ the median so thus we can say they are more angular and less abraded. Conversely spit 32-33 once again shows that 26 pieces are more abraded.

Table 4.34. Frequency test statistic for incomplete flakes.

Test Statistics[a]	
	Mean Dihedral Angle
n	180
Median	**168.5177**
Chi-Square	65.349[b]
df	12
Asymp. Sig.	.000
a. Grouping Variable: Depth Group	
b. 14 cells (50.0%) have expected frequencies less than 5. The minimum expected cell frequency is 1.0.	

Table 4.35. Frequency table for incomplete flakes; spits showing a dramatic increase or decrease in frequency are highlighted and their values emboldened.

Frequencies														
		Depth Group												
		22-23	23-24	24-25	25-26	26-27	27-28	28-29	29-30	30-31	31-32	32-33	33-34	34-35
Mean Dihedral Angle	> Median	**13**	16	**2**	**3**	**1**	5	4	6	3	2	**26**	5	0
	<= Median	**12**	19	**18**	**19**	**9**	1	0	2	2	0	**2**	1	0

SFD n = 426

For SFD (Table 4.36), we reject the null hypothesis because *p* = 0.000 and thus there is a statistically significant difference as groups are different to one another. Regarding frequencies for SFD (Table 4.37), a large component of the sample is balanced between more and less abraded in the upper spits (21-25 feet). In the lower spits (26-27 foot depth), comparisons show that 41 pieces are less abraded pieces while 9 are abraded, but in the very next spit this is the opposite and 27-28 foot depth are more abraded. Spits at 29-30 foot depth show a high degree of abraded pieces, while lower spits 32-33 show a low amount of less abraded pieces.

Table 4.36. Frequency test statistic for SFD.

Test Statistics[a]	
	Mean Dihedral Angle
n	426
Median	**171.2181**
Chi-Square	44.530[b]
df	11
Asymp. Sig.	.000
a. Grouping Variable: Depth Group	
b. 4 cells (14.3%) have expected frequencies less than 5. The minimum expected cell frequency is 1.0.	

Table 4.37. Frequency table for SFD; Spits showing a dramatic increase or decrease in frequency are highlighted and their values emboldened.

Frequencies														
		Depth Group												
		22-23	23-24	24-25	25-26	26-27	27-28	28-29	29-30	30-31	31-32	32-33	33-34	34-35
Mean Dihedral Angle	> Median	46	33	15	15	**9**	**21**	20	**24**	10	0	**2**	0	2
	<= Median	49	30	19	18	**41**	**6**	15	**10**	2	0	**4**	0	0

The Name Chamber SFD n = 51

For the Name Chamber (Table 4.38) we fail to reject the null hypothesis as $p = 0.203$. Thus there is little or no difference between depths within the Name Chamber, and we accept that spits are homogenous. However, the sample size is very small but Table 4.39 describes pieces from between 3 and 8 metres as being less abraded than pieces from 10 metres.

Table 4.38. Frequency test statistic for the Name Chamber.

Test Statistics[a]	
	Mean Dihedral Angle
n	51
Median	173.9000
Chi-Square	4.608[b]
df	3
Asymp. Sig.	.203
a. Grouping Variable: Depth Group	
b. 2 cells (25.0%) have expected frequencies less than 5. The minimum expected cell frequency is 1.1.	

Table 4.39. Uniformly distributed frequency table for the Name Chamber.

Frequencies					
		Depth Group			
		3 m	8 m	10 m	Tourist Path 28 m
Mean Dihedral Angle	> Median	3	5	**10**	1
	<= Median	**12**	**10**	8	**2**

All samples n = 739 (excluding Name Chamber)

For the entire sample (Table 4.40), we reject the null hypothesis ($p = 0.000$) and thus there is a statistically significant difference across the Oldowan spits. Across the entire sample (Table 4.41), it is apparent that variation exists. The major range of variation seems to lie in the between spits at 22-30 foot depths. Between the upper spit at 22-23 foot there is significantly more abrasion while conversely spits at 23-27 foot depths are less abraded. Spits at a deeper 28-31 foot depth show a higher degree of abrasion.

Table 4.40. Frequency test statistic for all samples.

Test Statistics[a]	
	Mean Dihedral Angle
n	739
Median	170.4567
Chi-Square	43.135[b]
df	13
Asymp. Sig.	.000
a. Grouping Variable: Depth Group	
b. 4 cells (14.3%) have expected frequencies less than 5. The minimum expected cell frequency is 1.5.	

Table 4.41. Median frequency table for all samples; spits showing a dramatic increase or decrease in frequency are highlighted and their values emboldened.

Frequencies															
		Depth Group													
		21-22	22-23	23-24	24-25	25-26	26-27	27-28	28-29	29-30	30-31	31-32	32-33	33-34	34-35
Mean Dihedral Angle	> Median	27	**77**	54	**27**	**25**	**29**	**29**	29	**34**	13	1	16	5	3
	<= Median	27	**58**	58	**41**	**44**	**38**	**15**	21	**13**	7	5	37	6	0

4.9 Results: Summary

Chapter 4 has provided a more detailed mapping of the western area of the site. This section improves the spatial record for certain areas of the site which were not detailed in the schematic representations provided by Kuman and Clarke (2000), which had been based largely on site contents by square. It also provides a reconstructed boundary between the M4/M5 deposits that is more accurate than previous schematics which were based solely off the excavation grid. Captions and photographs for the specific areas of the site explain the details. Most notable are features such the accurate location of the StW 53 infill and associated parts of M5 which were previously eroded away by solution pockets. The location of a large flowstone curtain which separates M5 from M4 is significant because it describes a period of subsidence where a void was created and later filled with calcite. The accurate location of the entrance to the Name Chamber is depicted and shows exactly where smaller lithics winnowed down from the base of M5E into the Name Chamber.

Section 4.2 of this chapter has presented the results of the abrasion study on M5E Oldowan artefacts and those in the underlying Nambe Chamber, which were evaluated using simple descriptive statistical values for each tool component compared to the computer-generated ideal CAD models. Statistical methods and results were based on non-parametric tests: the Coefficient of Variation (CV), Spearman's Rho, Kruskal-Wallis. Spearman's Rho tested the strength of correlation between individual variables of 3D surfaces that could be compared to CAD models. The Kruskal-Wallis test was important to measure multiple grouped variables and helped to analyse how much artefacts varied between their designated depths. Chunks and incomplete flakes are varied between depths which could be due to their high degree of angularity. Complete flakes from the Oldowan and Name Chamber showed homogeneity, the reason for this could be a sample size issue or a similar rate of abrasion within the Name Chamber may have occurred.

The frequency tables compared how often tool types fluctuated above or below the median dihedral angle for any given spit depth and showed that the greatest depth where abrasion occurred was between spits with 24-27 and 32-33 foot depths. The significance of these results is discussed in Chapter 5.

Chapter 5

5. Discussion

This chapter first summarises the results of the spatial mapping of the Sterkfontein deposits. It then discusses how and why the abrasion analysis shows that artefacts have become more abraded the deeper they are within the Oldowan deposit and why the above described results are significant.

5.1 Stratigraphic interpretations from the spatial mapping

By using GIS, I was able to create a highly accurate spatial map of the western half of the site and record details for certain features that have created complexity for these breccias, such as areas where dissolution had occurred and later admitted younger infills in some areas and not others. My GIS mapping of the site depicts specific features that differ from previous existing schematics that were only plotted based on excavated squares (e.g., Clarke 1994; Kuman and Clarke 2000). What is of most importance in this study is that the mapping describes the extent of the artefact-bearing infills and shows the features that relate to the reworking of the sediments. It is important to understand how and where these features influence the site, and to provide greater detail than was previously available. My spatial mapping provides detail of features such as the true extent of the artefact-bearing infill of M5, the position of the lower Name Chamber connection, flowstone formation, and the distribution of remnant areas of M4 breccia, both where it occurs and where it has been eroded away.

Of notable mention is the expansion of the limits of the M5 deposits to the north and the accurate plotting of these deposits. The connection between the Name Chamber feeding shaft and the M5E deposits (SquareR57) was first identified by Robinson (1962) and clarified by Clarke (1994) by feeding a hosepipe from the Extension site down into the Name Chamber. My map depicts the location of the link to the underground cave, but the surrounding breccia is now buried under a recent collapse and details of the breccias are no longer visible.

The plan also shows the location of various solution pockets, but those in the eastern half of M5 are now excavated away. It can, however, be noted that the M5E deposits were extensively affected by solution pockets that allowed MSA artefacts to contaminate the Acheulean eastern deposits up to a depth of 22 feet (Kuman 1994a; Kuman & Clarke 2000). This mixing of lithics from different periods thus restricted the information that could be obtained from the Acheulean levels in M5E.

The M5 West Acheulean deposits are more robust as they are heavily calcified and were unaffected by the decalcification that created the erosion channel which admitted the Post-M6 Infill. Excavations of the Lincoln Cave and the L63 area (Reynolds *et al.* 2003, 2007) found that some artefacts eroded out of the eastern portion of the M5 West Acheulean entered the Lincoln Caves deposits, along with MSA. My GIS map displays the specific location of the excavated connection to the Lincoln Cave (at L63) and accurately plots the distribution of the M5 capping flowstone (between M64 and L63), with M6 deposited on top of that flowstone. M6 survives as a hanging remnant, but presumably it was once a larger deposit. The younger Post-M6 Infill formed within the erosional channel which broke up large parts of the capping flowstone. Fragments of the capping flowstone are shown in Figures 4.8 and 4.9 intermixed with the Post-M6 breccia. The map shows the full extent of the Post-M6 deposit.

The StW 53 Infill (Figure 4.17) is important because it is characterised as a remnant of a late M4 breccia and contains a hominid cranium and several hominid teeth but no stone tools (Clarke 1994; Kuman & Clarke 2000). This infill was also affected by solution pockets, and conjoining portions of the StW 53 cranium were excavated from both solid and decalcified breccias. Currently work is being carried out by Laurent Bruxelles and Dominic Stratford to clarify the chronological sequence for this part of the site.

Previous mapping of this sector of the site has never been done using a GIS framework, and Figures 4.2 and 4.4 of the spatial map show the extent of M5 in the south where M5 filled an area of M4 that had collapsed. M5 formed up against a flowstone curtain that starts in the southwestern portion of the site and traverses west to east before it is affected by a solution pocket within the StW 53 Infill. M5 formed up against M4 in the central portion of the site (Figure 4.18), and the boundary between these members is shown by a red line. From lines U66 - V59, a flowstone curtain formed against the southernmost section of M4 after a period of subsidence, and M5 was deposited against this curtain. It is evident that M5 entered after the curtain formed because there is interdigitating of M5 sediments between the speleothem fingers (Figure 4.12). In some parts of M5, broken flowstone from this curtain can be seen incorporated in the deposit (Figure 4.15). A large portion of M4 south, behind the flowstone curtain, is eroded away and only a few remnants cling to the curtain (Figure 4.15). This mapping work now demonstrates the complexity of the site as a whole and its transformations through time.

5.2 Abrasion studies at STK

Kuman & Field (2009) stated that it would be important to do an analysis of the abraded component of the Oldowan assemblage from Sterkfontein M5 in order to investigate any sections of reworked breccia within the site. For this study I have gone a few steps further and described abrasion by artefact type namely: flakes, incomplete flakes, chunks and SFD in the Oldowan assemblage. This approach brought about interesting questions regarding the study of 3D surfaces and how different methodologies can be used to quantify abrasion of a given surface, the results of which will be discussed in this section. For example, mathematical and statistical analyses were used to test my hypotheses about what to expect for the Oldowan artefacts in relation to shape models. A large portion of this study was mathematical and some of my more hypothetical approach was based on a comparison between computer-produced ideal models and real world lithics. When considering data at such fine resolution, it is important to describe the trends that were predicted to occur in the computer-created data, and then compare them to the real world lithics.

My abrasion study of the artefacts that came from the M5E Oldowan and those that moved into the Name Chamber are all the more important considering the reworking that has affected the Oldowan deposit. This study of abrasion with Micro-CT has clarified what happens to artefacts when materials shift in a site. In this study the degree of abrasion between artefacts from M5E and those in the Name Chamber is quite minimal. This reflects a good integrity for the Oldowan Assemblage despite such movement. My interpretation of artefact abrasion is related to a more detailed understanding of how the movement of deposits can affect lithics, and in particular, how it can be detected in lithics if high enough resolution is applied with scanning.

5.3 Geometric CAD models and statistical analysis

In my methods, I discussed my creation of three standard geometric models to demonstrate how un-abraded versus abraded surfaces are characterised. This involved studying the way that triangles envelop a surface that is considered classically 'sharp/angular' or 'round' and how their dihedral angles, faces and edge lengths relate to each other. This provided me with a basis for comparison of the artefact data.

The main hypothesis was that an object that is much 'sharper' would align best to a cube, which by definition has 'sharp' right-angled edges, longer edge lengths and very specific dihedral angles (0º, 90º, 180º). A cube's dihedral angles would be represented graphically in a bimodal distribution (Figure 3.20). A 'rounder' object would have a more homogeneous pattern of open dihedral angles (nearing 170º) over its surface, more faces and shorter more similar edge lengths. A sphere's graphical dihedral angle distribution would be unimodal (Figure 3.20), because it is more uniform in its characteristics.

In other words, I expect an object that resembles a cube to have many areas that are long and flat which would mean that in 3D the surface would have fewer but larger triangles/faces and longer edge lengths between them. The larger and flatter these surfaces in terms of volume, the longer the resulting edge lengths. This is because a 3D mesh tries to simplify the image as best it can. Conversely, because a sphere has little or no continuous flat relief, I expect there to be more triangles/faces and much smaller and similar edge lengths. From this, I predict that more angular or what could be called 'sharp' or less abraded pieces will have fewer triangular faces. Larger lengths for 'rounder' or more abraded pieces will have more triangular faces and more similar edge lengths.

Regarding comparisons of dihedral angles, which formed the basis for whether something is construed as more or less abraded for its entire surface, it is important to remember that, because none of the natural examples I analysed will be an exact cube or sphere, I chose an intermediate midpoint value (169º) based on my data results to suggest whether an object is quantifiably more or less abraded. By analysing each piece's surface in its entirety, I could list descriptive values that may vary with each class of tool. I was able to categorise them as either 'approaching more abraded' or 'approaching less abraded'. The conclusions for these data are discussed below.

The Coefficient of Variation (CV) was also applied to highlight how much dispersion takes place around the mean for each stone tool type. Statistical techniques were applied to the data, the results of which are discussed below.

Technical Notes: A pyramid with a square base is difficult to account for shape because it not only closely resembles the properties of a cube with angles on the base of (0º, 180º) but it also tapers into a shape with very acute and difficult to measure dihedral angles. I feel the pyramid model does not prove as intuitive a basis for modelling as the cube and sphere. This model could perhaps be used in the future for comparison with lithics that exhibit extremely acute dihedral angles ≤ 90º and are of far simpler contour than those studied here. At this time it is hard to compare this shape to any real world examples investigated in this research as very few real values came close to this model.

5.4 Abrasion Index

This study aimed to analyse how abraded the entire surface of any given tool in the M5 Oldowan assemblage is and quantify it for the first time at this site.

Standardizing the abrasion index values

Based on my data results and geometric models, it was very clear that the value range is between about 163º-173º for most of the dihedral angles on any given piece. I decided that angles should be given a standard midpoint of 169º, which is the median value for my entire sample. My spherical model dihedral values are very close to this. This means that any angles less than 169º would be considered more acute, compared to any angles larger than 169º which would be more obtuse. It is important to note that the range of angles is constrained by computational processes that would never exist in real world examples unless we were dealing with artificial structures (or machined objects). Bearing this in mind, it was important to choose a set midpoint that is based on the data being presented by the real world tools. Thus, mathematically I refer to an angle x that is more obtuse where $x > 169º$ (more abraded) and more acute where $x < 169º$ (less abraded).

The most important result of the purely descriptive data is what we can glean from the dihedral angle data for each tool type and also what the Coefficient of Variation data tells us. It is clear from Tables 4.2 to 4.6 that chunks (DA = 165.2º and CV = 2.2%) and incomplete flakes (DA = 167.4º and CV = 2.1%) are tool shapes that can be considered less abraded in terms of our quantifiable index than Flakes and SFD. Chunks and incomplete flakes both display a higher degree of dispersion around the mean.

Flakes (DA = 168.3º and CV = 1.6%) and SFD (DA = 171º and CV = 0.8%) have a much higher range in terms of our index and fall closer to a more abraded state, and both have low to moderate CV dispersion characteristics. The results from our Name Chamber sub-sample (DA = 173.7º and CV = 0.4%) are of particular interest because the SFD has a higher dihedral angle than the SFD from the upper deposit, concluding that, as SFD moved lower into the site, it was subjected to more abrasion, either as a result of direct contact with surrounding debris or more likely because of distance travelled coupled with this association. The fact that chunks and incomplete flakes quantifiably display a lower dihedral angle or less abraded state most likely has something to do with their innate overall forms. Kuman & Field (2009) describe incomplete flakes as including both flake fragments and flakes lacking a platform which, as a result of their breaks, appear to have more angular components than most SFD. They describe chunks as angular or block-like entities that we can definitively state are most similar to our geometric cube model. Abrasion revealed on the chunks and incomplete flakes most closely resembles my experimental geometric standard cube model. We should remember though that these minor differences in abrasion are related to small differences in shape.

Complete flakes have a DA of 168.3º probably because they are flatter and longer (mean length of 34.6 mm compared to incomplete flakes with a mean length of 26.5 mm) and thus display a larger dihedral angle. In other words, the fact that complete flakes probably have a very intact cutting edge could explain why the dihedral angle is verging on becoming more acute. The SFD in the Oldowan Sterkfontein dominates the assemblage for pieces < 20 mm, making up almost 84.17% of the total sample (Kuman & Field 2009). I was quantitatively able to describe my SFD sample as much more abraded than any other tool type. Of particular interest is that our Name Chamber sub-sample is even more abraded (or approaching more obtuse at 173.7º) than its upper Oldowan counterpart, proving that as pieces move through the deposits, the mechanical stresses they undergo results in more abrasion on their surfaces, which is quantified here. It demonstrates that movement of the smallest lithics within all of the deposits is significantly greater, whether within the main site assemblage or in the Name Chamber.

Statistical component

Using a Spearman's Rho non-parametric test, I was able to show whether or not values were statistically significant and to what degree they were correlated to each other. I was able to test my geometric standard model theories against my real-world assemblages.

Table 4.11 compares the volume of the sample to the number of faces. The null hypothesis (H_0) is that there is little or no relationship between the volume and number of faces, and the alternative hypothesis (H_a) is that the volume and number of faces are related. The results show that both the relationship between volume and number of faces are statistically significant because the *p* value is lower than the α value and highly positively correlated (p = 0.762). This means that as volume increases, so do number of faces.

The H_o for the relationship between volume and mean edge length says that the two are not related. Table 4.13 demonstrates that a statistically significant difference exists, and thus the null hypothesis is rejected. The alternative hypothesis thus states that the two are related beyond a measure of chance and correlate at p = -0.62, which is a strong correlation coefficient. Because this is a negative correlation, we can say that as volume decreases; mean edge length increases, which supports my theory for the way in which 3D surfaces function.

In Table 4.15, additional correlations between mean edge length and number of triangle faces are displayed, and these are statistically significant. The alternative hypothesis helps us conclude a relationship with a strong negative correlation of p = -0.628. This definitively means that as mean edge length decreases the number of faces increases.

Table 4.17 illustrates a very interesting statistically significant result because volume displays a strong negative correlation with dihedral angle at p = - 0.562. Thus as volume increases, dihedral angles decrease or become more acute. The reasons for this could be due to the way a surface mesh is created and interpreted by Avizo. It is possible that computational programmes carry a volume threshold limit that manifests past a certain volume, and thus they split faces into new faces with more acute new angles when the threshold is reached (Kristian Carlson pers. comm.). This result is unexpected and needs to be investigated further.

5.5 Specified edge sub-study

For this sub-study case, I took five random pieces in each artefact category from within my data set and analysed their specific visually recognisable edges (refer to methodology section). I wanted to test what kind of dihedral angles I would get by looking solely at the main edge of a tool and comparing it to the average dihedral angle of those same five tools using my initial overall surface analysis method. The results show the difference first in the dihedral angle average of each section of the tool: top, mid and lower, and then compressed into a total average for the tool based on its three sections. The above-mentioned entire surface analysis was then performed and the results documented in Tables 4.7 to 4.10.
My results show that while some individual cases (mainly chunks) vary significantly from our primary method, the two methods yield pretty much the same results. The only difference is that the specific edge analysis can select regions of study, but at the price of taking about five times longer than my primary method which took about five minutes per tool. Another advantage of a complete surface analysis, as opposed to a sectoral study, is that there is no need for a specified alignment to be done. Alignment when studying any specific sectors of stone tools is something that is widely debated among researchers and there is little consensus on a unified method (Grosman 2008).

5.6 Kruskal-Wallis statistical analysis

A Kruskal-Wallis (or one way ANOVA) test was performed for the dihedral angle of each artefact type as a group in order to measure variability or lack thereof within the sample throughout individual spit depths (21-34 feet or approximately 6.4-10.3m). The Kruskal-Wallis test is important because it can measure multiple grouping variables at once and helped me analyse how much artefacts vary between their designated depths. The reported effect size is used to calculate the percentage of variability that takes place between groups if we know a difference exists but we cannot specify where it exists. The null hypothesis (H_0) for these tests is that 'groups are homogeneous', and our alternative hypothesis (H_a) is that 'groups are different'.

The mean dihedral angle for chunks, incomplete flakes, and SFD were all measured as statistically significant. Once again chunks and incomplete flakes display a variability difference between samples. I hypothesize that this is because of their high degree of angularity that influences the outcome of intergroup comparisons. Complete flakes from the Oldowan and the Name Chamber SFD tested $p > 0.05$ and thus the H_0 was accepted, leading to the conclusion that there is homogeneity between groups. The reason for this could be a sample size issue or it could simply mean that these categories have undergone a similar rate of abrasion within the Name Chamber leading them to be more similar. I hypothesize the reason for this is because the feeding shaft of the Name Chamber is so narrow that pieces underwent the same type and rate of abrasion. This fact indeed requires further investigation. Another important characteristic to note about SFD and complete flakes is that they both have flat edges and in some cases SFD are just a smaller type of complete flake, which is why they may respond correspondingly to abrasion.

5.7 Frequency tables

The results of the frequency tables listed in Chapter 5 display some very interesting trends. Frequency tables list the number of tool categories across spit depth and count how many times individual tools fall higher or lower than the median dihedral angle value of that particular category (this median value is listed in the descriptive table for each value). The importance of this is that we can compare it to our Median dihedral angle index and describe what spit depths indicate a more or less abraded component. Again a test for statistical significance is carried out in the frequency tables with a H_0 that frequencies are homogeneous by depth, with the H_a that frequencies differ by depth. Once again, chunks, incomplete flakes and SFD are statistically different and flakes and the Name Chamber lithics are deemed homogeneous.

I noticed various trends in the frequency tables, and to further illustrate these trends I had emboldened and highlighted the spits of interest. It is noticeable that in certain spits pieces are distributed either above or below the median value and tend to cluster in groups either side of the median. Even though Tables 4.30 and 4.31 for complete flakes are statistically homogeneous in terms of frequency, we can see a few small differences in the 21-24 foot spits (high up in the infill), where more pieces are visibly different from the rest and are clustered together with values greater than the median, and thus more abraded. For chunks (Tables 4.32-4.33), values for spits from 22-25 feet are ≤ median, suggesting that in these levels of the infill pieces are more angular and less abraded. However, in the 32-33 foot spits, there are 12 pieces out of a total of 74 pieces (8.8%) that are above the median, suggesting that at this depth chunks are more abraded because their median is higher than the average dihedral angle midpoint.

For incomplete flakes (Tables 4.34-4.35), spits from 24-26 feet exhibit the most difference and are lower in value than the median, suggesting again a less abraded state. However, within spit 32-33 feet (the same as for chunks) a large number of pieces have values greater than the median, leading us to believe that there is a trend within the spit with 32-33 foot depth and that more abrasion has taken place in the lower levels of the site. For SFD (Tables 4.36-4.37), a large component of the sample is balanced between more and less abraded in the upper spits (21-25 feet). Spits with 26-27 foot depth comparisons show that 41 pieces are less abraded pieces while 9 are abraded, but in the very next spit that reverses and 21 pieces from spits with 27-28 foot depth are more abraded. Spits with 29-30 foot depth show a high degree of abraded pieces. Across the entire sample (see Tables 4.40-4.41), it is apparent that variation exists, although the values are evenly distributed; however the majority of differences still lie in spits with 24-27 and 32-33 foot depths.

The results discussed above once again illustrate just how complex karst environments and their associated assemblages can be. This study has worked towards providing some additional methodology, and for the first time, it has provided some quantitative values with which to better understand the Sterkfontein Caves site in terms of its secondary context and reworking of some material.

5.8 Discussion: Summary

Chapter 5 has discussed the results in terms of their significance for a more precise spatial mapping of the site, to improve on the previous schematic maps, and the degree of abrasion that can be detected with high resolution MicroCT scanning..

Of great importance in this study is that the mapping describes the extent of the artefact-bearing infills and shows notable features that relate to the reworking of the sediments. It is important to understand how and where these features influence the site and affect the lithic assemblages, as it provides greater details about micro-level site formation processes than was previously available in more schematic studies. Of particular interest was the re-examined northerly extent of the M5 deposits, the large flowstone curtain that separates an eroded section of M4 from the south portion of M5 (Squares U66, V66-V60, W60) and the accurate location of the entrance of the shaft in Square R57 where materials from the Oldowan were shown to have winnowed into the Name Chamber.

This chapter then described abrasion on tool types from the Oldowan assemblage (n = 739) using Spearman's Rho, Kruskal-Wallis and basic descriptive statistics. Results were based on a comparison between computer-produced ideal models and the actual Oldowan and Name Chamber lithics. Considering data at such fine resolution using this type of comparison proved useful.

The three standard geometric models (cube, sphere and pyramid) demonstrate how un-abraded versus abraded surfaces are characterised. The main hypothesis was that an object that is much 'sharper' would align best to a cube with right-angled edges, longer edge lengths and specific dihedral angles (0º, 90º, 180º). A 'rounder' object would have a more homogeneous pattern of open dihedral angles (nearing 170º) over its surface, more faces and shorter / more similar edge lengths. A Spearman's Rho test was used to compare Oldowan scanned surfaces against user-generated CAD models. The results show that the relationship between volume and number of faces is statistically significant and highly positively correlated (p = 0.762). This means that as volume increases, so do the number of faces. The relationship between volume and mean edge length correlates at p = -0.62, which is a strong correlation coefficient. This correlation is negative. Thus, as volume decreases mean edge length increases, supporting my theory for the way in which 3D surfaces function.

According to the abrasion index, lithics with a dihedral angle below 169º are considered less abraded and those with a DA greater than 169º are more abraded; chunks (DA = 165.2º) and incomplete flakes (DA = 167.4º) are less abraded, while Flakes (DA = 168.3º) and SFD (DA = 171º) are more abraded. Reworked SFD from the lower Name Chamber are the most abraded component (DA = 173.7º).

A Kruskal-Wallis (one way ANOVA) was performed for the DA of each artefact type in order to measure variability, or lack thereof, within the sample for individual spit depths. Chunks, incomplete flakes, and SFD all tested statistically significant showing difference between groups. Conversely complete flakes from the Oldowan and the Name Chamber SFD showed homogeneity between groups. The reasons for this require further investigation.

Similarly, frequency statistics were used to test how many artefacts fell below or exceeded the median index value (169º) in order to account for abrasion by depth. For the overall sample, it is clear that spit depths of 24-27 and 32-33 feet showed the most variations, with the deeper lithics being more abraded which was an important result of this study.

Chapter 6

6. The Sterkfontein Caves in context

This chapter summarizes the overall context of the site, from the nature of the catchment area which accumulated an extensive M5 lithic assemblage, to the importance of hominid finds, the environmental conclusions and the overall behavioural implications. This chapter also provides some perspective on the way the methods applied here can benefit archaeological research in the future.

Sterkfontein is undoubtedly one of the most unique and information-rich sites in southern Africa. Since the first fossil discovery of a hominid in 1936, the caves have yielded hundreds of hominid specimens, many thousands of associated faunal remains, palaeoenvironmental indicators (based on faunal taxa, isotopic studies and fossil wood), and the largest intact Oldowan and Early Acheulean stone tool assemblages in southern Africa. The Sterkfontein sequence has yielded an enormous amount of physical evidence regarding hominids, most notably the complete skeleton of *Australopithecus prometheus* from M2, along with hundreds of other *Australopithecus* specimens within the caves (Clarke & Kuman 2019). *Paranthropus robustus* and early *Homo* fossils are less common at Sterkfontein but are still present in the deposits. The hominid responsible for producing the Oldowan stone tool assemblage is most likely *Homo habilis* (Stratford *et al.* 2016). Other important research at the caves has shown that faunal remains and isotopic studies are useful for critically interpreting and comparing environmental change during shifting periods of human evolution.

Most recently M2 was dated to ca. 3.67 Ma using cosmogenic burial dating (Granger *et al.* 2015). Currently M4 is estimated on fauna to be ca 2.4 - 2.8 Ma based on bovid fauna (Vrba 1982) or ca. 3.3 Ma (Clarke 2013). The Oldowan stone tool component (cosmogenically dated to ca. 2.18 Ma) is massively important because it is the largest and earliest in southern Africa. The site of Swartkrans, located only about 1 km from Sterkfontein, is only the second site with a similar lithic profile and has Oldowan artefacts ca. 2.2 Ma (Kuman *et al.* 2021). The younger Acheulean breccia in M5 is estimated to be ca 1.7-1.4 Ma based on the fauna and the early archaeology (Kuman & Clarke 2000).

Karst sites, although problematic in their formation, are important because they capture valuable deposits that can be used to study human and cultural evolution, and the depositional processes of these sites are important to understand. Karst system sites have been described by Sherwood & Goldberg (2001) as highly effective sediment traps, which are also referred to as 'keyhole sites' that preserve archaeological materials. Karst environments can consist of shallow rock shelters with stable land surfaces or deep cavernous labyrinths within bedrock completely protected from the elements and devoid of light (Mandel *et al.* 2017). In the Cradle of Humankind, caves such as Sterkfontein are primarily formed by the dissolution of limestone underground, leading to steep vertical openings by which sediments and archaeological assemblages accumulate. Deposition of artefacts is often accelerated by hydraulic action, slope wash or gravity but also can be disturbed by these same factors.

It is essential to study site formation processes carefully and with high resolution techniques before we can address Oldowan behaviour at Sterkfontein. The results of high resolution methodologies for studying site formation at Sterkfontein and how such methods could be used to study other sites in the future are discussed in the concluding section (6.1).

6.1 Conclusions

Isotopic research by Luyt & Lee-Thorp (2003) showed that the catchment area of the M5E Oldowan was stable, and large shady trees probably attracted hominids over time to the cave entrance (Kuman 2003). Research to clarify the nature of movement of lithics into the cave and its stratigraphic detail is important. Stratford *et al.* (2012) showed that a portion of artefacts from the base of M5E had winnowed down a hole into the Name Chamber below. Although it was shown that SFD and large numbers of microfauna were known to have winnowed down from the base of the M5E Oldowan deposit into the depths of the Name Chamber, abrasion of lithics could not be detected macroscopically, so Micro-CT scanning was used in the current study.

It is important to trace artefacts that have experienced reworking because it gives us the opportunity to investigate the site formation circumstances through the processes directly affecting the artefacts and deposits. This study has offered some perspectives on mechanical diagenesis through the use of Micro-CT scanning. Unlike traditional scanning electron microscopy (SEM) which produces 2D images, Micro-CT scanning produces 3D models where morphologies can be analysed both internally and externally. Geoarchaeological research, integrated with 3D analysis both spatially within a site and for the landscape, has been used at many notable South African sites such as: Blombos Cave (Archer *et al.* 2015; Henshilwood *et al.* 2001a), Klasies River (Wurz *et al.* 2018), Pinnacle Point (Karkanas & Goldberg 2010; Marean *et al.* 2010) and Wonderwerk Cave (Chazan *et al.* 2012). Multi-faceted research is useful for any site (Katsianis *et al.* 2017), including Sterkfontein as described in this study, and has helped to greatly improve understanding of spatial aspects of site formation, and thus cultural development in the earliest archaeology of the country.

The results of this study have confirmed that the Oldowan assemblage has good integrity, because the differences we see in abrasion states between the various artefact types and their different sizes are very small. This has been demonstrated through comparison of the Oldowan M5E assemblage with Oldowan lithics excavated from the underlying Name Chamber, where lithics were known to have moved through a 12.5 m long shaft to settle within the underground talus. Because abrasion produced during this process was not visible macroscopically, the use of high resolution methods proved useful. Stratford (2008) explained that about 90% of Name Chamber SFD was considered fresh at the time of excavation, and thus the use of accurate testing methodologies was beneficial to understanding and quantifying abrasion characteristics. Although the differences may be minor, they are demonstrated to be statistically significant, as values for the Name Chamber artefacts do show differences in abrasion to those from the M5E Oldowan. This analysis with Micro-CT at high resolution has now been shown as a methodology which can be applied to better understand complex karst environments.

The artefact surface analysis methodology posited here describes many different eventualities that could influence the difference in values. Thus I carried out extensive testing using geometric models to provide templates for fresh versus abraded pieces, against which the actual Oldowan lithics were compared. The comparative results obtained for study of abrasion on the whole surface of an artefact versus only the edges yielded virtually identical results, because the complete surface result includes values for the edges. As study of the specific edges took much longer to accomplish, analysis of the entire surface is demonstrated to be effective and preferable, which is another outcome of this study. My abrasion study has shown that the Oldowan has maintained its integrity despite the very complicated movement and reworking of sediments within the site. The SFD from the upper Oldowan deposit was shown to have experienced some abrasion (DA = 171º) but not as significant as the SFD from the underlying Name Chamber (DA = 173.7º).

The GIS spatial plan produced in this study now provides more detail for infills and karst features within the western half of the site than any previous plans had been able to do. The plan shows the detail of features that contributed to both site formation and disturbance, and it will serve as a reference should any further excavations be carried out at the site in future. Additionally the mapping carried out in this study has added more information about the site than the previous schematic diagram (Kuman & Clarke 2000), which was created based on plots of faunal, lithic and hominid contents within excavated squares. The new study now shows features such as a large flowstone curtain to the south of M5 that separates it from an eroded-away section of M4 that had not previously been mapped. The position of an extensive flowstone that caps M5 located in the north of the site is now shown in detail, as is the entrance to the Name Chamber feeding shaft located at square R 57.

Other work is already being carried out at Sterkfontein to integrate the surface-exposed stratigraphic members with the subterranean deposits within the cave system into a greater GIS spatial framework. My research is thus a tool that provides pieces of the puzzle catering to this much larger objective, and it will be used to improve future research on the stratigraphy within the caves. In addition, high resolution analysis of abrasion levels for lithics within the karst site of Sterkfontein has proven useful for understanding reworked contexts within the site. The dynamics of both the overall surface method and the method for studying specific edges have proven resilient across a number of test factors and should provide a new and flexible medium for studying archaeological questions that pertain to site formation, particularly in reworked contexts. While such sites are limited in number, they provide key assemblages representing the earliest archaeology in southern Africa.

6.2 Micro-CT scanning and potential future applications

It must be understood that the greater focus of this work is actually very specific. This study concentrates very heavily on testing the degree of reworking of the Oldowan deposits, coupled with a way to more accurately identify and clarify the complex stratigraphic features that influence site formations. Bearing this in mind, the research described here undoubtedly displays potential for study of other complex karst sites inside and outside the Cradle of Humankind.

The use of Micro-CT scanning is a gateway to high resolution studies of artefacts, and even though it is not accessible to many archaeologists, it is an extremely versatile tool should one consider it, particularly for overcoming problems of small artefact size and those with reflective surfaces such as quartz, which often appears fresh to the naked eye. Some prior studies using Micro-CT include Pargeter *et al.* (2017), who studied fracture analytics of quartz artefacts, and Bradfield (2016), who adapted a version of lithic macro-fracture analysis to investigate the internal features of bone tools. Both studies show that there is great potential for inter-field analysis or combined techniques for artefact examination. Comparison of archaeological material to a fresh experimental flaking assemblage would be another application.

In the greater Cradle of Humankind area, various other sites with lithics exist. Most notable is Swartkrans (see Figure 1.1), which is situated nearby and is most similar to Sterkfontein in terms of its lithic assemblages. Like Sterkfontein, it has provided a distinct Oldowan occupation with a sizable SFD component within a quartz-dominated assemblage, but raw material was available from surface outcrops close to the site and cores were not intensively reduced (Kuman *et al.* 2018). At Sterkfontein, core reduction was more intensive, with more effort to transport better raw materials into the site from nearby river gravels (Kuman & Field 2009). Micro-CT of the Swartkrans lithics could potentially be used for a future study that compares quartz obtained from the gravels to the quartz from surface outcrops. Quartz from the gravels has fewer flaws in it, having survived movement in the river, while quartz from outcrops can have more flaws and internal imperfections in it (Kuman & Field 2009). Micro-CT is thus a tool we can use to study these differences to gain a better understanding of how and why hominids selected certain raw materials above others.

Another potential site where the method could be applied is the Cave of Hearths, a karst cave site located in the Makapansgat Valley, in the Limpopo Province of South Africa. It is a limestone cavern containing an extensive record of Early, Middle and Later Stone Age accumulations, as well as Iron Age layers. Discovered by C. van Riet Lowe in 1937, the site was extensively excavated and described by Revil John Mason in the early 1950s (Mason 1988). Later a more detailed study of the site was published by McNabb & Sinclair (2009), which included a re-interpretation of Mason's description of the Acheulean in the three earliest beds (McNabb 2009).

McNabb (2009) describes that the ESA beds (1-3) were deposited onto a hard travertine flowstone that formed on a layer of bat guano. The talus deposit exhibited a minor slope as material accumulated below a cave entrance. A swallow hole near the rear wall of the cave formed during the MSA and displaced some of the deposits about 4 metres below the base of Bed 1. However, the consolidated nature of the Acheulean deposits led Mason to believe that these beds were largely *in situ*, with the hominids living within the cave and knapping inside its limits. McNabb (2009) disputed this assumption first on the basis that the deposits were disturbed biologically and by sedimentary processes, and secondly by noting that SFD was largely absent from Mason's assemblage. To McNabb, this meant that the assemblage was incomplete, and either knapping took place outside of the cave or the large majority of SFD was transported away through the swallow hole and could not be recovered. Because the deposits had been removed through excavation, stratigraphy could not provide a clear explanation. McNabb (2009) describes non-quartzite tools as weathered to a large degree, and he discounted them in his study because quartzite was the dominant raw material. Apparently quartzite was readily available from natural outcrops just outside of the cave and from the nearby river gravels. Overall, however, McNabb thought that tool production took place at the entrance to the cave, with larger blanks being transported into the cave and only minimally worked once inside, which is probably the more likely explanation for the paucity of SFD. If SFD had been preserved at Cave of Hearths, it could have been used to glean some information about site formation. However, there are large numbers of flakes in varied sizes within the collection that could be studied with Micro-CT scanning to address the question of abrasion of lithics. Such work could potentially provide some evidence as to the level of hydraulic energy influencing the deposition of material in the cave (and perhaps for the weathered lithics), or its reworking within the cave system.

Swartkrans and Cave of Hearths are thus only two examples of sites where such applications might have some potential to help decipher aspects of site formation through the high resolution scanning of artefacts.If we can quantify abrasion for SFD at Sterkfontein perhaps, we can apply this methodology to other sites either within or outside of the Cradle of Humankind in order to better understand a distinct loss or over-representation of material within assemblages.

Another example of future abrasion studies could include a comparison of Oldowan material in M5E to Acheulean tools in M5W, which are known to have undergone different processes of deposition and more weathering at the surface prior to deposition. This is something the author is looking to investigate further to provide a better understanding of Member 5 overall.

References

Abel, R.L., Ashton, N.M., Parfitt, S.A., Lewis, S.G., Scott, B., Stringer, C. 2011. Digital preservation and dissemination of ancient lithic technology with modern micro-CT. *Computers & Graphics* 35: 878-884.

Andrefsky, W. 2009. The analysis of stone tool procurement, production, and maintenance. *Journal of Archaeological Research* 17(1): 65-103.

Archer, W. & Braun, D.R. 2010. Variability in bifacial technology at Elandsfontein, Western Cape, South Africa: a geometric morphometric approach. *Journal of Archaeological Science* 37: 201-209.

Archer, W., Gunz, P., van Niekerk, K.L., Henshilwood, C.S., McPherron, S.P. 2015. Diachronic change within the Still Bay at Blombos Cave, South Africa. *PLoS One* 10(7): e0132428.

Archer, W., Pop, C., Rezek, Z., Schlager, S., Lin, S.C., Weiss, M., Dogandzic, T., Desta, D., McPherron, S.P. 2017. A geometric morphometric relationship predicts stone flake shape and size variability. *Archaeological and Anthropological Sciences* 36(38): 1945-1954.

Avery, D.M., Stratford, D.J., Sénégas, F. 2010. Micromammals and the formation of the Name Chamber at Sterkfontein, South Africa. *Geobios* 43: 379-387.

Bamford, M.K. 1999. Pliocene wood from an early hominid cave deposit, Sterkfontein, South Africa. *South African Journal of Science* 95: 231-237.

Barham, L. 1987. The bipolar technique in Southern Africa: A replication experiment. *South African Archaeological Bulletin* 42(145): 45-50.

Berna, F., Goldberg, P., Horwitz, L.K., Brink, J., Holt, S., Bamford, M., Chazan, M. 2012. Microstratigraphic evidence of in situ fire in the Acheulean strata of Wonderwerk Cave, Northern Cape province, South Africa. *Proceedings of the National Academy of Sciences* 109(20): 1215-1220.

Bewley, R.H., Crutchley, S.P., Shell, C.A. 2005. New light on an ancient landscape: LiDAR survey in the Stonehenge World Heritage Site. *Antiquity* 79: 636-647.

Bicket, A.R., Rendell, H.M., Claridge, A., Rose, P., Andrews, J., Brown, F.S. 2009. A multiscale geoarchaeological approach from the Laurentine shore (Castelporziano, Lazio, Italy). *Géomorphologie: relief, processus, environnement* 15(4): 241-256.

Birkeland, P.W., Machette, M.N., Haller, K.M. 1991. *Soils as a Tool for Applied Quaternary Geology*. Utah: Utah Geological and Mineral Survey.

Bookstein, F.L. 1997. Landmark methods for forms without landmarks: morphometrics of group differences in outline shape. *Medical Image Analysis* 1: 225-243.

Bordes, F. 1961. Mousterian cultures in France. *Science* 134(3482): 803-810.

Boshoff, P., Durrheim, R., Fraser, A., Martini, J.E.J., Ralph, A., Sefton, M. 1990. The Lincoln-Fault cave system. *Bulletin South African Speleologists Association* 31: 60-64.

Bradfield, J. 2016. Fracture analysis of bone tools: a review of the micro-CT and macrofracture methods for studying bone tool function. In: Vitezovic, S. (ed.) *Close to the Bone: Current Studies in Bone Technologies*: 71-79. Belgrade: Institute of Archaeology.

Brain, C.K. 1958. *The Transvaal Ape-Man Bearing Cave Deposits*. *Memoirs of the Transvaal Museum*, No. 11, Pretoria: Transvaal Museum.

Broom, R. 1936. A new fossil anthropoid skull from South Africa. *Nature* 138: 486-488.

Brown., A.G. 1997. *Alluvial Geoarchaeology.* Cambridge: Cambridge University Press.

Bruxelles, L., Clarke, R., Maire, R., Ortega, R., Stratford, D. 2014. Stratigraphic analysis of the Sterkfontein StW 573 *Australopithecus* skeleton and implications for its age. *Journal of Human Evolution* 70: 36-48.

Bruxelles, L., Stratford, D., Maire, R., Pickering, T., Heaton, J., Beaudet, A., Kuman, K., Crompton, R., Carlson, K., Jashashvili, T., McClymont, J., Leader, G., Clarke, R. 2019. A multiscale stratigraphic investigation of the context of StW 573 'Little Foot' and Member 2, Sterkfontein Caves, South Africa. *Journal of Human Evolution* 133: 78-98.

Burgess, R.J. & Kvamme, K.L. 1978. A new technique for the measurement of artifact angles. *American Antiquity* 43(3): 482-487.

Bustoz-Pérez, G., Díaz, S., Baena, J. 2019. An experimental approach to degrees of rounding among lithic artifacts. *Journal of Archaeological Method and Theory* 26: 1243-1275.

Butzer, K.W. 1964. *Environment and Archaeology*. Chicago: Aldine.

Butzer, K.W. 1982. *Archaeology as Human Ecology: Method and Theory for a Contextual Approach*. New York: Cambridge University Press.

Butzer, K.W. 2008. Challenges for a cross-disciplinary geoarchaeology: the intersection between environmental history and geomorphology. *Geomorphology* 101(1-2): 402-411.

Cardillo, M. 2010. Some applications of Geometric Morphometrics to archaeology. In: Elewa, A.M.T. (ed.) *Morphometrics for Nonmorphometricians*: 325-341. Lecture Notes in Earth Science 124. Dordrecht: Springer.

Caruana, M.V., Carvalho, S., Braun, D.R., Presnyakova, D., Haslam, M., Archer, W., Bobe, R., Harris, J.W. 2014. Quantifying traces of tool use: a novel morphometric analysis of damage patterns on percussive tools. *Plos One* 9(11): 1-18.

Caruana, M.V. 2017. Lithic production strategies in the Oldowan assemblages from Sterkfontein member 5 and Swartkrans member 1, Gauteng province, South Africa. *Journal of African Archaeology* 15(1): 1-19.

Charlin, J. & Gonzalez-Jose, R. 2012. Size and shape variation in late Holocene projectile points of the Southern Patagonia: A geometric morphometric study. *American Antiquity* 77(2): 221-242.

Chase, A.F., Chase, D.Z., Weishampel, J.F., Drake, J.B., Shrestha, R.L. 2011. Airborne LiDAR, archaeology, and the ancient Maya landscape at Caracol, Belize. *Journal of Archaeological Science* 38(2): 387-398.

Clarke, R.J. 1994. On some new interpretations of Sterkfontein stratigraphy. *South African Journal of Science* 90(4): 211-214.

Clarke, R.J. 1998. First ever discovery of a well-preserved skull and associated skeleton of *Australopithecus. South African Journal of Science* 94(10): 460-463.

Clarke, R.J. 1999. Discovery of complete arm and hand of the 3.3 million-year-old *Australopithecus* skeleton from Sterkfontein. *South African Journal of Science* 95: 477-480.

Clarke, R.J. 2002. Newly revealed information on the Sterkfontein Member 2 *Australopithecus* skeleton. *South African Journal of Science* 98(11): 523-526.

Clarke, R.J. 2006. A deeper understanding of the stratigraphy of Sterkfontein fossil hominid site. *Transactions of the Royal Society of South Africa* 61(2): 111-120.

Clarke, R.J. 2007. Taphonomy of Sterkfontein *Australopithecus* skeletons. In: Pickering, T.R., Schick, K., Toth, N. (eds.) *Breathing Life into Fossils: Taphonomic Studies in Honor of C.K. (Bob) Brain*: 167-173. Bloomington (Indiana): Stone Age Institute Press.

Clarke, R.J. 2012. A brief review of history and results of 40 years of Sterkfontein excavations. In: Reynolds, S.C. & Gallaghar, A. (eds.) *African Genesis: Perspectives on Hominin Evolution*: 120-141. Cambridge: Cambridge University Press.

Clarke, R.J. 2013. *Australopithecus* from Sterkfontein Caves, South Africa. In: Reed, K.E., Fleagle, J.G. and Leakey, R.E. (eds.) *The Paleobiology of Australopithecus, Vertebrate Paleobiology and Paleoanthropology*: 105-123. Dordrecht: Springer.

Clarke, R.J. 2017. *Homo habilis*: the inside story. In: Sahnouni, M., Semaw, S., Garaizar, J.R. (eds.) *Proceedings of the II Meeting of African Prehistory*: 25-51. Burgos: Centro Nacional de Investigación sobre la Evolución Humana.

Clarke, R.J. & Kuman, K. 2019. The skull of StW 573, a 3.67 Ma *Australopithecus prometheus* skeleton from Sterkfontein Caves, South Africa. *Journal of Human Evolution* 134: 1-31.

Clarke, R.J. & Tobias, P.V. 1995. Sterkfontein Member 2 foot-bones of the oldest South African hominid. *Science* 269(5223): 521-524.

Coe, R. 2002. It's the Effect Size, Stupid. What Effect Size is and why it is Important. Presented at annual conference of the British Educational Research Association. England: University of Exeter.

Cooke, H.B.S. 1938. The Sterkfontein bone breccia: a geological note. *South African Journal of Science* 35(12): 204-208.

Corti, M. 1993. Geometric Morphometrics: an extension of the revolution. *Trends in Ecology & Evolution* 8(8): 302-303.

Coules, H.E., Orrock, P.J., Seow, C.E. 2019. Reflectance Transformation Imaging as a tool for engineering failure analysis. *Engineering Failure Analysis* 105: 1006-1017.

Couzens, R.A. 2012. An analysis of the symmetry of Large Cutting Tools within the South African Acheulean. Unpublished MSc dissertation, Johannesburg: University of the Witwatersrand.

Crabtree, K. 1971. Overton Down experimental earthwork. *Wiltshire 1968, Proceedings of the University of Bristol Spelæological Society* 12(3): 237-244.

Crompton, S. 2007: Layers of perception. *Proceedings of the 35th International Conference on Computer Applications and Quantitative Methods in Archaeology (CAA)* 10: 147-152.

Crowther, R.A., Henderson, R., Smith, J.M. 1996. MRC image processing programs. *Journal of Structural Biology* 116(1): 9-16.

Curnoe, D. & Tobias, P.V. 2006. Description, new reconstruction, comparative anatomy and classification of the StW 53 cranium, with discussions about the taxomony of other Southern African early *Homo* remains. *Journal of Human Evolution* 50: 36-77.

Curwen, C.E. 1930. Neolithic camps. *Journal of Antiquity* 4: 22-54.

Delson, E. 1984. Cercopithecid biochronology of the African Plio-Pleistocene: Correlation among eastern and southern hominid-bearing localities. *Courier Forschungsinstitut Senckenberg* 69(1): 199-218.

Delson, E. 1988. Chronology of South African australopith site units. In: Grine, F.E., (ed.) *Evolutionary History of the 'Robust' Australopithecines*: 317-324. New York: Aldine.

De Lombre-Hermida, A., Bargalló, A., Huguet, R., Vallverdu, J., García-Antón, M.D., Mosquera, M., Ollé, A., Ramos, R.S., Bernal, M.T. 2015. The lithic industry of Sima del Elefante (Atapuerca, Burgos, Spain) in the context of Early and Middle Pleistocene technology in Europe. *Journal of Human Evolution* 82: 95-106.

Dibble, H.L. & Bernard, M.C. 1980. A comparative study of basic edge angle measurement techniques. *American Antiquity* 45(4): 857-865.

Dibble, H.L. & Chase, P. 1981. A new method of recording artifact shape. *American Antiquity* 46: 178-187.

Eren, M.I., Dominguez-Rodrigo, M., Kuhn, S.L., Adler, D.S., Ian Le, Bar-Yosef, O. 2005. "Defining and measuring reduction in unifacial stone tools." *Journal of Archaeological Science* 32(8): 1190-1201.

Eren, M.I. & Sampson, C.G. 2009. Kuhn's geometric index of unifacial stone tool reduction (GUIR): does it measure missing flake mass? *Journal of Archaeological Science* 36(6): 1243-1247.

Ferring, C.R. 1994. Late Quaternary geology of the upper Trinity River basin, Texas. Unpublished Doctoral dissertation, The University of Texas. Dallas: The University of Texas.

Field, A.S. 1999. An analytical and comparative study of the Earlier Stone Age archaeology of the Sterkfontein Valley. Unpublished MSc dissertation, Departments of Archaeology and Anatomical Sciences. Johannesburg: University of the Witwatersrand.

Flügel, E. 2004. *Microfacies of Carbonate Rocks: Analysis, Interpretation and Application*. Berlin: Springer Science & Business Media.

French, C.A. 2003. *Geoarchaeology in Action: Studies in Soil Micromorphology and Landscape Evolution*. London: Routledge.

Galland, A., Queffeleca, A., Caux, S., Bordes, J.B. 2019. Quantifying lithic surface alterations using confocal microscopy and its relevance for exploring the Châtelperronian at La Roche-à-Pierrot (Saint-Césaire, France). *Journal of Archaeological Science* 104: 45-55.

Gero, J. & Mazzullo, J. 1984. Analysis of artifact shape using Fourier Series in closed form. *Journal of Field Archaeology* 11(3): 315-322.

Goldberg, P. & Berna, F. 2010. Micropmorphology and context. *Quarternary International* 214(1-2): 56-62.

Goldberg, P. & Macphail, R.I. 2006. *Practical and Theoretical Geoarchaeology*. Oxford: Blackwell Publishing.

Goldberg, P. & Sherwood, S.C. 2006. Deciphering human prehistory through the geoarcheological study of cave sediments. *Evolutionary Anthropology* 15(1): 20-36.

Goldberg, P., Miller, C.E., Schiegl, S., Ligouis, B., Berna, F., Conard, N., Wadley, L. 2009. Bedding, hearths, and site maintenance in the Middle Stone age of Sibudu cave, KwaZulu-Natal, South Africa. *Archaeological and Anthropological Sciences* 1(2): 95-122.

Gould, R.A., Koster, D.A., Sontz. L.A. 1971. The lithic assemblage of the Western Desert Aborigines of Australia. *American Antiquity* 36: 149-169.

Granger. D., Gibbon, R., Kuman, K., Clarke, R.J., Bruxelles, L. Caffee, M. 2015. New cosmogenic burial ages for Sterkfontein Member 2 *Australopithecus* and Member 5 Oldowan. *Nature* 522(7554): 85-88.

Grosman, L. 2016. Reaching the point of no return: The computational revolution in archaeology. *Annual Review of Anthropology* 45: 129-145.

Grosman, L., Smikt, O., Smilansky, U. 2008. On the application of 3-D scanning technology for the documentation and typology of lithic artifacts. *Journal of Archaeological Science* 35(12): 3101-3110.

Grosman, L., Goldsmith, Y., Smilanksy, U. 2011a. Morphological analysis of Nahal Zihor handaxes: a chronological perspective. *PaleoAnthropology* 2011: 203-215.

Grosman L., Sharon, G., Goldman-Neuman, T., Smikt, O., Smilansky, U. 2011b. Studying post-depositional damage on Acheulean bifaces using 3-D scanning. *Journal of Human Evolution* 60(4): 398-406.

Grosman, L., Ovadia, A., Bogdanovsky, A. 2014. Neolithic masks in the digital world. In: Hershamn, D. (ed.) *Face to Face: the Oldest Masks in the World*: 60-89. Jerusalem: the Israel Museum.

Hassan, F.A. 1978. Sediments in archaeology: methods and implications for palaeoenvironmental and cultural analysis. *Journal of Field Archaeology* 5(2): 197-213.

Hassan, F. 1979. Geoarchaeology: The Geologist and Archaeology. *American Antiquity* 44(2): 267-270.

Haynes, C.V. 1964. Fluted projectile points: their age and dispersion: stratigraphically controlled radiocarbon dating provides new evidence on peopling of the new world. *Science* 145(3639): 1408-1413.

Henshilwood, C.S., d'Errico, F., Marean, C.W., Milo, R.G., Yates, R. 2001a. An early bone tool industry from the Middle Stone Age at Blombos Cave, South Africa: implications for the origins of modern human behaviour, symbolism and language. *Journal of Human Evolution* 41(6): 631-678.

Henshilwood, C.S., Sealy, J.C., Yates. R., Cruz-Uribe, K., Goldberg, P., Grine, F.E., Klein, R.G., Poggenpoel, P., van Niekerk, K., Watts, I. 2001b. Blombos Cave, Southern Cape, South Africa: Preliminary report on the 1992–1999 excavations of the Middle Stone Age levels. *Journal of Archaeological Science* 28(4): 421-448.

Herries, A.I.R. & Shaw, J. 2011. Palaeomagnetic analysis of the Sterkfontein palaeocave deposits: implications for the age of the hominin fossils and stone tool industries. *Journal of Human Evolution* 60(5): 523-539.

Herzlinger, G., Goren-Inbar, N., Grosman, L. 2017. A new method for 3-D geometric morphometric shape analysis: the case study of handaxe knapping skill. *Journal of Archaeological Science: Reports* 14: 163-173.

Herzlinger, G. & Goren-Inbar, N. 2019. Beyond a cutting edge: a morpho-technological analysis of Acheulian handaxes and cleavers from Gesher Benot Ya'aqov, Israel. J*ournal of Palaeolithic Archaeology* 3(1): 33-58.

Herzlinger, G. & Grosman, L. 2018. AGMT3-D: a software for 3-D landmarks-based geometric morphometric shape analysis of archaeological artifacts. *PLoS One* 13(11): e0207890.

Hiscock, P. 1982. The real meaning of edge angles? *Australian Archaeology* 14(1): 79-85.

Holliday, T.W. 1997. Body proportions in Late Pleistocene Europe and modern human origins. *Journal of Human Evolution* 32(5): 423-448.

Hughes, A.R. & Tobias, P.V. 1977. A fossil skull probably of the genus *Homo* from Sterkfontein, Transvaal. *Nature* 265(5592): 310-312.

Hughes, P.D. 2010. Geomorphology and Quaternary stratigraphy: the roles of morpho-, litho, and allostratigraphy. *Geomorphology* 123(3-4): 189-199.

Jewell, P.A. 1963. *The Experimental Earthwork of Overton Down, Wiltshire, 1960.* London: British association for the advancement of science.

Karkanas P. & Goldberg P. 2010. Site formation processes at Pinnacle Point Cave 13B (Mossel Bay, Western Cape Province, South Africa): resolving stratigraphic and depositional complexities with micromorphology. *Journal of Human Evolution* 59(3-4): 256-273.

Karkanas P. & Goldberg P. 2013. Micromorphology of cave sediments. In: Shroder, J.F. & Frumkin, A. (eds.) *Treatise on Geomorphology*: 286-297. Karst Geomorphology, vol 6. San Diego: Academic Press.

Karkanas, P. & Goldberg, P. 2018. *Reconstructing Archaeological Sites: Understanding the Geoarchaeological Matrix*. New Jersey: John Wiley & Sons.

Katsianis, M., Mavridis, F., Tankosić, Z. 2017. A 3D spatial approach to post-excavation study as exemplified at the Agia Triada Cave, Karystos. In: Tankosić, Z., Mavridis, F., Kosma, M. (eds.) *An island between two worlds. The archaeology of Euboea from Prehistoric to Byzantine times*: 133-145. Papers and Monographs from the Norwegian Institute at Athens, vol 6. Athens: Norwegian Institute.

Keeley, L.H. 1974. Technique and methodology in microwear studies: a critical review. *World Archaeology* 5(3): 323-336.

Kibii, J.M. 2004. Comparative taxonomic, taphonomic and palaeoenvironmental analysis of 4-2.3 million-year-old Australopithecine cave infills at Sterkfontein. Unpublished PhD thesis. Johannesburg: University of Witwatersrand.

Kibii, J.M. & Clarke, R.J. 2003. A reconstruction of the StW 431 *Australopithecus* pelvis based on newly discovered fragments. *South African Journal of Science* 99(5): 225-226.

Kraft, J.C., Rapp Jr, G., Aschenbrenner, S.E. 1975. Late Holocene paleogeography of the coastal plain of the Gulf of Messenia, Greece, and its relationships to archaeological settings and coastal change. *Geological Society of America Bulletin* 86(9): 1191-1208.

Kuman, K. 1994a. The archaeology of Sterkfontein: past and present. *Journal of Human Evolution* 27(6): 471-495.

Kuman, K. 1994b. The archaeology of Sterkfontein: Preliminary findings on site formation and cultural change. *South African Journal of Science* 90(4): 215-219.

Kuman, K. 2003. Site formation in the early South African Stone Age sites and its influence on the archaeological record. *South African Journal of Science* 99(5-6): 1-5.

Kuman, K. & Clarke R.J. 2000. Stratigraphy, artefact industries and hominid associations for Sterkfontein, Member 5. *Journal of Human Evolution* 38(6): 827-847.

Kuman, K. & Field, A.S. 2009. The Oldowan Industry from Sterkfontein Caves, South Africa. In: Schick, K. and Toth, N. (eds.) *Approaches to the Earliest Stone Age*: 151-170. Bloomington: Stone Age Institute Press.

Kuman, K., Sutton, M.B., Pickering, T., Heaton, J.L. 2018. The Oldowan industry from Swartkrans cave, South Africa, and its relevance for the African Oldowan. *Journal of Human Evolution* 123: 52-69.

Kuman, K., Granger, D.E., Gibbon, R.J., Pickering, T.R., Caruana, M.V., Bruxelles, L., Clarke, R.J., Heaton, J.L., Stratford, D. and Brain, C.K., 2021. A new absolute date from Swartkrans Cave for the oldest occurrences of *Paranthropus robustus* and Oldowan stone tools in South Africa. *Journal of Human Evolution 156*: 103000.

Langejans, G. 2012. Micro-residue analysis on Early Stone Age tools from Sterkfontein, South Africa: a methodological enquiry. *South African Archaeological Bulletin* 67(196): 200-213.

Lerma J.L., Navarro S, Seguí, A.E., Cabrelles M. 2014. Range-based versus automated marker-less image-based techniques for rock art documentation. *The Photogrammetric Record* 29(145): 30-48.

Lin, S.C.H., Douglass, M.J., Holdaway, S.J., Floyd, B. 2010. The application of 3D laser scanning technology to the assessment of ordinal and mechanical cortex quantification in lithic analysis. *Journal of Archaeological Science* 37(4): 694-702.

Luyt, C.J. & Lee-Thorp, J.A. 2003. Carbon isotope ratios of Sterkfontein fossils indicate a marked shift to open environments c. 1.7 Myr ago. *South African Journal of Science* 99(5): 271-273.

Lycett, S.J., Von Cramon-Taubadel, N., Foley, R. 2006. A crossbeam co-ordinate calliper for morphometric analysis of lithic nuclei: A description, test and empirical examples of application. *Journal of Archaeological Science* 33(6): 847-861.

Lycett, S.J. & Chauhan, P.R. 2010. *New Perspectives on Old Stones: Analytical Approaches to Palaeolithic Technologies*. New York: Springer.

Mandel, R.D., Goldberg, P., Holliday, V.T. 2017. Site Formation Processes. In: Gilbert, A.S., Goldberg, P., Holliday, V.T., Mandel, R.D., Sternberg, R.S. (eds.) *Encyclopedia of GeoArchaeology: Encyclopedia of Earth Sciences Series*: 797-817. Dordrecht: Springer.

Marean, C.W., Bar-Matthews, M., Fisher, E., Goldberg, P., Herries, A., Karkanas, P., Nilssen, P.J., Thompson, E. 2010. The stratigraphy of the Middle Stone Age sediments at Pinnacle Point Cave 13B (Mossel Bay, Western Cape Province, South Africa). *Journal of Human Evolution* 59(3-4): 234-255.

Martini, J.E., Wipplinger, P.E., Moen, H.F., Keyser, A. 2003. Contribution to the speleology of Sterkfontein Caves, Gauteng Province, South Africa *International Journal of Speleology* 34(1): 43-69.

Mason, J.R. 1962. The Sterkfontein stone artefacts and their maker. *South African Archaeological Bulletin* 17: 109-125.

Mason, R.J. 1988. *Cave of Hearths, Makapansgat, Transvaal*. Johannesburg: University of the Witwatersrand.

McKee, J.K. 1993. Faunal Dating of the Taung hominid fossil deposit. *Journal of Human Evolution* 25(5): 363-376.

McNabb, J. 2009. The ESA stone tool assemblage from the Cave of Hearths, Beds 1-3. In: McNabb, J. & Sinclair, A. (eds.) *The Cave of Hearths: Makapan Middle Pleistocene Research Project: Field research by Anthony Sinclair and Patrick Quinney, 1996-2001*: 75-102. BAR international series, vol 1. University of Southampton: Archaeopress.

McNabb, J. & Sinclair, A. 2009. An overview of the archaeological history of the Cave of Hearths and its lithic assemblages. In: McNabb, J. & Sinclair, A. (eds.) *The Cave of Hearths: Makapan Middle Pleistocene Research Project: Field research by Anthony Sinclair and Patrick Quinney, 1996-2001*: 12-28. BAR international series, vol 1. University of Southampton: Archaeopress.

McPherron, S.P. 2000. Handaxes as a measure of the mental capabilities of early hominids. *Journal of Archaeological Science* 27(8): 655-663.

McPherron, S.P. & Dibble, H.L. 1999. Stone tool analysis using digitized images: examples from the Lower and Middle Paleolithic. *Lithic Technology* 24(1): 38-52.

McPherron, S.P., Braun, D.R., Dogandzic, T., Archer, W., Desta, D., Lin, S. 2014. An experimental assessment of the influences on edge damage to lithic artifacts: a consideration of edge angle, substrate grain size, raw material properties, and exposed face. *Journal of Archaeological Science* 49: 70-82.

Montet-White, A. 1973. *Le Malpas Rockshelter: a Study of Late Palaeolithic Technology in its Environmental Setting*. Lawrence: University of Kansas Publications in Anthropology.

Morales, J.I., Lorenzo, C., Verges, J.M. 2013. Measuring retouch intensity in lithic tools: a new proposal using 3D scan data. *Journal of Archaeological Method Theory* 22(2): 543-558.

Nash, D.T. & Petraglia, M.D. 1987. Natural formation processes and the archaeological record. *BAR International Series* 352, 204. Oxford: Cambridge University Press.

Nielsen, A.E. 1991. Trampling the archaeological record: an experimental study. *American Antiquity* 56(3): 483-503.

Niven, L., Steele, T., Finke, H., Gernat, T., Hublin, J. 2009. Virtual skeletons: using a structured light scanner to create a 3D faunal comparative collection. *Journal of Archaeological Science* 36(9): 2018-2023.

Ogola, C. 2009. The Sterkfontein western breccias: stratigraphy, fauna and artefacts. Unpublished PhD thesis. Johannesburg: University of the Witwatersrand.

O' Regan, H.J. 2007. A revision of the carnivora from Member 5, Sterkfontein, South Africa, based on reassessment of published material and site stratigraphy. *Annals of the Transvaal Museum* 44(1): 209-214.

Pargeter, J., Bam, L., De Beer, F., Lombard, L. 2017. Microfocus X-Ray Tomography as a method for characterising macro-fractures on quartz backed tools. *South African Archaeological Bulletin* 72(206): 148-155.

Partridge, T.C. 1978. Re-appraisal of lithostratigraphy of Sterkfontein hominid site. *Nature* 275(5678): 282-287.

Partridge, T.C. 1993. Report provided in the *27th Annual Report, Palaeo-Anthropology Research Unit*, Dept. of Anatomy and Human Biology, University of the Witwatersrand Medical School (office of P.V. Tobias).

Partridge, T.C. 2005. Dating of the Sterkfontein hominids: progress and possibilities. *Transactions of the Royal Society of South Africa* 60(2): 107-109.

Partridge, T.C. & Watt, I.B. 1991. The stratigraphy of the Sterkfontein hominid deposit and its relationship to the underground cave system. *Palaeontologia Africana* 28: 35-40.

Patterson, L.W. 1980. Measurement of stone artifact edge angles. *Flintknappers' Exchange* 3(2): 11-13.

Pickering, T.R. 1999. Taphonomic interpretations of the Sterkfontein early hominid site (Gauteng, South Africa) reconsidered in light of recent evidence. Unpublished PhD thesis. Madison: University of Wisconsin.

Pickering, T.R., Clarke, R.J., Moggi-Cecchi, J. 2004. The role of carnivores in the accumulation of the Sterkfontein Member 4 hominid fossil assemblage: a taphonomic reassessment of the complete hominid fossil sample (1936-1999). *American Journal of Physical Anthropology* 125(1): 1-15.

Pickering, T.R. & Kramers, J.D. 2010. Re-appraisal of the stratigraphy and determination of new U-Pb dates for the Sterkfontein hominin site, South Africa. *Journal of Human Evolution* 59(1): 1-17.

Rajani, M.B., Patra, S.K., Verma, M. 2009. Space observation for generating 3D perspective views and its implication to the study of the archaeological site of Badami in India. *Journal of Cultural Heritage* 10: 20-26.

Rapp Jr., G.R. & Hill, C.L. 1998, *Geoarchaeology: The Earth-Science Approach to Archaeological Interpretation*. New Haven Connecticut: Yale University Press.

Räsänen, M.E., Auri, J.M., Huitti, J.V., Klap, A.K., Virtasalo, J.J. 2009. A shift from lithostratigraphic to allostratigraphic classification of Quaternary glacial deposits. *GSA Today* 19(2): 4-11.

Re, A., Corsi, J., Demmelbauer, M., Martini, M., Mila, G., Ricci, C. 2015. X-ray tomography of a soil block: a useful tool for the restoration of archaeological finds. *Heritage Science* 3(1): 1-7.

Reading, H.G. & Levell, B.K. 1996. Controls on the sedimentary rock record. In: Reading, H.G. (ed.) *Sedimentary Environments: Processes, Facies and Stratigraphy*: 5-36, 3rd ed. Cambridge: Blackwell Science.

Reed, K.E. 1997. Early hominid evolution and ecological change through the African Plio-Pleistocene. *Journal of Human Evolution* 32(2-3): 289-322.

Renfrew, C. 1976. Archaeology and the Earth Sciences. In Davidson, D.A. &. Shackley, M.L (eds.) *Geoarchaeology: Earth Science and the Past*: 1-5. Boulder: Colorado Westview Press.

Renfrew, C. & Bahn, P. 2004. *Archaeology: Theories, Methods and Practice*. London: Thames & Hudson Ltd.

Reynolds, S.C., Vogel J.C., Clarke, R.J., Kuman, K. 2003. Preliminary results of excavations at Lincoln Cave, Sterkfontein, South Africa, *South African Journal of Science* 99: 286-289.

Reynolds, S.C., Clarke, R.J., Kuman, K. 2007. The view from the Lincoln Cave: mid to late Pleistocene fossil deposits from Sterkfontein hominid site, South Africa. *Journal of Human Evolution* 53(3): 260-271.

Richardson, E., Grosman, L., Smilansky, U., Werman, M. 2013. Extracting scar and ridge features from 3D-scanned lithic artifacts. In: Earl, E., Sly, T., Wheatley, D., Romanowska, I., Papadopolous, K., Murrieta-Flores, P., Chrysanthi, A. (eds.) *Archaeology in the Digital Era*: 83-92. Amsterdam: Amsterdam University Press.

Robinson, J.T. 1957. Occurrence of stone artefacts with *Australopithecus* at Sterkfontein (parts 1 and 2). *Nature* 180(4585): 521-524.

Robinson, J.T. 1962. Sterkfontein stratigraphy and the significance of the extension site. *South African Archaeological Bulletin* 17(66): 87-107.

Roe, D.A. 1964. The British lower and middle Palaeolithic: some problems, methods of study and preliminary results. *Proceedings of the Prehistoric Society* 30: 245-267.

Salvador, A. 1994. *International Stratigraphic Guide: a Guide to Stratigraphic Classification, Terminology, and Procedure*. Trondheim: International Union of Geological Sciences.

Saragusti, I., Karasik, A., Sharon, I., Smilansky, U. 2005. Quantitative analysis of shape attributes based on contours and section profiles in artifact analysis. *Journal of Archaeological Science* 32(6): 841-853.

Schick, K. & Clark, J.D. 2003. Biface technological development and variability in the Acheulean industrial complex in the Middle Awash region of the Afar Rift, Ethiopia. In Soressi, M., & Dibble, H.L. (eds.) *Multiple Approaches to the Study of Bifacial Technologies*: 1-30. Philadelphia: Museum of Anthropology and Archaeology.

Schick, K.D. & Toth, N.P. 1994. *Making Silent Stones Speak: Human Evolution and the Dawn of Technology*. New York: Simon and Schuster.

Schiffer, M.B. 1972. Archaeological context and systemic context. *American Antiquity* 37: 156-165.

Schiffer, M.B. 1983. Toward the identification of formation processes. *American Antiquity* 48(4): 675-706.

Semenov, S.A. 1964. *Prehistoric Technology: An Experimental Study of the Oldest Tools and Artefacts from Traces of Manufacture and Wear*. London: Cory, Adams & Mackay.

Shackley, M.L. 1974. Stream abrasion of flint implements. *Nature* 248(5448): 301-302.

Shackley, M.L. 1975 *Archaeological Sediments*. London: Butterworth.

Sherwood, S.C. & Goldberg, P. 2001. A geoarchaeological framework for the study of karstic cave sites in the eastern woodlands. *Midcontinental Journal of Archaeology* 26(2): 145-167.

Shott, M. J. & Trail, B.W. 2010. Exploring new approaches to lithic analysis: laser scanning and Geometric Morphometrics. *Lithic Technology* 35(2): 195-220.

Siegel, P.E. 1985. Edge angle as a functional indicator: a test. *Lithic Technology* 14(2): 90-94.

Slice, D.E. 2007. Geometric Morphometrics. *Annual Review of Anthropology* 36: 261-281.

Sonnenfeld, J. 1962. Interpreting the function of primitive implements. *American Antiquity* 28(1): 56-65.

Spry, C., Foley, E., Kurpiel, R., Turnbull, J. 2019. Identifying quartz artefacts in archaeology and cultural heritage management: issues, approaches and a new open access project. In: Spry, C., Foley, E., Kurpiel, R., Turnbull, J. (eds.) *Excavations, Surveys and Heritage Management in Victoria*: 77-83. Melbourne: La Trobe University.

Stein, J.K. 1993, Scale in Archaeology, Geosciences, and Geoarchaeology. In: Stein, J.K. & Linse. A.R. (eds.) *Effects of Scale on Archaeological and Geoscientific Perspectives*. Geological Society of America Special Paper 283: 1-10. Boulder Colorado: I. B. Taurus.

Stein, J.K. 2001. A review of site formation processes and their relevance to geoarchaeology. In: Goldberg, P., Holliday, V.T., Herring, C.V. (eds.) *Earth Sciences and Archaeology*: 37-54. Boston: Springer.

Stiles, D.N. & Partridge, T.C. 1979. Results of recent archaeological and palaeoenvironmental studies at the Sterkfontein Extension Site. *South African Journal of Science* 75(8): 346-352.

Stratford, D.J. 2008. *A Study of Newly Discovered Lithics from Earlier Stone Age Deposits at Sterkfontein*. Unpublished MSc Thesis, SGAES. Johannesburg: University of the Witwatersrand.

Stratford, D.J. 2011. Cave excavation: some methodological and interpretive considerations. *Cave and Karst Science* 38(3): 111-116.

Stratford, D.J., Bruxelles, L., Clarke, R.J., Kuman, K. 2012. New stratigraphic interpretations of the fossil and artefact-bearing deposits of the Name Chamber, Sterkfontein. *South African Archaeological Bulletin* 67(197): 159-167.

Stratford, D.J. & Val, A. 2015. The macrovertebrate fossil assemblage from the Name Chamber, Sterkfontein: taxonomy, taphonomy and implications for site formation processes. *Paleontologia Africana* 50: 1-17.

Stratford, D., Heaton, J. L., Pickering, T. R., Caruana, M. V., Shadrach, K. 2016. First hominin fossils from Milner Hall, Sterkfontein, South Africa. *Journal of Human Evolution* 91(16): 167-173.

Stratford, D.J., Merlo, S., Brown, S. 2016. The development of a new geospatial framework for the palaeoanthropological site of the Sterkfontein Caves, Cradle of Humankind, Gauteng, South Africa. *Journal of Field Archaeology* 41(2): 211-221.

Sumner, T.A. & Riddle, T.R.A. 2008. A virtual Paleolithic: assays in photogrammetric three-dimensional artifact modelling. *Paleoanthropology* 2008: 158-169.

Susman, R.L., Stern, J.T., Jungers, W.L. 1984. Arboreality and bipedality in the Hadar homonids. *Folia primatologica* 43(2-3): 113-156.

Tallavaara, M., Manninen, M.A., Hertell, E., Rankama, T. 2010. How flakes shatter: a critical evaluation of quartz fracture analysis. *Journal of Archaeological Science* 37(10): 2442-2448.

Tobias, P.V. 1991. *The Skulls, Endocasts and Teeth of Homo habilis. Olduvai Gorge, Volume IV.* Cambridge: Cambridge University Press.

Tobias, P.V. & Hughes, A.R. 1969. The new Witwatersrand University excavation at Sterkfontein: progress report, some problems and first results. *South African Archaeological Bulletin* 24(95-96): 158-169.

Tringham, R., Cooper, G., Odell., G, Voytek, B., Whitman, A. 1974. Experimentation in the formation of edge damage: a new approach to lithic analysis. *Journal of Archaeology* 1(1-2): 171-196.

Underhill, D. 2007. Subjectivity inherent in by-eye symmetry judgements and the large cutting tools at the Cave of Hearths, Limpopo Province, South Africa. *Papers from the Institute of Archaeology* 18: 101-113.

Valletta, F., Smilansky, U., Goring-Morris, A.N., Grosman, L. 2020. On measuring the mean edge angle of lithic tools based on 3-D models: a case study from the southern Levantine Epipalaeolithic. *Archaeological and Anthropological Sciences* 12(2): 49-68.

Viallet, C. 2019. A new method of Three-Dimensional morphometry for analyzing the functional potentialities of bifaces. Contribution to the study of artefacts from AU P3 from the “Caune de l’Arago” (France). *Prehistoric Palaeontology* 18(2): 236-250.

Villagran, X.S., Strauss, A., Alves, M., Oliveira, R.E. 2019. Virtual micromorphology: The application of micro-CT scanning for the identification of termite mounds in archaeological sediments. *Journal of Archaeological Science: Reports* 24: 785-795.

Vrba, E.S. 1976. The Fossil Bovidae of Sterkfontein, Swartkrans and Kromdraai. *Memoirs of the Transvaal Museum* 21. Pretoria: Transvaal Museum.

Vrba, E.S. 1980. The significance of bovid remains as indicators of environment and predation patterns. In: Behrensmeyer, A.K. & Hill, A.P. (eds.) *Fossils in the Making*, 247-271. Chicago: University of Chicago Press.

Vrba, E.S. 1982. Biostratigraphy and chronology, based particularly on Bovidae, of Southern hominid associated assemblages: Makapansgat, Sterkfontein, Taung, Kromdraai, Swartkrans; also Elandsfontein (Saldanha), Broken Hill (now Kabwe) and Cave of Hearths. *Proceedings of Congress international de paleontologie humaine* 2: 707-752.

Wadley, L. & Jacobs, Z. 2006. Sibudu Cave: background to the excavations, stratigraphy and dating. *Southern African Humanities* 18(1): 1-26.

Wadley, L., Sievers, C., Bamford, M., Goldberg, P., Berna, F., Miller, C. 2011. Middle Stone Age bedding construction and settlement patterns at Sibudu, South Africa. *Science* 334(6061): 1388-1391.

Walker, R.G. & Cant, D.J. 1984. *Facies models: Geoscience* Canada Reprint Series 1: 317. Calgary Alberta: Geological Association of Canada.

Walker, J., Cliff, R.A., Latham, A.G. 2006. U-Pb Isotopic Age of the StW 573 hominid from Sterkfontein, South Africa. *Science* 314(5805): 1592-1594.

Waters, M.R. 1992. *Principles of Geoarchaeology: A North American Perspective*. Tucson: University of Arizona Press.

Weiner, S. & Bar-Yosef, O. 1990. States of preservation of bones from prehistoric sites in the Near East: a survey. *Journal of Archaeological Science* 17(2): 187-196.

White, W.B. 2007. Cave sediments and the paleoclimate. *Journal of Cave and Karst studies* 69(1): 76-93.

White, J.P. & Thomas, D.H. 1972. What mean these stones? Ethnotaxonomic models and archaeological interpretations in the New Guinea Highlands. In: Clarke, D.L. (ed.) *Models in Archaeology*: 275-308. London: Routledge.

Wilkinson, M.J. 1973. Sterkfontein Cave System: evolution of a karst form. Unpublished MA thesis. Johannesburg: University of the Witwatersrand.

Wilkinson, M.J. 1983. Geomorphic perspectives on the Sterkfontein Australopithecine breccias. *Journal of Archaeological Science* 10(6): 515-529.

Wilmsen, E.N. 1970. *Lithic Analysis and Cultural Inference: A Paleo-Indian Case.* Tucson: University of Arizona Press.

Wynn, T. & Tierson, F. 1990. Regional comparison of the shapes of later Acheulean handaxes. *American Anthropologist* 92(1): 73-84.

Wurz, S., Bentsen, S.E., Reynard, J., van Pletzen-Vos, L., Brenner, M., Mentzer, S., Pickering, R., Green, H. 2018. Connections, culture and environments around 100 000 years ago at Klasies River main site. *Quarternary International* 495: 102-115.

Zaidner, Y. & Grosman, L. 2015. Middle Paleolithic sidescrapers were resharped or recycled? A view from Nesher Ramla, Israel. Quaternary International 361: 178-187.